



# Flow and Distribution of Non-aqueous Phase Liquids

Kevin G. Mumford, Bernard H. Kueper and  
Robert J. Lenhard

# *Flow and Distribution of Non-aqueous Phase Liquids*

*The Groundwater Project*

**Kevin G. Mumford** *PhD*

*Professor, Civil Engineering,  
Queen's University,  
Kingston, Ontario, Canada*

**Bernard H. Kueper** *PhD*

*Professor Emeritus, Civil Engineering,  
Queen's University,  
Kingston, Ontario, Canada*

**Robert J. Lenhard** *PhD*

*Former Senior Scientist, US National Laboratories;  
Former Program Manager/Group Manager  
Southwest Research Institute  
San Antonio, Texas, United States*

***Flow and Distribution of  
Non-aqueous Phase Liquids***

*The Groundwater Project  
Guelph, Ontario, Canada*

The Groundwater Project relies on private funding for book production and management of the Project.

Please consider [donating to the Groundwater Project](#)   
so books will continue to be freely available.

Thank you.

All rights reserved. This publication is protected by copyright. No part of this book may be reproduced in any form or by any means without permission in writing from the authors (to request permission contact: [permissions@gw-project.org](mailto:permissions@gw-project.org)). Commercial distribution and reproduction are strictly prohibited.

GW-Project works can be downloaded for free from [gw-project.org](http://gw-project.org). Anyone may use and share [gw-project.org](http://gw-project.org) links to download GW-Project's work. It is not permissible to make GW-Project documents available on other websites nor to send copies of the documents directly to others. Kindly honor this source of free knowledge that is benefiting you and all those who want to learn about groundwater.

Copyright © 2024 Kevin G. Mumford, Bernard H. Kueper, and Robert J. Lenhard  
(The Authors)

Published by the Groundwater Project, Guelph, Ontario, Canada, 2024.

Flow and Distribution of Non-aqueous Phase Liquids/ Kevin G. Mumford, Bernard H. Kueper and Robert J. Lenhard.

89 p.

DOI: <https://doi.org/10.62592/YXXN4737>.

ISBN: 978-1-77470-069-3

Please consider signing up to the GW-Project mailing list to stay informed about new book releases, events, and ways to participate in the GW-Project. When you sign up to our email list, it helps us build a global groundwater community. [Sign up](#).

APA (7th ed.) Citation:

Mumford, K. G., Kueper, B. H., & Lenhard, R. J. (2024). *Flow and distribution of non-aqueous phase liquids*. The Groundwater Project. <https://doi.org/10.62592/YXXN4737>.



*Domain Editors:* Eileen Poeter and John Cherry.

*Board:* John Cherry, Shafick Adams, Gabriel Eckstein, Richard Jackson, Ineke Kalwij, Renée Martin-Nagle, Everton de Oliveira, Marco Petitta, and Eileen Poeter.

*Cover Image:* Kueper, 1990.

## Dedication

This Groundwater Project Book is dedicated to Drs. Friedrich Schwillie and Art Corey, who both made tremendous contributions to our understanding of non-aqueous phase liquids in soil and groundwater systems:

- Dr. Friedrich Schwillie, the former chief groundwater hydrologist at the Federal Institute of Hydrology in Koblenz, West Germany, had the acumen in the 1970s to recognize that dense, halogenated solvents and petroleum hydrocarbons posed threats to soil and groundwater systems throughout industrialized areas of the world.
- Dr. Art Corey, former professor in the Department of Agricultural Engineering at Colorado State University, USA, had a laser focus on the fundamentals of multiphase flow, which we were able to extend to other non-aqueous phase liquid systems in both soil and groundwater.

These accomplished individuals not only inspired us but countless others as well—too many to mention—who have dedicated their careers to the understanding of non-aqueous phase liquids in soil and groundwater systems.

# Table of Contents

<b>DEDICATION .....</b>	<b>V</b>
<b>TABLE OF CONTENTS.....</b>	<b>VI</b>
<b>THE GROUNDWATER PROJECT FOREWORD .....</b>	<b>VIII</b>
<b>FOREWORD .....</b>	<b>IX</b>
<b>PREFACE .....</b>	<b>X</b>
<b>ACKNOWLEDGMENTS.....</b>	<b>XII</b>
<b>1 INTRODUCTION.....</b>	<b>1</b>
1.1 MULTIPLE FLUIDS IN POROUS MEDIA.....	1
1.2 PURPOSE.....	3
1.3 NOMENCLATURE.....	4
1.4 LIGHT NON-AQUEOUS PHASE LIQUIDS (LNAPLs) .....	5
1.5 DENSE NON-AQUEOUS PHASE LIQUIDS (DNAPLs) .....	6
1.6 LIFE CYCLE OF A NAPL SOURCE ZONE.....	9
1.7 RELEVANT EXERCISES .....	12
<b>2 PARAMETERS IMPORTANT TO NAPL FLOW .....</b>	<b>13</b>
2.1 OVERVIEW.....	13
2.2 QUANTIFICATION OF FLUID CONTENT.....	13
2.3 INTERFACIAL TENSION .....	16
2.4 WETTABILITY AND CONTACT ANGLE.....	17
<b>3 CAPILLARY PRESSURE .....</b>	<b>21</b>
3.1 CAPILLARY PRESSURE ASSOCIATED WITH SINGLE INTERFACES.....	21
3.2 MACROSCOPIC CAPILLARY PRESSURE .....	24
3.3 DRAINAGE, IMBIBITION, AND CAPILLARY PRESSURE-SATURATION CURVES.....	26
3.4 RESIDUAL FORMATION AND FLUID TRAPPING .....	30
3.5 MATHEMATICAL CAPILLARY PRESSURE-SATURATION EXPRESSIONS .....	31
3.6 SCALING CAPILLARY PRESSURE CURVES .....	33
3.7 RELEVANT EXERCISES .....	34
<b>4 RELATIVE PERMEABILITY .....</b>	<b>35</b>
4.1 EFFECTIVE PERMEABILITY AND THE EXTENSION OF DARCY'S LAW .....	35
4.2 RELATIVE PERMEABILITY CURVES.....	36
4.3 MATHEMATICAL RELATIVE PERMEABILITY-SATURATION EXPRESSIONS .....	37
<b>5 DNAPL AND LNAPL DISTRIBUTION.....</b>	<b>39</b>
5.1 DNAPL DISTRIBUTION IN DNAPL-WATER SYSTEMS .....	39
5.2 NAPL DISTRIBUTION IN THREE-FLUID SYSTEMS .....	42
5.3 LNAPL DISTRIBUTION .....	47
5.4 RELEVANT EXERCISES .....	50
<b>6 VISUAL EXAMPLES OF DNAPL AND LNAPL MIGRATION .....</b>	<b>51</b>
6.1 DNAPL MIGRATION THROUGH HETEROGENEOUS SAND.....	51
6.2 LNAPL MIGRATION FOLLOWED BY A WATER TABLE FLUCTUATION .....	52
<b>7 SUMMARY.....</b>	<b>55</b>
<b>8 EXERCISES.....</b>	<b>56</b>
EXERCISE 1 .....	56

EXERCISE 2 ..... 56

EXERCISE 3 ..... 56

EXERCISE 4 ..... 56

EXERCISE 5 ..... 56

EXERCISE 6 ..... 57

EXERCISE 7 ..... 57

EXERCISE 8 ..... 57

EXERCISE 9 ..... 58

**9 REFERENCES ..... 59**

**10 BOXES..... 66**

    BOX 1 - ADDITIONAL EQUATIONS FOR AIR-NAPL-WATER SYSTEMS ..... 66

**11 EXERCISE SOLUTIONS ..... 71**

    SOLUTION EXERCISE 1..... 71

    SOLUTION EXERCISE 2..... 71

    SOLUTION EXERCISE 3..... 71

    SOLUTION EXERCISE 4..... 72

    SOLUTION EXERCISE 5..... 73

    SOLUTION EXERCISE 6..... 74

    SOLUTION EXERCISE 7..... 75

    SOLUTION EXERCISE 8..... 77

    SOLUTION EXERCISE 9..... 80

**12 NOTATIONS ..... 84**

**13 ABOUT THE AUTHORS ..... 87**

## The Groundwater Project Foreword

The United Nations (UN) - Water Summit on Groundwater held from 7 to 8 December 2022 at the UNESCO headquarters in Paris, France, concluded with a call for governments and other stakeholders to scale up their efforts to better manage groundwater. The intent of the call to action was to inform relevant discussions at the UN 2023 Water Conference held from 22 to 24 March 2023 at the UN headquarters in New York City. One of the required actions is *strengthening human and institutional capacity*, for which groundwater education is fundamental.

The 2024 World Water Day theme is *Water for Peace*, which focuses on the critical role water plays in the stability and prosperity of the world. The [UN-Water website](#)<sup>↗</sup> states that *more than three billion people worldwide depend on water that crosses national borders*. There are 592 transboundary aquifers, yet most countries do not have an intergovernmental cooperation agreement in place for sharing and managing the aquifer. Moreover, while groundwater plays a key role in global stability and prosperity, it also makes up 99 percent of all liquid freshwater—accordingly, groundwater is at the heart of the freshwater crisis. *Groundwater is an invaluable resource*.

The Groundwater Project (GW-Project), a registered Canadian charity founded in 2018, is committed to advancement of groundwater education as a means to accelerate action related to our essential groundwater resources. We are dedicated to *making groundwater understandable* and, thus, enable *building the human capacity for sustainable development and management of groundwater*. To that end, the GW-Project creates and publishes high-quality books about *all-things-groundwater*, for all who want to learn about groundwater. Our books are unique. They synthesize knowledge, are rigorously peer reviewed and translated into many languages, and are free of charge. An important tenet of GW-Project books is a strong emphasis on visualization: Clear illustrations stimulate spatial and critical thinking. The GW-Project started publishing books in August 2020; by the end of 2023, we had published 44 original books and 58 translations. The books can be downloaded at [gw-project.org](http://gw-project.org)<sup>↗</sup>.

The GW-Project embodies a new type of global educational endeavor made possible by the contributions of a dedicated international group of volunteer professionals from a broad range of disciplines. Academics, practitioners, and retirees contribute by writing and/or reviewing books aimed at diverse levels of readers including children, teenagers, undergraduate and graduate students, professionals in groundwater fields, and the general public. More than 1,000 dedicated volunteers from 70 countries and six continents are involved—and participation is growing. Revised editions of the books are published from time to time. Readers are invited to propose revisions.

We thank our sponsors for their ongoing financial support. Please consider donating to the GW-Project so we can continue to publish books free of charge.

**The GW-Project Board of Directors, January 2024**

## Foreword

Groundwater contamination was not perceived to be a major problem until the early 1980s when recognition was triggered by the common finding of chlorinated solvents in public water-supply wells and monitoring wells at industrial and military sites in the United States and West Germany. Within a decade or so, similar findings came from all industrialized countries where studies were undertaken.

Occurrence of non-aqueous phase liquid (NAPL) groundwater contamination was not new; chemicals such as trichloroethylene, methylene chloride, and chloroform had been entering aquifers from leaks, spills, and disposals for decades, and their contamination of groundwater was not suspected even though the solvents were used abundantly at hundreds of thousands of locations world-wide. Maximum acceptable concentrations in drinking water had not been specified by regulators for any of these chemicals for decades and their presence was not apparent by either taste or odor.

Groundwater sampling for solvents did not begin until the late 1970s as overall awareness of organic chemicals in the environment grew. Although awareness of these chemicals in groundwater arose in the early 1980s, there was delay in recognizing that:

1. these oil-like liquids dissolved sparingly in water (i.e., they are immiscible liquids),
2. they easily entered aquifers where they moved rapidly, and
3. their high density relative to water made them common as contaminants deep in aquifers relative to gasoline and other petroleum products that are generally lighter than water.

This book describes the physics of both denser-than-water and lighter-than-water immiscible liquids in the subsurface. The basis of this book is knowledge about the fundamentals of fluid mechanics, laboratory experiments, field experiments, and investigations of contaminated sites. Knowledge from these sources is essential for understanding how and why petroleum products behave much differently than the denser-than-water immiscible liquids and for understanding why it is so difficult to remediate subsurface contamination by dense immiscible liquids.

The authors of this book have published numerous papers, book chapters, and monographs on the topic based on their laboratory, field, theoretical, and mathematical work. They are experienced in teaching the subject matter and providing consulting advice. Drs. Mumford and Kueper are professors of civil engineering at Queen's University in Canada and Dr. Lenhard is a US government researcher.

John Cherry, The Groundwater Project Leader  
Guelph, Ontario, Canada, March 2024

## Preface

This book focuses on the behavior of non-aqueous phase liquids (NAPLs) in porous media as a subset of the more general topic of multiphase flow. Many NAPLs are manufactured organic chemicals; their release to the subsurface has resulted in much of the known groundwater contamination in industrialized nations. These chemicals include what have become known as LNAPLs (light non-aqueous phase liquids)—such as gasoline, diesel fuel, heating oil, and jet fuel—and DNAPLs (dense non-aqueous phase liquids), which include chlorinated solvents used as cleaning and degreasing chemicals in many types of manufacturing industries as well as creosote, coal tar, and polychlorinated biphenyls (PCBs).

The importance of LNAPLs was recognized in the 1930s by the petroleum industry. By the 1960s, there were impressive monographs on their flow and distribution in the subsurface based on rigorous laboratory and theoretical research, one of which was *Groundwater Pollution in Porous Media by Fluids Immiscible with Water* by Dr. Frederick Schwillie (1981). Schwillie went on to become the first to recognize the importance of chlorinated solvent DNAPLs in groundwater and published a landmark monograph in 1984 based on research conducted in the laboratory that he directed in Germany. Schwillie's monograph was in German and James Pankow translated it to English as *Dense Chlorinated Solvents in Porous and Fractured Media* [↗](#) in 1988. This published work was impressive in its attention to photographs from pioneering laboratory experiments, which continue to inspire people working in this area, including for the visual demonstrations presented in this book.

Building on the work of Schwillie, a team of researchers associated with the University Consortium for Chlorinated Solvents Research conducted theoretical research as well as laboratory and field experiments that resulted in the publication of *Dense Chlorinated Solvents and Other DNAPLs in Groundwater* (1996) edited by James Pankow and John Cherry. This book is available on the [Groundwater Project website](#) [↗](#).

Work by Art Corey, including his *Mechanics of Immiscible Fluids in Porous Media* [↗](#) (first published in 1986 and republished in 1994) was also an important early reference on this subject. Corey provided a fundamental understanding of capillary pressure-saturation-relative permeability relationships in porous media.

In the spirit of those early works, this book aims to synthesize and summarize information concerning the fundamental properties and processes that control how LNAPLs and DNAPLs migrate in the subsurface. This includes conceptual diagrams to help readers appreciate the complexities associated with multiphase flow in porous media, where subtle differences in subsurface and fluid properties often control migration and result in substantial lateral spreading rather than vertical flow. Building on this conceptual understanding, the content progresses from an introduction of fluid saturation, interfacial tension, and wettability to a fundamental explanation of capillary pressure and relative

permeability. These are key concepts needed to understand NAPL migration, interpret field observations, and develop numerical models.

This book concludes with a discussion of more detailed concepts specific to LNAPL and DNAPL and presents a series of images from controlled releases in the laboratory to highlight—in a detailed and visual way—important aspects of NAPL flow and distribution. We have chosen to present conceptual figures together with photographs from the field and laboratory throughout this book to help readers develop an intuitive understanding of these complex, and often invisible, phenomena. As such, this book is intended to be an introductory book suitable for upper year undergraduate students and first-time graduate students, as well as practitioners looking to understand fundamental processes. We hope that this introduction leads you to find NAPL flow, with its pore-scale complexities and macroscale implications, to be the endlessly fascinating topic that has captivated our curiosity for decades.

## Acknowledgments

We deeply appreciate the thorough and useful reviews of and contributions to this book by the following individuals:

- ❖ Richard E. Jackson, Geofirma Engineering Ltd. and adjunct professor, Earth and Environmental Sciences, University of Waterloo, Waterloo, Canada;
- ❖ David McWhorter, emeritus professor, Civil and Environmental Engineering, Colorado State University, USA;
- ❖ Tom Sale, emeritus professor, Civil and Environmental Engineering, Colorado State University, USA;
- ❖ Neil Thomson, professor, Civil and Environmental Engineering, University of Waterloo, Waterloo, Canada;
- ❖ Everton de Oliveira, president of Hidroplan and director-president of the Instituto Água Sustentável (Sustainable Water Institute), Brazil;
- ❖ Ariel Nunez Garcia, postdoctoral fellow, Queen's University, Kingston, Canada;
- ❖ Brian Moore, undergraduate researcher, Queen's University, Kingston, Canada;
- ❖ Matthys Dippenaar, associate professor, Engineering Geology and Hydrogeology, University of Pretoria, South Africa; and
- ❖ Connie Bryson, editor, The Groundwater Project, Canada.
- ❖ John Cherry, Morwick-G360 Institute, University of Guelph, Guelph, Ontario, Canada;
- ❖ Guy Patrick, Senior Contaminant Hydrogeologist, Patrick Consulting, Victoria, British Columbia, Canada.

We are grateful for Amanda Sills and the Formatting Team of the Groundwater Project for their oversight and copyediting of this book. We thank Eileen Poeter (emeritus professor, Colorado School of Mines, Golden, Colorado, USA) for reviewing, editing, and producing this book.

The sources of materials presented in figures and tables are acknowledged in the captions; however, figures and tables without a citation to source are original to this book.

# 1 Introduction

## 1.1 Multiple Fluids in Porous Media

Groundwater scientists and engineers are often concerned with the flow of a single fluid—water—through porous or fractured subsurface material; hydrogeology is primarily concerned with understanding this flow. However, in many situations, more than one fluid is present in the subsurface. For example, in soils near the ground surface and above the water table, air and water coexist in the pore space between grains.

The flow of water and air is important for infiltration and irrigation, and the amount of water in the pore space plays an important role in unsaturated soil mechanics. In oil and gas reservoirs, the flow of oil, gas, and water controls the recovery of natural resources. In each of these examples, the presence of an additional fluid phase (or phases) affects the amount of water in the pore space and the pathways available for that water to flow through the pore network. An understanding of other fluids in the pore space is not only important because of their effect on groundwater flow but also because groundwater is part of an interconnected hydrological system that involves water as well as dissolved and suspended material in that water. Some compounds (e.g., chemicals, solutes) can move between pore fluids by mass transfer across fluid–fluid interfaces; an understanding of how other fluids are distributed alongside groundwater in a pore space is critical for understanding that exchange of mass.

This book focuses on a class of fluids referred to as *non-aqueous phase liquids* (NAPLs), whose behavior in vadose and groundwater systems has much in common with fluid behavior in unsaturated soil and in oil and gas reservoirs. Over the last several decades, considerable attention has been paid to NAPLs in soil and groundwater (Schwille, 1981; Mercer & Cohen, 1990; Corey, 1994; Pankow & Cherry, 1996; Kueper et al., 2003; Mayer & Hassanizadeh, 2005; Kueper et al., 2014; Rivett et al., 2014; Essaid et al., 2015). Many NAPLs are anthropogenic industrial liquids that are hazardous to human and ecological health. Consequently, a comprehension of NAPL flow and fate in the subsurface is important for understanding, investigating, and predicting the consequences of historic or improper disposal and accidental releases of NAPLs to subsurface environments.

NAPLs are generally classified according to their density relative to water: as *light non-aqueous phase liquids* (LNAPLs) or *dense non-aqueous phase liquids* (DNAPLs). That difference in density is important and is the first predictor of where a NAPL will be distributed in the subsurface. For example, an LNAPL released at ground surface will flow downward through the vadose zone, and its flow path will be affected by contrasts in both water content and subsurface material properties (Figure 1).

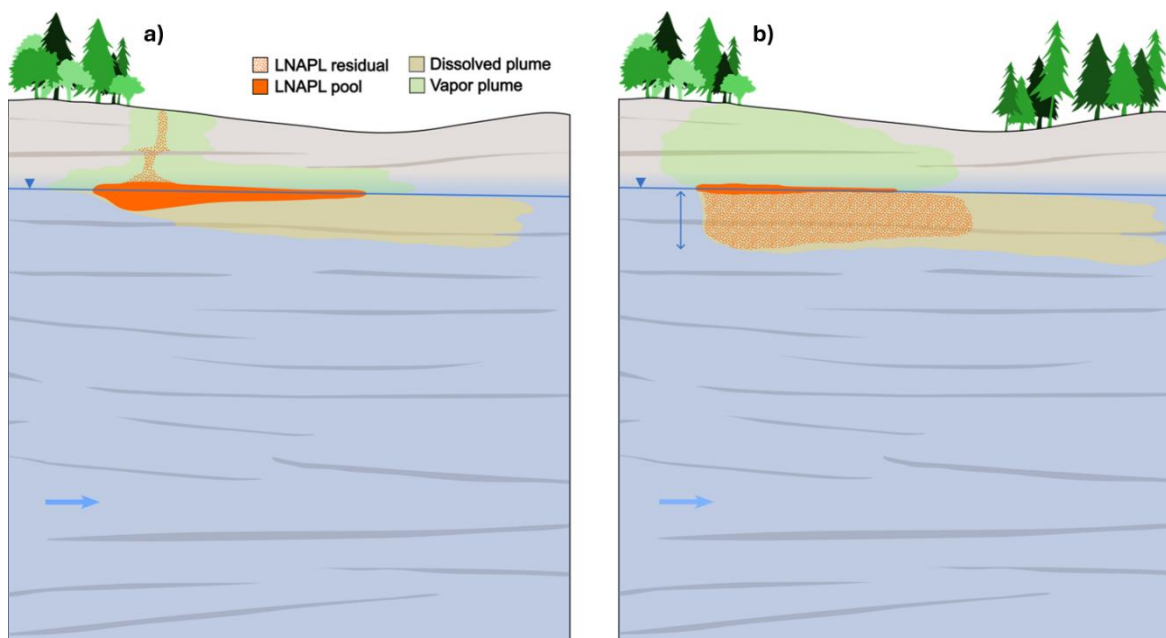


**Figure 1** - Conceptual model of a LNAPL release to a water-table aquifer with groundwater flowing from left to right. a) After LNAPL migration downward through the unsaturated (vadose) zone, leaving residual LNAPL along its path, then accumulating in the vicinity of the capillary fringe and depressing the water-saturated region. b) After LNAPL has been depleted and vertically redistributed (shown by the vertical double-headed arrow) by fluctuation of the water table, creating a smear zone of residual (entrapped) LNAPL below the water table. Vaporization in the unsaturated zone and dissolution in the saturated zone within the pool and smear zone result in the formation of a vapor plume and a dissolved plume, respectively.

Contrasts between layer properties can result in lateral spreading of LNAPL at the boundaries of those layers. If the LNAPL is able to break through or flow around a layer then it can continue to flow downward toward the water table, provided sufficient LNAPL volume is present. Lateral spreading also can occur once the LNAPL reaches the water-saturated capillary fringe with the LNAPL remaining in the vicinity of the water table due to its buoyancy (although not strictly above the water table as discussed in Section 5.3).

In contrast, a DNAPL released at the ground surface will flow downward through the vadose zone but will not be significantly impeded by the water table (subject to entry pressure requirements discussed in Section 5.1; Figure 2). Gravity continues to drive DNAPL deeper into the subsurface, with substantial lateral spreading dictated by geological heterogeneity. In fact, although early conceptual figures often depicted DNAPL as moving downward directly below its release location at or near ground surface, it is much more common for DNAPL to move laterally before moving downward because of the strong influence of capillary barriers (described in Section 5.1). In other words, DNAPL moves sideways to move down. Lateral spreading is relatively unaffected by the water hydraulic gradient.

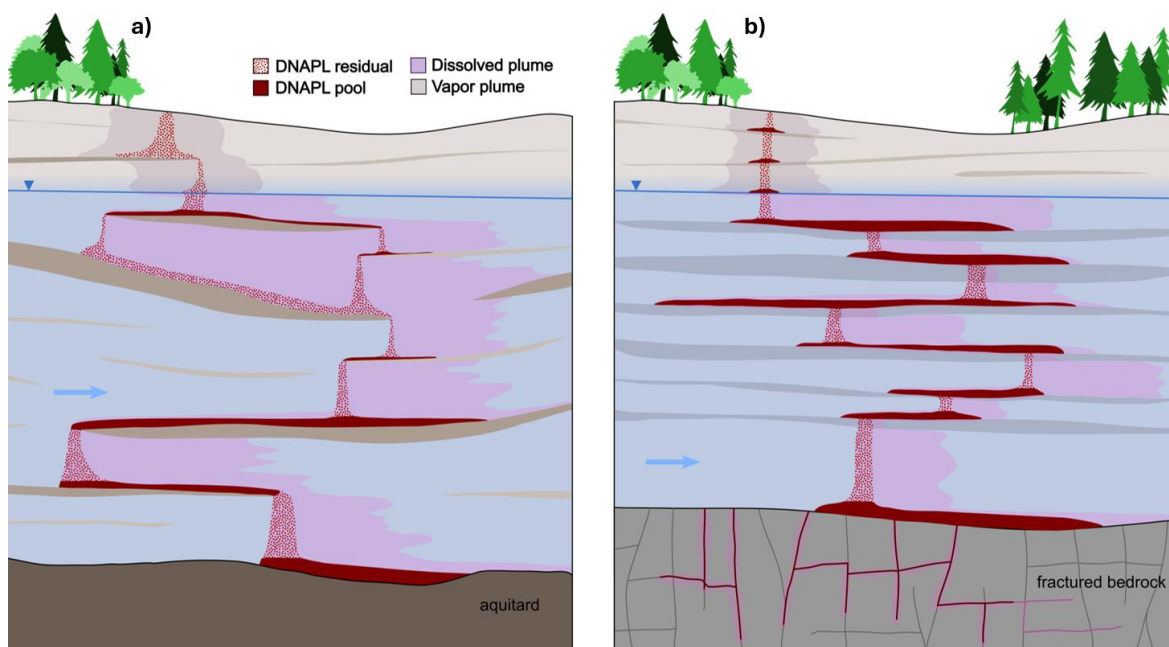


**Figure 2** - Conceptual model of a DNAPL release into a heterogeneous sandy aquifer with groundwater flow from left to right containing a) discontinuous silt and clay layers, and b) continuous layers of finer sand, both of which act as capillary barriers. Downward DNAPL migration in the saturated zone is only possible following bypass or breakthrough of these barriers. DNAPL is present as both pools and residual, with pools present on top of the capillary barriers. DNAPL can also enter fractures in bedrock or clay, if present, and these media do not necessarily provide an impenetrable boundary. Vaporization in the unsaturated zone and dissolution in the saturated zone result in the formation of a vapor plume and a dissolved plume, respectively.

By virtue of their respective densities, LNAPL is likely to be primarily distributed above the water-saturated zone, while DNAPL can be found at substantial depths within the water-saturated zone. NAPLs with densities near but still less than water will behave as LNAPLs but can transform to DNAPLs as the lighter components of the NAPL are depleted (e.g., Roy et al., 2004). Importantly, although they are typically treated as immiscible liquids when assessing their flow in porous media, most NAPLs are not perfectly immiscible because they have finite aqueous solubilities and vapor pressures. Therefore, once released to the subsurface and in contact with water or air, NAPLs dissolve in water and vaporize into air. Generally, NAPLs dissolve in water at low concentrations (sparingly soluble), often creating large and persistent plumes of dissolved organic compounds that can be hazardous even at low ( $\mu\text{g/L}$ ) concentrations. NAPLs partitioning into the air is based primarily on their vapor pressures; there are examples of both volatile and non-volatile NAPLs.

## 1.2 Purpose

The purpose of this book is to introduce the fundamental mechanisms, properties, and mathematical relationships that control and describe the flow of NAPLs in porous media. NAPL flow in porous media is a subset of the more general topic of *multiphase flow* in porous media; much of what is discussed here also applies to air and water in the vadose zone, and to free gas phase in groundwater. In addition, material in this book serves as a

complement to topics related to groundwater contamination, as well as strategies for the investigation and remediation of NAPL-impacted sites. The focus here is on capillary-dominated displacement. Instabilities related to viscous and gravity forces are not addressed (e.g., Toussaint et al., 2012; Ewing & Berkowitz, 1998; Kueper & Frind, 1988).

This book is organized into six sections. Section 2 introduces parameters that are important for understanding, describing, and simulating NAPL flow in porous media. Section 3 explains the concept of capillary pressure, which links pressures in the air (gas), water, and NAPL phases, as well as approaches used to describe capillary pressure at a macroscopic scale. Section 4 describes the related concept of relative permeability, which dictates the resistance to the flow of multiple fluids in a pore space. The emphasis of Sections 3 and 4 is on two-fluid (e.g., NAPL–water) systems.

Section 5 introduces selected concepts specific to LNAPL and DNAPL in the subsurface, including a discussion of three-fluid systems. Finally, Section 6 presents two laboratory demonstrations (along with links to videos) to highlight the key concepts of LNAPL and DNAPL flow that are presented in this book. These six sections are followed by a summary, exercises for the reader to test and develop their knowledge, and additional detail on the mathematics that describe flow in three-fluid (air–NAPL–water) systems.

The material in this book is by no means an exhaustive treatment of NAPLs in the subsurface; readers are encouraged to seek additional information available through The Groundwater Project, as well as studies published in the scientific and engineering literature and guidance documents issued by various government agencies.

### 1.3 Nomenclature

Key terminology used to describe NAPL flow in porous media is defined throughout this book. This includes some terminology that was originally proposed by petroleum engineers for their needs that was later adopted and, in some cases, redefined by hydrogeologists for their requirements. For example, NAPL *pools* are subsurface regions in which the pore space is mostly, but not completely, occupied by NAPL. The NAPL in pools exists in a connected network of pores and is potentially mobile.

Unlike NAPL pools, NAPL *residual* refers to NAPL that is immobile, but it is defined differently depending on the number of fluids present. In a two-fluid (NAPL–water) region, NAPL residual refers to disconnected blobs and ganglia that are surrounded (occluded) by water. However, in a three-fluid (air–NAPL–water) region (e.g., the vadose zone), NAPL residual refers only to NAPL in films, bypassed pores, and pendular rings; water-occluded NAPL is referred to as *entrapped* NAPL. NAPL residual is discussed in more detail in Sections 3.4 and 5.2.

## 1.4 Light Non-Aqueous Phase Liquids (LNAPLs)

LNAPLs include a wide range of organic liquids but in the context of groundwater contamination are most often associated with petroleum hydrocarbons. These include gasoline and diesel fuel, heating oil, jet fuel, kerosene, and feedstock such as crude oil. LNAPLs also include organic solvents such as alkanes and aromatics, including benzene and toluene. Organic solvents can occur as components in fuels and as compounds used in chemical manufacturing. LNAPL releases can be associated with a variety of storage and fluid transfer infrastructure, including above ground and underground storage tanks and pipelines, as well as with fluid handling operations. LNAPL releases can occur at, for example, manufacturing facilities, refineries, terminals, filling stations, airports, and military bases (Rivett et al., 2014). Smaller-scale releases can also be associated with domestic use (e.g., home heating oil) or commercial and industrial facilities.

Examples of LNAPLs are listed in Table 1, along with fluid properties that affect their movement and fate in groundwater systems. These properties include those that affect flow (density, viscosity, interfacial tension) and those that affect the partitioning to water and air (solubility and vapor pressure, respectively). Solubility and vapor pressure are listed only for individual chemicals (components), and not for multicomponent LNAPLs, as those properties are functions of the LNAPL composition.

**Table 1** - Properties of example LNAPLs.

LNAPL	Density (g/cm <sup>3</sup> )	Dynamic viscosity (cP)	Solubility (mg/L)	Vapor pressure (mm Hg)	Interfacial tension (mN/m)	
					NAPL–water	Air–NAPL
<b>Single components<sup>1</sup></b>						
Benzene	0.87	0.60	1,750	95.2	35	28.9
Toluene	0.86	0.55	535	28.1	36.1	28.5
Ethylbenzene	0.86	0.68	152	7.00	35.5	29.3
m-Xylene	0.86	0.81	130	1.00	36.4	29.0
<b>Petroleum fuel mixtures<sup>2</sup></b>						
Petrol (Gasoline)	0.67–0.80	0.62			52	
Avgas	0.71	2.3			37	
Kerosene	0.81	2.3			47–49	
Diesel	0.87	2.7			50	
Bunker C	0.9 <sup>3</sup>	45,030			40	

<sup>1</sup>Mercer & Cohen (1990) at 20–30 °C and air–NAPL interfacial tension at 20 °C

<sup>2</sup>Rivett et al. (2014) at 15 °C, air–NAPL interfacial tension for mixtures not reported

<sup>3</sup>Also reported as a DNAPL, with a density up to 1.1 g/cm<sup>3</sup>

Although releases of a single component can occur, LNAPLs are typically found in groundwater systems as multicomponent liquids. This is particularly true for petroleum fuels. Therefore, LNAPL composition—and specific aspects of LNAPL behavior associated with that composition—is site-specific. Nevertheless, the fate of each individual chemical component is important because the composition of the LNAPL may change over time as those chemicals partition from the LNAPL to the water and/or air.

Once released to the subsurface, LNAPL can threaten environmental quality through a variety of processes. The migration of LNAPL through the subsurface and its subsequent discharge to surface water can affect that surface water by creating oil sheens, which impacts aquatic organisms and potentially compromises drinking water supplies. Organic compounds in LNAPL can partition to surrounding groundwater (dissolve), creating a dissolved plume that can be transported in the direction of groundwater flow (Figure 1) towards drinking water wells or surface water.

The dissolved plumes created by LNAPL dissolution are limited to the shallow saturated zone (i.e., near the water table and connected to the LNAPL source), with deeper vertical movement created only by transverse vertical dispersion or vertical hydraulic gradients, including those created by recharge. Deeper plumes can also be created by the “smearing” of LNAPL due to fluctuations of the water table (Figure 1), such that a larger cross section of LNAPL is available for contact with flowing groundwater (e.g., Dobson et al., 2007). Biogeochemical reactions with the dissolved organic compounds in the plume can further reduce groundwater quality through reduction in dissolved oxygen and changes in metal, nitrogen, and sulfur speciation.

In addition to the formation of a dissolved plume in the saturated zone, volatile organic compounds can partition from the LNAPL or the impacted groundwater into soil gas and move into buildings—which is referred to as *vapor intrusion*—thereby reducing indoor air quality. A detailed description of mass transfer (dissolution and vaporization) and the associated reactive transport processes are outside the scope of this book and are discussed in more detail elsewhere. They are an important consideration at LNAPL-impacted sites, in part because groundwater and soil gas are more mobile than LNAPL (once a release has stopped), resulting in plumes that are larger than the LNAPL source. However, an understanding of plume formation and the subsequent reactive transport pathways starts with an understanding of LNAPL flow and distribution in the subsurface.

## 1.5 Dense Non-Aqueous Phase Liquids (DNAPLs)

Like LNAPLs, DNAPLs include many different chemicals associated with a variety of industries and applications. These include chlorinated solvents such as trichloroethene (TCE) and tetrachloroethene (PCE) that have been used as cleaning and degreasing chemicals. Due to their widespread use and persistence, TCE and PCE are two of the most frequently detected groundwater contaminants in industrialized areas of the world (e.g., Zogorski et al., 2006). DNAPLs also include pesticides and polychlorinated biphenyls (PCBs), a group of liquids used primarily as insulating oils in transformers. DNAPLs also include coal tar and creosote (e.g., Jackson et al., 2006), historic byproducts of coal gasification processes that consist mainly of polycyclic aromatic hydrocarbons (PAHs).

Coal tar is a byproduct associated with former manufactured gas plants (MGPs), and creosote is an industrial liquid used primarily as a wood preservative.

Because of their widespread uses across multiple industries, there are many DNAPL-impacted sites worldwide. Releases at DNAPL-impacted sites can be associated with storage tanks and fluids handling, as well as burn pits and waste lagoons, and can occur at manufacturing facilities, solvent recyclers, dry cleaners, and chemical production facilities (Kueper & Davies, 2009). Examples of chlorinated solvent DNAPLs and selected fluid properties are listed in Table 2.

**Table 2** - Properties of example DNAPLs.

DNAPL	Density (g/cm <sup>3</sup> ) <sup>1</sup>	Dynamic viscosity <sup>1</sup> (cP)	Solubility (mg/L) <sup>1</sup>	Vapor pressure (mm Hg) <sup>1</sup>	Interfacial tension (mN/m) <sup>2</sup>	
					NAPL–water <sup>3</sup>	Air–NAPL
<b>Carbon tetrachloride</b>	1.59	0.97	825	109	45.0	27.0
<b>Trichloroethene</b>	1.46	0.57	1,100	75	34.5	29.5
<b>Tetrachloroethene</b>	1.63	0.9	200	18.9	44.4	32.9
<b>1,2-dichloroethane</b>	1.25	0.84	8,500	82.1	30	32.6
<b>1,1,1-trichloroethane</b>	1.35	0.84	1,300	124.6	45	25.8
<b>cis-1,2-dichloroethene</b>	1.28	0.48	3,500	205	30	24

<sup>1</sup>from Pankow & Cherry (1996) at 25 °C

<sup>2</sup>from Mercer & Cohen (1990) at 20–25 °C

<sup>3</sup>Textbook values of interfacial tension for laboratory-grade NAPLs such as chlorinated solvents are often higher than those found during field investigations, which typically range between 10 and 25 mN/m. DNAPLs encountered at field sites typically have lower interfacial tensions than laboratory-grade DNAPLs because of exposure to impurities during their use and in the subsurface.

Although the use of DNAPL as chemical feedstock can result in the release of single-component liquids, multicomponent DNAPLs are common. Multicomponent DNAPLs can form during chemical manufacturing, through co-disposal at former solvent recycling facilities, and through degreasing operations where DNAPL solvents (e.g., cutting oils and lubricants) are used to remove LNAPLs. An example of a multicomponent DNAPL is provided in Table 3.

**Table 3** - Composition of DNAPL from S-AREA as percent by mass<sup>1</sup> (Cohen & Mercer, 1993).

Compound	S-AREA OW-213F
Chlorobenzene	0.8
Dichlorobenzene	0.6
Trichlorobenzene	11.5
Tetrachlorobenzene	32
Pentachlorobenzene	6.4
Hexachlorobenzene	1.6
Toluene	0.1
Chlorotoluene	0.9
Dichlorotoluene	0.9
Total benzene hexachlorides	0.4
Carbon Tetrachloride	1.0
Trichloroethene	0.4
Tetrachloroethene	13
Hexachloroethane	1.1
Hexachlorobutadiene	4.2
Hexachlorocyclopentadiene	12
Octachlorocyclopentadiene	14
Endosulfan II	0.3
Mirex	0.1
<b>Total</b>	<b>100.5</b>

<sup>1</sup>Total composition > 100 percent reflects the uncertainty in laboratory analysis

Like LNAPLs, DNAPLs may threaten environmental quality through dissolution into groundwater to create a dissolved plume of organic compounds that potentially discharges to surface water or impacts drinking water wells, or through vaporization to soil gas and subsequent vapor intrusion into buildings (Figure 2). The rate of DNAPL dissolution into flowing groundwater is typically very slow given the low aqueous solubilities of most DNAPLs. As a result, a DNAPL source zone (the portion of subsurface that contains DNAPL) present below the water table can remain in place for decades to centuries (Kueper et al., 2014), even if remedial action is taken because remediation does not completely remove the DNAPL.

The potential hazards associated with such long-lived source zones are made worse because components in many DNAPLs, including chlorinated solvents, have an adverse effect on human health at low ( $\mu\text{g/L}$ ) concentrations. For example, a single 208 L (55 gallon) drum of TCE can theoretically contaminate  $6 \times 10^{10}$  L of water at a concentration of  $5 \mu\text{g/L}$ , a common regulatory standard. On average throughout the world, each person uses about 250 L of domestic water per day so one spilled drum of TCE could theoretically contaminate a day's worth of water used by 3 percent of the world population. In addition, DNAPL source zones often extend much deeper in the subsurface than LNAPL source zones, leading to the formation of much deeper plumes and potential impacts on deeper aquifers.

The complexity of DNAPL source zones produces complex plumes due to variable dissolution rates from residual and pooled sub-regions (relatively low and high NAPL

saturations) as well as multiple transport processes, including diffusion, mechanical dispersion, sorption, and reaction. Importantly, even if DNAPL is prevented from entering a low-permeability layer that acts as a capillary barrier, dissolved compounds in the plume can diffuse into that layer, later acting as a source of contamination (Section 1.6).

Dissolution from DNAPL source zones is also often found to be rate-limited (i.e., resulting in dissolved concentrations that are less than the solubility limit), which depends on the DNAPL distribution (source architecture) and must be accounted for when interpreting dissolved concentrations measured in groundwater samples collected at DNAPL-impacted sites. As discussed for LNAPL, one needs to understand the source in order to understand the plume.

Waste management practices at industrial facilities have changed dramatically over the years. For example, it was common from the 1940s through to the early 1980s to dispose of LNAPLs and DNAPLs in unlined ponds, unlined burn pits, unlined landfills, and directly to the ground surface. Waste management practices in the USA improved in the mid to late 1980s with the implementation of modern environmental regulations such as the passage in 1980 of the Comprehensive Environmental Response, Compensation and Liability Act (CERCLA), also known as Superfund. To further put things into historical perspective, Schuille (1981) was the first English language publication to present the concept of heavier-than-water solvents sinking below the water table, and the term non-aqueous phase liquid (NAPL) was first coined in 1981 during studies of a hazardous waste landfill in Niagara Falls, New York, USA (Pankow & Cherry, 1996).

Commercial laboratories offering services for the analysis of organic compounds in groundwater samples were not readily available from the 1940s through to the 1970s, a time period during which large volumes of organic NAPLs were released to the subsurface throughout industrialized countries worldwide. It was not until 1979 that EPA published a series of analytical methods that employed gas chromatography/mass spectrometry (GC/MS) for determining organic compounds in wastewater (not groundwater) (Pankow & Cherry, 1996). Analytical methods for determining concentrations of organic chemicals in groundwater samples followed. By the 1990s, commercial laboratories providing analyses of organic compounds in groundwater samples were readily accessible and available to practitioners.

## 1.6 Life Cycle of a NAPL Source Zone

A NAPL source zone is defined as the overall volume of the subsurface that contains NAPL. Both LNAPL and DNAPL source zones age with time; the discussion here focuses on a DNAPL source zone, with similar concepts applicable to an LNAPL source zone.

DNAPL distribution (architecture) in the subsurface is dependent on the elapsed time since the original DNAPL release occurred. As discussed by Kueper and others (2014), the DNAPL source zone goes through five life cycle stages beginning with an initial release

of DNAPL to the subsurface and culminating in complete DNAPL depletion, with contamination persisting due to the diffusion of organic compounds out of lower-permeability zones (often referred to as *back-diffusion*) and desorption of organic compounds from solids. The stages are described here and illustrated in Figure 3 and its associated animation.

- *Stage 1 (Source On - Figure 3a)* refers to the period of time during which DNAPL releases to the subsurface are occurring. DNAPL releases can be short in duration, such as the sudden failure of a storage vessel, or longer in duration, such as slow leaks from pipes, sumps, and disposal ponds operating for years or decades.
- *Stage 2 (DNAPL Redistribution - Figure 3b)* corresponds to the period of time during which releases to the subsurface are no longer occurring, but the DNAPL is still migrating in the subsurface until it reaches an equilibrium distribution. The duration of Stage 2 depends on several factors including the volume of DNAPL released, the DNAPL viscosity, the permeability of the subsurface, the geologic structure, and the DNAPL-water interfacial tension.
- During *Stage 3 (Dissolution, Aging, and Diffusion - Figure 3c)*, DNAPL is slowly depleted as a result of vaporization into air and dissolution into groundwater. For a multicomponent DNAPL, the aqueous solubility of each component is a function of its *mole fraction* (i.e., the number of moles of that component relative to the total number of moles) in the DNAPL. As the DNAPL dissolves into groundwater, the components with higher effective solubility are depleted faster than those with lower effective solubility. Over time, the DNAPL is therefore enriched in components with lower effective solubility and the dissolved phase plume becomes depleted in the components having initially higher effective solubility. The practical implication of this is that groundwater practitioners should expect to see changes in the plume chemistry over time. Similar aging effects will occur in the unsaturated zone as the DNAPL components with higher effective vapor pressure are depleted faster than those with lower effective vapor pressure. Another important aspect of Stage 3 (as well as Stages 1 and 2) is that dissolved phase contaminants are diffusing into lower-permeability media such as silts and clays where little groundwater flow occurs.
- *Stage 4 (DNAPL Depletion - Figure 3d)* refers to the point in time at which all DNAPL has been depleted as a result of vaporization and dissolution. The amount of time required to reach Stage 4 is dependent on several factors including the volume of DNAPL released, the aqueous and vapor phase solubility of the DNAPL, and the groundwater velocity.

- During Stage 5 (Back Diffusion and Desorption - Figure 3e), dissolved phase plumes are being sustained by back-diffusion out of lower-permeability media into higher-permeability media, and desorption.

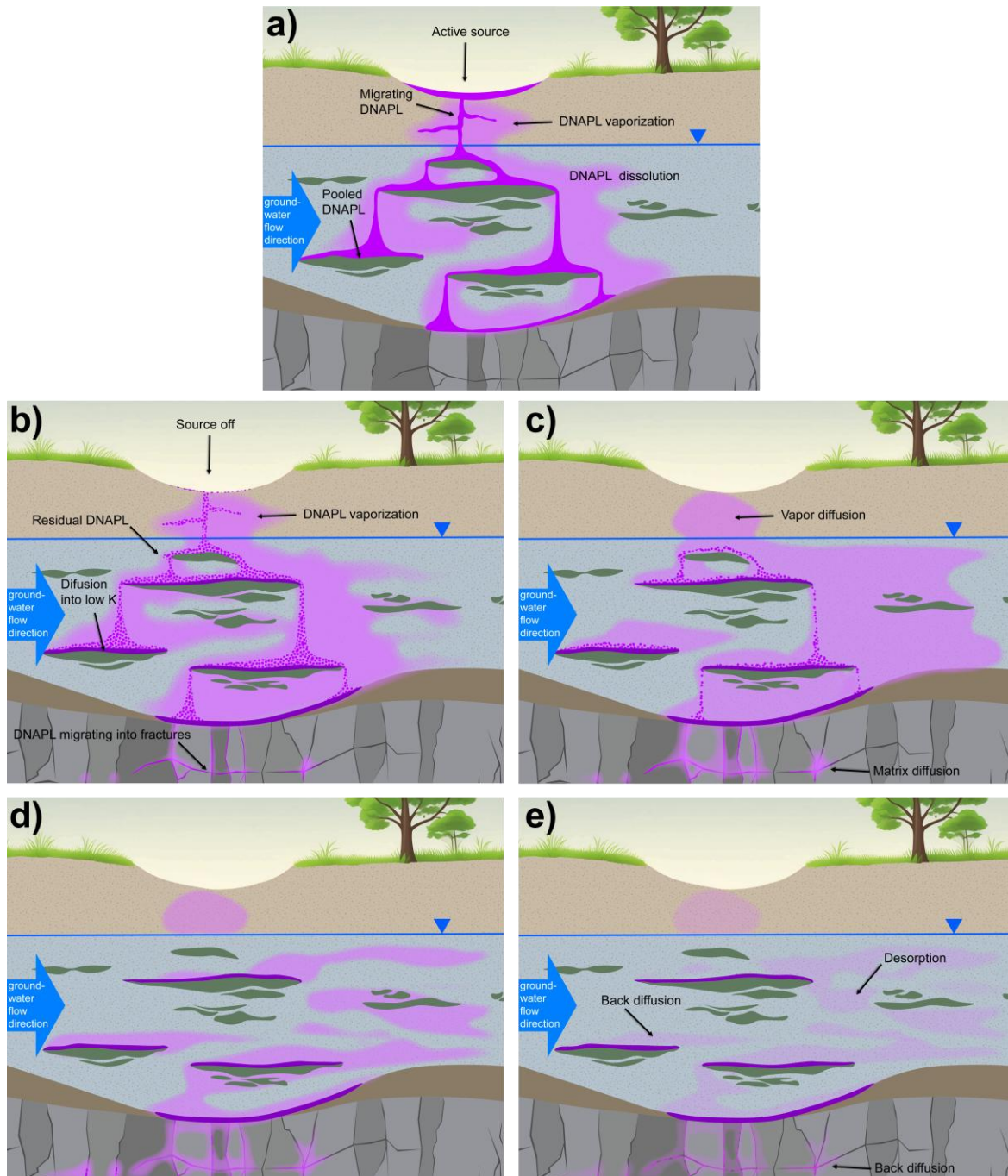


**Figure 3** - Life cycle stages of a DNAPL source zone. a) Stage 1 DNAPL is being released to the subsurface where it migrates in response to geologic heterogeneity. b) Stage 2 DNAPL no longer enters the subsurface but redistributes within the subsurface until it reaches an equilibrium condition. c) Stage 3 DNAPL slowly depletes due to vaporization and dissolution, while dissolved DNAPL diffuses into lower permeability media. d) Stage 4 DNAPL has been depleted, only dissolved and sorbed contaminants remain. e) Stage 5 Dissolved contaminant plumes are sustained by back diffusion from lower permeability media and desorption (after Kueper et al., 2014). [The stages are brought to life by this video](#).

The amount of time required to progress through all five life cycle stages depends on a number of factors including, but not limited to, the following:

1. volume of DNAPL released,
2. vapor pressure and solubility of the DNAPL,
3. groundwater velocity, and
4. proportion of low permeability diffusive sinks.

This book focuses on processes relevant to early stages of the DNAPL source zone life cycle (Stages 1 and 2) during which migration and entrapment processes dominate. These early stages determine the source zone architecture that is available for Stage 3. Many of the NAPL sites under investigation today are in Stage 3; Stages 3 through 5 are discussed further in Kueper et al. (2014) and Sale et al. (2008, 2018).

## 1.7 Relevant Exercises

The following Exercises give the reader practice working with the material presented in Section 1 *Introduction*:

[Exercise 1](#) ↴ prompts the reader to think about hazardous liquids in their home.

[Exercise 2](#) ↴ examines sites associated with DNAPL release.

[Exercise 3](#) ↴ looks at multicomponent NAPLs.

[Exercise 4](#) ↴ asks the reader to use the information presented in Table 1 and Table 2 to calculate the minimum volume of water required to dissolve an organic solvent and a chlorinated solvent.

## 2 Parameters Important to NAPL Flow

### 2.1 Overview

Many of the parameters that are used to describe water flow (single-phase flow) in porous media (e.g., Woessner & Poeter, 2020) are equally important to multiphase flow. These include fluid properties (e.g., density and viscosity) and porous media properties (e.g., porosity, intrinsic permeability, and the degree of heterogeneity and anisotropy). Many of these are defined over a representative elementary volume (REV), which includes many grains and pores.

Although these parameters are important for the description of NAPL flow in porous media, they are not sufficient. Additional parameters are required to describe the simultaneous presence of multiple fluids in the pore space, and the interfaces created by those multiple fluids. These include both fluid–solid interfaces (water–solid and, potentially, NAPL–solid) and fluid–fluid interfaces (NAPL–water, air–NAPL and air–water). Throughout this book the gas phase is referred to as air because that is the most relevant gas under most conditions at NAPL-impacted sites—although the concepts and equations discussed can be readily applied to other gases. These properties are defined at a microscopic (pore, interface) scale in this section. Sections 3 and 4 discuss how the properties are incorporated into macroscopic-scale flow.

### 2.2 Quantification of Fluid Content

Porosity is the ratio of the volume of pore space to the total volume of a sample of a porous medium (Woessner & Poeter, 2020). Similarly, we can describe the volume occupancy of water, NAPL, and air in a porous medium as shown in Equations (1),(2), and (3).

$$\theta_w = \frac{V_w}{V_T} \quad (1)$$

$$\theta_n = \frac{V_n}{V_T} \quad (2)$$

$$\theta_a = \frac{V_a}{V_T} \quad (3)$$

where:

$\theta_w$  = volumetric water content (dimensionless)

$\theta_n$  = volumetric NAPL content (dimensionless)

$\theta_a$  = volumetric air content (dimensionless)

$V_w$  = volume of water ( $L^3$ )

$V_n$  = volume of NAPL ( $L^3$ )

$$\begin{aligned} V_a &= \text{volume of air (L}^3\text{)} \\ V_T &= \text{total volume of pore space (L}^3\text{)} \end{aligned}$$

$\theta_w$ ,  $\theta_n$ , and  $\theta_a$  are also referred to as the water-, NAPL-, and air-filled porosities, respectively.

Given that the sum of the water, NAPL, and air volumes is equal to the total pore (void) volume ( $\sum_{i=w,n,a} V_i = V_v$ ), it follows that the sum of the water-, NAPL-, and air-filled porosities is equal to the total porosity ( $\sum_{i=w,n,a} \theta_i = V_v/V_T = \theta_T$ ). Furthermore, for a water-saturated porous medium, with no NAPL or air in the pore space,  $\theta_w = \theta_T$ .

It is also common to express fluid occupancy as a *saturation*, which represents a volumetric fraction of a sample's pore volume rather than of its total sample volume as shown in Equations (4), (5), and (6).

$$S_w = \frac{V_w}{V_v} \quad (4)$$

$$S_n = \frac{V_n}{V_v} \quad (5)$$

$$S_a = \frac{V_a}{V_v} \quad (6)$$

where:

$$S_w = \text{water saturation (dimensionless)}$$

$$S_n = \text{NAPL saturation (dimensionless)}$$

$$S_a = \text{air saturation (dimensionless)}$$

This is not to be confused with the concept of saturation as it relates to aqueous solubility, where a saturated solution is a solution containing the maximum solute concentration.

A fluid-filled porosity is equal to the product of that fluid's saturation and the total porosity; the sum of the saturations is equal to unity ( $\sum_{i=w,n,a} S_i = 1$ ). A release of NAPL (either LNAPL or DNAPL) to the subsurface above the water-saturated capillary fringe commonly results in the occupation of the pore space by a combination of water, NAPL, and air (i.e., water, NAPL, and air saturations are all greater than zero). Even in the vicinity of the capillary fringe and the water table, LNAPL and air can be entrapped as a result of water table fluctuations. Nevertheless, this section will focus on two-fluid systems that contain water and NAPL, with a discussion of three-fluid systems presented in Section 5.2.

As discussed further in Section 3, fluids exist in several forms and locations in the subsurface. For example, NAPL can exist as a continuous phase throughout a portion of the pore space, or it can exist as disconnected blobs (*ganglia*). This has significant implications for NAPL mobility. The NAPL and water are also not distributed uniformly throughout the pore space, with NAPL preferentially occupying the larger pores.

The physicochemical properties of the fluids and solids control which fluids contact solid surfaces and which fluids contact other fluid surfaces (further explained in Section 2.4). For most NAPLs, water is assumed to be the wetting fluid and will contact the solid surfaces and occupy the smaller pore spaces when either air or NAPL is present in two-fluid systems. However, in some two-fluid systems (e.g., portions of petroleum reservoirs), NAPL will be the wetting fluid and occupy the smaller pore spaces in preference to water or brine—for example, for crude oil (e.g., Tiab & Donaldson, 1996) as well as some NAPLs recovered from field sites (e.g., Dwarakanath et al., 2002). Examples of residual and pooled NAPL are shown in Figure 4.

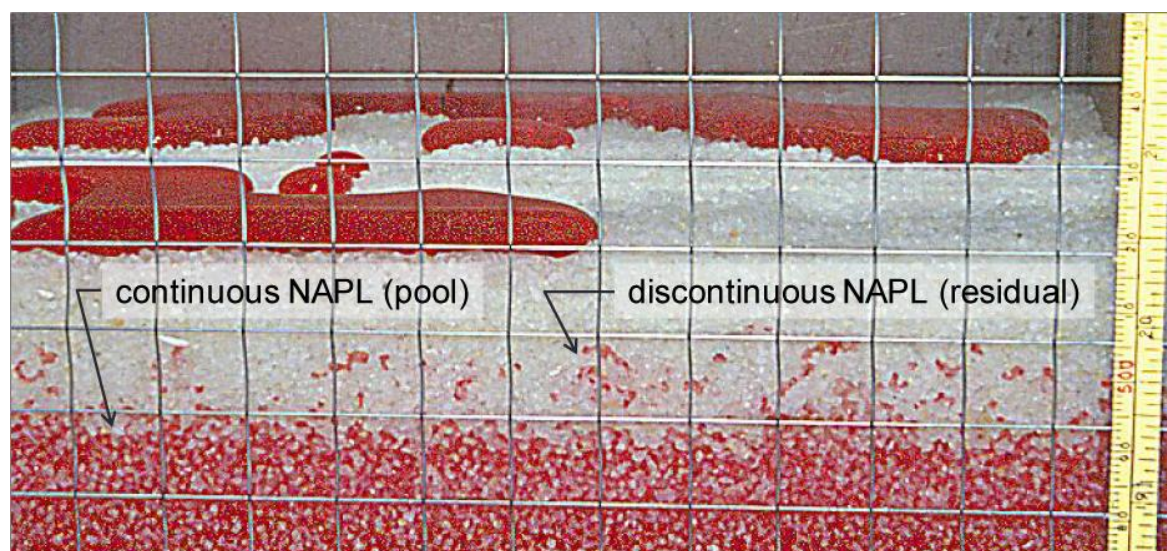


**Figure 4** - Photo of a water-saturated laboratory sand box experiment (Kueper, 1996) showing red-dyed tetrachloroethene (PCE) DNAPL in silica sand. The accumulations of DNAPL on top of the silica sand cannot penetrate because the capillary pressure at the base of the accumulations does not exceed the entry pressure of the silica sand, as described in Section 3.1.

The visual assessment of NAPL saturations in field samples can be difficult. Some NAPLs are colorless and are not easily differentiated from water. In addition, low NAPL saturations (less than 10 percent of pore space) are difficult to detect visually but can still be an important source of groundwater contamination. For this reason, a variety of NAPL presence and saturation indicators, both direct and indirect, are typically employed in field investigations (Kueper & Davies, 2009).

Figure 5 presents a variety of photographs of DNAPLs encountered in the subsurface. Figure 5a shows dark brown DNAPL present in a sand layer situated between adjacent layers of clay. The core was obtained at a chemical manufacturing facility. The DNAPL is present at sufficient saturation such that it can freely flow out of the sand. Figure 5b shows pink-colored DNAPL present in fine- to medium-grained sand lenses (Kueper et al., 1993) and the DNAPL is present at insufficient saturation to freely flow out of the sand lenses. Figure 5c shows red-colored DNAPL present in medium-grained sand (Kueper et al., 1993) and the DNAPL is present at sufficient saturation to freely flow out of the sand.

The saturation at which DNAPL is mobile depends on the pore structure and saturation history and is typically greater than 30 percent.



**Figure 5** - Photographs of DNAPL encountered in the subsurface showing a) and c) DNAPL at sufficient saturation to flow out of the sand and (b) DNAPL at insufficient saturation to flow out of the sand. Pink- and red-colored DNAPL is the result of dye added as part of field experiments (photographs by B. Kueper).

## 2.3 Interfacial Tension

Molecules on either side of a fluid–fluid interface experience an imbalance of forces because of different NAPL-to-NAPL and water-to-water (cohesive) and NAPL-to-water, air-to-NAPL, and air-to-water (adhesive) forces. For example, while the water molecules in the bulk phase in Figure 6 experience no net force, water molecules at the NAPL–water interface experience a net force away from the interface toward the water molecules in the bulk phase. The water molecules at the interface have less binding energy than those in the bulk phase, and this missing energy is associated with a free surface energy (Adamson, 1990). Because energy is required to separate a fluid, binding energy is treated as negative and free surface energy (missing binding energy) as positive. This free surface energy represents the energy that must be put into a system to create new interfacial area and can be expressed as an energy per unit area (e.g.,  $\text{J}/\text{m}^2$ ) or a force per unit length (e.g.,  $\text{N}/\text{m}$ ). Commonly, this is called *interfacial tension* for an interface between any two fluids. *Surface tension* is a more specific term that is commonly used for an interface between a liquid and air. In the context of NAPL flow in porous media, interfacial tension is often used to describe the NAPL–water interfacial tension, while surface tension is used to describe the air–NAPL or air–water interfacial tension.

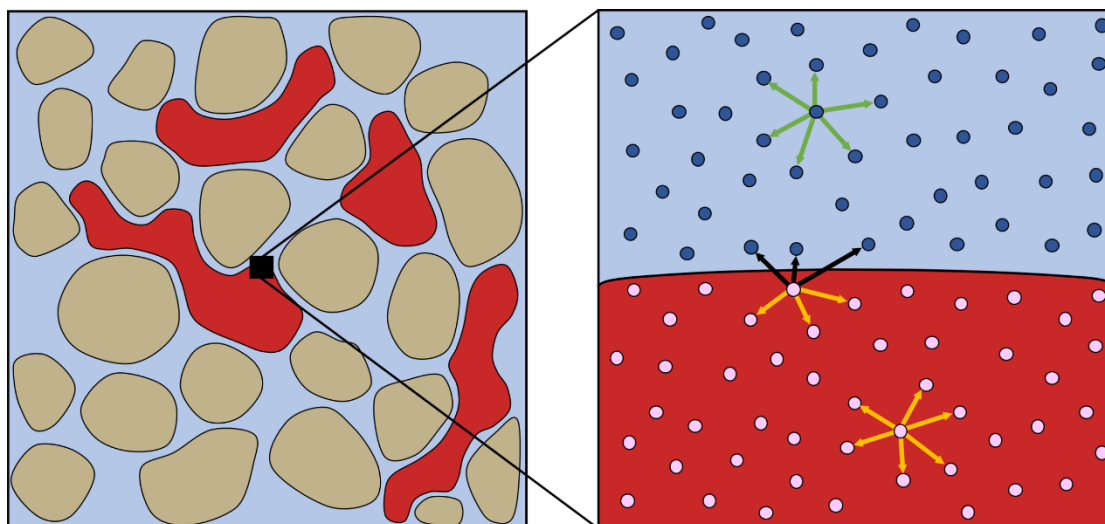


**Figure 6** - Conceptual illustration of intermolecular forces in the bulk phases of fluid 1 (blue) and fluid 2 (red) and at the fluid–fluid interface, where forces between fluid 1 molecules (green arrows) and between fluid 2 molecules (yellow arrows) are different than those between fluid 1 and fluid 2 molecules (black arrows).

Conceptualizations of interfacial tension based on energy per unit area or force per unit length (Adamson, 1990) are both useful. Thinking about a discrepancy of intermolecular forces leading to differences in binding energy is helpful to understand why various fluid pairs have different interfacial tensions, and why those tensions might change. For example, it is expected that increasingly similar forces between molecules on either side of an interface leads to a lower interfacial tension. On the other hand, forces acting tangential to an interface are helpful in establishing conceptual models linking pressure and gravity. This is used in Section 3.

The interfacial tension of NAPLs encountered at field sites is often less than those listed in Table 1 and Table 2. Mixtures of components, the possible presence of surfactants, and impurities imparted to the NAPL during its use and subsequent migration through the subsurface alter the intermolecular forces, with a corresponding lowering of interfacial tension. As a result, while theoretical values of interfacial tension may be useful for screening-level calculations, site-specific measurements are important for more detailed evaluations. A variety of techniques are available to measure interfacial tension including use of ring, plate, and drop-shape tensiometers; a variety of commercial laboratories perform this service. While textbook values of interfacial tension for laboratory grade NAPLs such as chlorinated solvents may be in excess of 40 mN/m, site-specific values typically range between 10 and 25 mN/m.

## 2.4 Wettability and Contact Angle

Wettability is the tendency of one fluid to spread over a solid surface in the presence of another fluid. Like interfacial tension, it is controlled by the forces between molecules in each phase and between phases. The wettability depends on both the solid and the two fluids. In the case of NAPL and water in porous media, this creates three interfaces (water–

solid, NAPL–solid and NAPL–water) and a one-dimensional contact line where the NAPL–water interface meets the solid surface.

Wettability can be expressed and quantified using the magnitude of the *contact angle*, which can be measured between the NAPL–water interface and the solid surface (Figure 7), although alternate wettability indices from the petroleum industry are also used (e.g., Dwarakanath et al., 2002). If the contact angle measured through a fluid is less than 90°, that fluid is referred to as the *wetting fluid*. Conversely, if the contact angle measured through a fluid is greater than 90 degrees, that fluid is referred to as the *nonwetting fluid*. The fluid through which the contact angle is measured is somewhat arbitrary. Therefore, an understanding of the system being studied and the basis of the measurement is important when reporting or interpreting contact angles. While 90 degrees is a convenient threshold for defining a change from wetting to nonwetting conditions, intermediate wetting conditions are also defined in practical applications. One such definition is for contact angles between approximately 60 degrees and 130 degrees to define *intermediate wetting*, while those less than 60 degrees define *wetting*, and those greater than 130 degrees define *nonwetting* conditions (Morrow, 1976). Furthermore, if the contact angle is 0 degrees through one fluid, that fluid is referred to as being *perfectly wetting*.

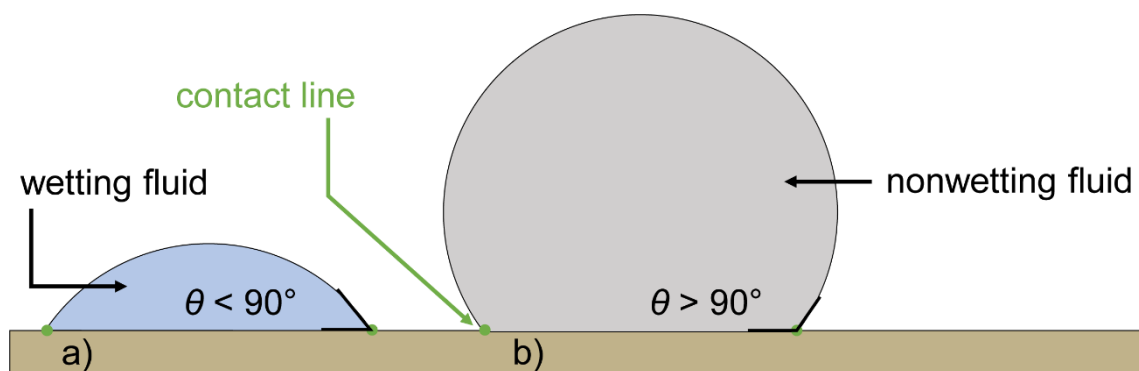


**Figure 7** - Conceptual cross-section of a drop of a) wetting fluid and b) nonwetting fluid on a solid surface.

The determination of wettability and contact angle are important in multiphase flow because the affinity of one fluid over another for the solid surface dictates both the preferential pore occupancy and the magnitude of capillary forces caused by interfacial tension, with subsequent effects on capillary pressure, relative permeability, and capillary trapping discussed in Sections 3 and 4.

Theoretically, the contact angle is defined by a balance of forces acting at the contact line, referred to as Young's equation (Adamson, 1990). Written for a NAPL–water fluid pair, this is shown in Equation (7).

$$\sigma_{sn} - \sigma_{sw} = \sigma_{nw} \cos \theta \quad (7)$$

where:

- $\sigma_{sn}$  = solid–NAPL interfacial tension ( $\text{MT}^{-2}$ ) typically in mN/m  
 $\sigma_{sw}$  = solid–water interfacial tension ( $\text{MT}^{-2}$ )  
 $\sigma_{nw}$  = NAPL–water interfacial tension ( $\text{MT}^{-2}$ )  
 $\theta$  = contact angle (*dimensionless*)

Although conceptually useful, Equation (7) is difficult to apply because solid–fluid interfacial tensions are not known. Instead, the contact angle is treated as an empirical parameter, typically measured by imaging a drop of liquid placed on a solid surface (*sessile drop*). In samples from most NAPL-impacted sites, NAPL is considered to be the nonwetting fluid in the presence of water (Figure 8), and the wetting fluid in the presence of air. However, some NAPL-wet and mixed-wet systems have been reported for NAPLs recovered from field sites (e.g., Dwarakanath et al., 2002) and in the petroleum industry they have been found to occur in certain circumstances under near surface conditions (Salathiel, 1973). For example, organic compounds (e.g., asphaltenes) containing hydrophilic and hydrophobic functional groups (Ramirez-Corredores, 2017) may attach to solids or water films on solid surfaces, with the hydrophobic end creating NAPL-wet pores. This condition is commonly called *mixed-wet* in petroleum reservoirs, but it is also possible for this to occur in NAPL-impacted media when these compounds are in the NAPL.

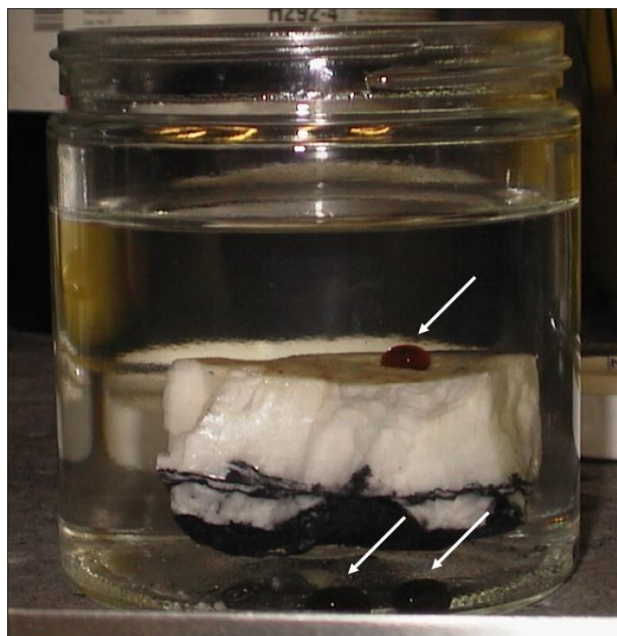


**Figure 8** - Droplet of PCB DNAPL nonwetting in the presence of water on calcite. Note also the two droplets of PCB DNAPL nonwetting in the presence of water on glass on the bottom of the jar. Droplets are indicated by the white arrows (photograph by B. Kueper).

This book makes use of a contact angle in situations where the contact line is assumed to be static and the properties of the solid surface are assumed to be uniform in space. Neither of these is generally true in the field, and the contact angle depends on

contact line direction (*hysteresis*) and velocity (*dynamic effects*) as well as surface roughness and surface chemistry (Dussan, 1979; Adamson, 1990). However, quasi-static assumptions can provide useful estimates of NAPL behavior, particularly in slower-moving systems. The impact of contact line direction on the contact angle is important in situations where NAPL is either invading or being removed from the pore space (decreasing or increasing water saturation) and is discussed further in Section 3 as part of a discussion of hysteresis.

A concept related to wettability is the *spreading coefficient* (Adamson, 1990; Zhou & Blunt, 1997), which is defined by a balance of forces similar to Equation (7) but applied to the contact line created by three fluids (e.g., the meeting of NAPL–water, air–NAPL, and air–water interfaces). The magnitude of the spreading coefficient dictates whether a NAPL will spread continuously over an air–water interface to create a pair of NAPL–water and air–NAPL interfaces, or contract into lenses separated by patches of air–water interface. This spreading behavior has important implications for the retention of NAPL in the vadose zone, where continuous NAPL films are able to flow but discontinuous NAPL is immobile (e.g., Hofstee et al., 1998).

## 3 Capillary Pressure

### 3.1 Capillary Pressure Associated with Single Interfaces

The differences in intermolecular forces at a fluid–fluid interface described in Section 2.3 result in free surface energy associated with that interface, which creates interfacial tension. To minimize the free surface energy, interfacial tension acts to contract the interface to reduce its surface area. The result is curvature of the interface and an increase in the fluid pressure on the inside (*concave* side) of the interface compared to the outside (*convex* side) of the interface, which maintains a balance of forces on the interface.

The difference in pressure between the fluids on the inside and outside of the curved interface is referred to as *capillary pressure*. Capillary pressure across a single interface depends only on the interfacial tension and the curvature of the interface. Therefore, in the absence of contact with a solid surface, the capillary pressure of an air bubble suspended in water is the same as the capillary pressure of a water drop with the same curvature suspended in air, where the inside fluid has the higher pressure in both cases. However, for multiphase flow in porous media, where fluid–fluid interfaces intersect solid surfaces to form contact lines, the direction of interface curvature is controlled by wettability, with the nonwetting fluid being on the inside of the curved interface. Therefore, for a NAPL–water system in which the NAPL is the nonwetting fluid, the capillary pressure is defined by Equation (8).

$$P_c = P_n - P_w \quad (8)$$

where:

$$P_c = \text{capillary pressure (ML}^{-1}\text{T}^{-2}\text{)}$$

$$P_n = \text{NAPL pressure (ML}^{-1}\text{T}^{-2}\text{)}$$

$$P_w = \text{water pressure (ML}^{-1}\text{T}^{-2}\text{)}$$

It is important to note that fluid and capillary pressures can be expressed in a variety of units. For example, pressures can be expressed as force per unit area (e.g., N/m<sup>2</sup>) or as an equivalent height of fluid, which is referred to as *pressure head* (e.g., cm of water). Units of pressure and head are commonly used, and the concepts discussed here are equally applicable to both. The relationship between capillary pressure and curvature is given by the Young-Laplace equation (Dullien, 1992) shown as Equation (9).

$$P_c = \sigma_{nw} \left( \frac{1}{R_1} + \frac{1}{R_2} \right) \quad (9)$$

where:

$$R_1 \text{ and } R_2 = \text{principal radii of curvature (L)}$$

Each principal radii of curvature is defined as the radius of a circle tangent to a curved surface at some point on that surface, oriented along two orthogonal planes normal to the surface at that point. If a mean radius of curvature is defined as shown in Equation (10),

$$R = \frac{1}{2} \left( \frac{1}{R_1} + \frac{1}{R_2} \right) \quad (10)$$

where:

$$R = \text{mean radius of curvature (L)}$$

then Equation (9) can be simplified to Equation (11).

$$P_c = \frac{2\sigma}{R} \quad (11)$$

In the special case of a spherical interface,  $R_1 = R_2 = R$  and  $R$  is the radius of the sphere. By convention,  $R_1$  and  $R_2$  are chosen to be positive such that  $P_c$  is positive. However,  $R_1$  and  $R_2$  have different signs if their centers of curvature lie on opposite sides of the interface. This can produce the interesting result of  $P_c = 0$  for  $R_1 = -R_2$  in Equation (9), which is the case for pendular rings of water at the contact points between grains.  $P_c = 0$  is also true for the case of  $R_1 = R_2 = \infty$  (flat interface, no curvature).

Capillary pressure is often related to pore sizes of a porous medium through analogies to *capillary rise*. For example, consider the rise of water (the wetting fluid) in a narrow tube with a circular cross section (capillary tube) suspended in a large reservoir of water, shown in Figure 9 for water and air.

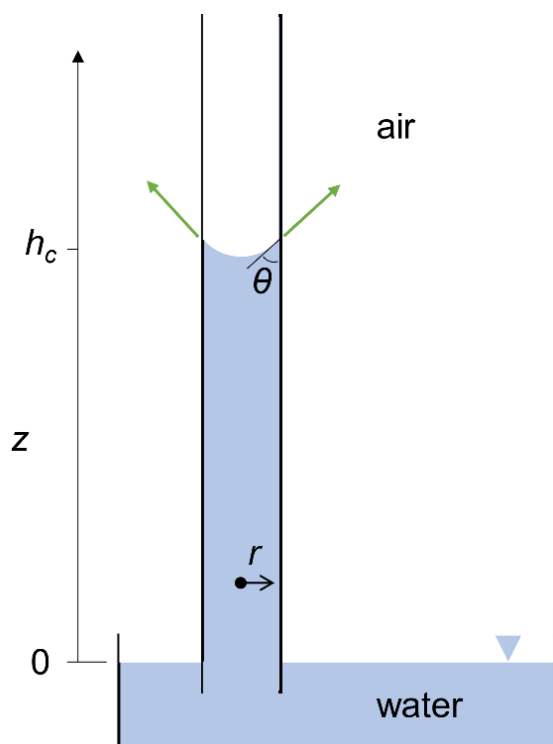


Figure 9 - Conceptual illustration of water rise in a capillary tube.

The air pressure (nonwetting fluid pressure) above both the tube and reservoir is equal to atmospheric pressure. The water rises up into the tube (capillary rise) from the free water surface by wetting the inside tube surface, pulled up by interfacial tension. As a consequence, the water pressure is negative in the capillary tube above the free water surface. A force balance on the column of water in the tube, once it comes to rest, is given by Equation (12).

$$2\pi r\sigma \cos \theta - \pi r^2 h_c \rho_w g = 0 \quad (12)$$

where:

- $r$  = radius of the tube (L)
- $h_c$  = height of water in the tube (L)
- $\rho_w$  = water density ( $ML^{-3}$ )
- $g$  = gravitational acceleration ( $LT^{-2}$ )

The first term is the capillary force: the product of the length of the contact line (in this case, the inner circumference of the tube) and the component of interfacial tension acting parallel to the tube wall. The second term is the weight of the water: the product of the water volume, water density, and gravitational acceleration.

A rearrangement of Equation (12) gives the capillary rise Equation (13)

$$h_c = \frac{2\sigma \cos \theta}{\rho_w g r} \quad (13)$$

For a static water column in the tube, the water pressure immediately below the air-water interface is shown by Equation (14).

$$P_{w(z=h_c)} = P_{w(z=0)} - \rho_w g h_c \quad (14)$$

Taking the water pressure at the reservoir surface to be equal to the air (atmospheric) pressure, together with Equation (13) and the definition of capillary pressure as  $P_c = P_a - P_w$  (analogous to Equation (8) but for air as the nonwetting fluid) gives Equation (15).

$$P_c = \frac{2\sigma \cos \theta}{r} \quad (15)$$

Equation (15) is remarkably similar to Equation (11) but uses the tube radius (analogous to a pore size) in place of the mean radius of curvature of the interface. In the special case of a contact angle of zero,  $R = r$  and Equations (11) and (15) are identical. However, it is important to note that although capillary pressure is fundamentally a function of the interfacial tension and the curvature of the interface, if measures of the porous medium are used to infer capillary pressure, then the wettability of the medium, expressed through the contact angle, must also be considered.

Capillary rise examples can serve as instructive analogies (e.g., to understand the height of the capillary fringe in coarse- versus fine-grained materials), although it is important to understand that many aspects of pore networks are not well represented by collections of straight, smooth-walled capillary tubes.

Similar analogies can be used to understand the concept of *entry pressure*, where a non-zero capillary pressure must be imposed to enable the invasion of NAPL into a water-filled pore. Consider, for example, NAPL above the grains of a water-saturated porous medium (Figure 10). According to Equation (8) and Equation (11) for  $P_n = P_w$ ,  $P_c = 0$  and  $R = \infty$ , and NAPL cannot enter the pore throats (Figure 10a). As  $P_c$  increases, the curvature of the interface increases (the mean radius of curvature decreases), but  $R$  remains greater than  $r/\cos\theta$ , where  $r$  here represents an effective radius of a pore throat (Figure 10b). Only after  $P_c$  is increased, such that  $R = r/\cos\theta$  and Equation (15) is satisfied, can NAPL enter the pore throats, starting with the largest available throats (Figure 10c).

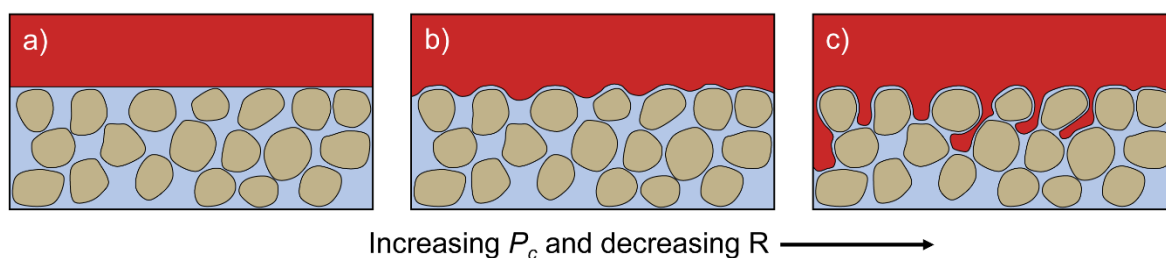


**Figure 10** - Conceptual illustration of NAPL invading a water-saturated porous medium, where the NAPL-water interface is a) not curved, b) slightly curved at slightly increased capillary pressure and c) more curved at higher capillary pressure, that allows NAPL to invade the medium, starting with the largest pore throats.

This analogy is useful because it illustrates that a pressure difference between NAPL and water may not be sufficient for NAPL to invade a water-saturated medium and form a continuous phase through that medium. It also illustrates that the pressure difference (capillary pressure) required for NAPL invasion is proportional to the cosine of the contact angle, and inversely proportional to the representative pore size of the medium.

### 3.2 Macroscopic Capillary Pressure

The previous discussion was focused on a single interface in a single tube, but the presence of multiple fluids in a porous medium creates many interfaces that extend over many pores of different size (Figure 4). It is not practical to know the radius of curvature, or the pore geometry and contact angle, in every pore for field application. However, their measurement in very small samples have been valuable in furthering the knowledge of fundamental processes (e.g., Wildenschild & Sheppard, 2013). Instead, as is done for many other properties important for describing flow in porous media, there is a need to define effective properties at the macroscopic scale. Therefore, a *macroscopic capillary pressure* is defined using Equation (8); however, the water pressure and NAPL pressure are measured (e.g., Dane & Topp, 2002) at the boundaries of a macroscopic sample (Figure 11) and the

capillary pressure is representative of an average interface curvature over many pores and interfaces. It is important to recognize this conceptual leap from the scale of a single interface to the macroscopic scale. As explained in the following text, a macroscopic description results in capillary pressure that depends on more than simply interfacial tension and the curvature of the interface. Some researchers have chosen to represent this macroscopic capillary pressure using different notation (e.g., Korteland et al., 2009). In this book, the conventional notation of  $P_c$ ,  $P_n$ , and  $P_w$  will be used. The scale is to be inferred from the context.

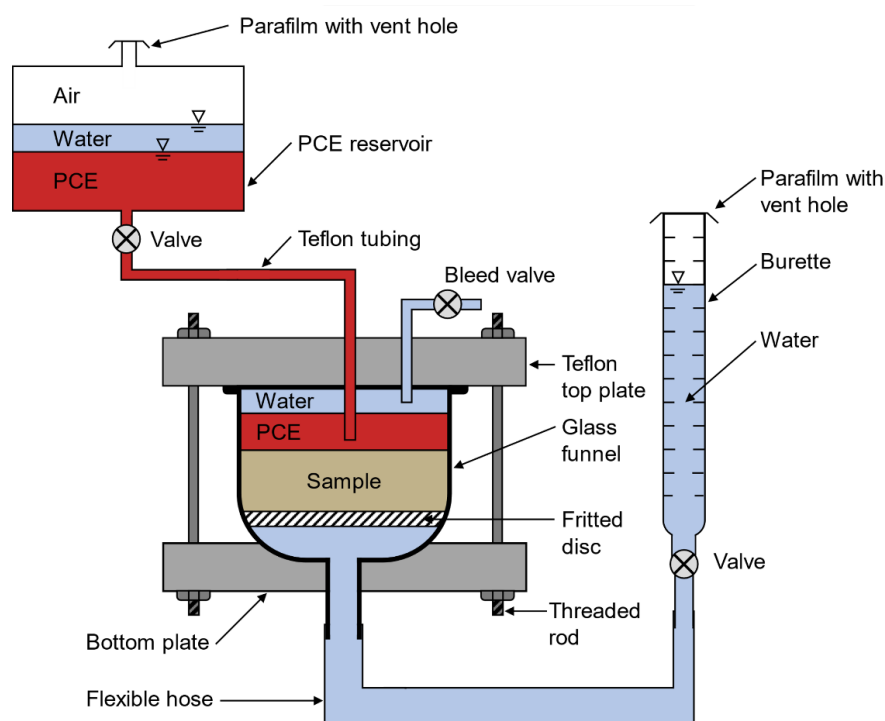


**Figure 11** - Device utilized to measure DNAPL-water capillary pressure curves (adapted from Kueper, 1989). The measured capillary pressure curves are presented and discussed in Kueper and Frind (1991).

The analogy illustrated in Figure 10 suggests that for a difference in NAPL and water pressure applied over many pores of different sizes, different sized pores will be invaded by NAPL at different capillary pressures (different interface curvatures). For the typical condition of NAPL as the nonwetting fluid, this invasion occurs from the largest pores to the smallest pores, with the largest pores being invaded at smaller curvature (larger radius of curvature). Therefore, it is the wettability of the porous medium that dictates preferential pore occupancy, with the wetting fluid generally occupying the smallest pore spaces and the nonwetting fluid occupying the largest pore spaces. The extent of that pore occupation (i.e., definition of small and large) is controlled by the magnitude of the capillary pressure.

It is important to note that this general characterization is also subject to the connectivity of the pore space, with larger pore spaces (pore bodies) surrounded by smaller

pore spaces (pore throats). This preferential occupancy results in a capillary pressure that is a function of fluid saturation at the macroscopic scale, which has significant implications for NAPL flow.

### 3.3 Drainage, Imbibition, and Capillary Pressure-Saturation Curves

Relationships between capillary pressure and saturation in porous media are determined by applying a pressure difference across a porous medium sample. For two-fluid NAPL–water systems, these relationships are typically measured using a sample that is initially water saturated, and the capillary pressure is raised by either lowering the water pressure or increasing the NAPL pressure (Figure 11). After each increment of capillary pressure, and after the system has reestablished mechanical equilibrium (i.e., the fluids are static), the change in water (and NAPL) saturation is calculated by measuring the water displaced from the sample.

Successive capillary pressure increments (both increasing and decreasing) result in the creation of *capillary pressure-saturation curves* (Figure 12). An alternate approach is to change the fluid saturation through controlled injection or withdrawal and measure the equilibrated water and NAPL pressures at the sample boundaries (Su & Brooks, 1980; Lenhard & Brooks, 1985; Lenhard & Parker, 1988).

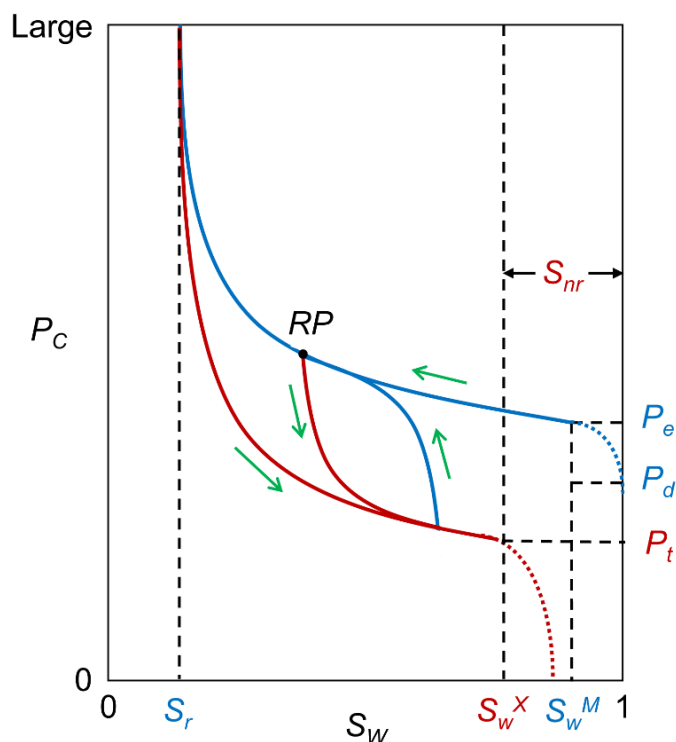


**Figure 12** - Conceptual representation of capillary pressure-saturation curves. Drainage curves are shown in blue and imbibition curves are shown in red. The presence of a macroscopically continuous, nonwetting fluid phase is represented by solid lines, while a macroscopically discontinuous phase is shown by dashed lines (modified after Kueper & Gerhard, 2014). Symbol definitions are listed in Table 4.

**Table 4 - Key capillary pressures and saturations.**

Name	Symbol	Description
Displacement pressure	$P_d$	Capillary pressure required for NAPL to enter the largest pore at the boundary of a porous medium sample during drainage.
Entry pressure	$P_e$	Capillary pressure required to create the first sample-spanning pathway of NAPL that allows NAPL flow during drainage.
Terminal pressure	$P_t$	Capillary pressure at which all NAPL is disconnected across a porous medium sample during imbibition such that NAPL flow ceases.
Reversal point	$RP$	Capillary pressure and saturation at which the direction of change is reversed (drainage to imbibition or imbibition to drainage). Represents the start of a scanning curve.
Emergent saturation	$S_w^M$	Water saturation that corresponds to the entry pressure and NAPL relative permeability greater than zero.
Extinction saturation	$S_w^X$	Water saturation that corresponds to the terminal pressure and a NAPL relative permeability of zero. Note that $S_w^X$ depends on $RP$ , with the maximum value of $S_w^X$ occurring for $RP$ at $S_w = S_r$ .
Residual water saturation	$S_r$	Minimum water saturation achievable on drainage.
Residual NAPL saturation	$S_{nr}$	Trapped NAPL saturation during imbibition. $S_{nr} = 1 - S_w^X$ depends on $RP$ .

The curve beginning at complete water saturation (upper blue curve in Figure 12) is referred to as the primary drainage curve. *Drainage* refers to the displacement of the wetting fluid (water) by the nonwetting fluid (NAPL) resulting in a decrease in the wetting fluid saturation and a corresponding increase in the nonwetting fluid saturation. The opposite process is *imbibition*, the displacement of the nonwetting fluid by the wetting fluid resulting in an increase in the wetting fluid saturation.

The shape of the primary drainage curve has several key characteristics. A small increase in capillary pressure above zero does not cause water to drain from a water-saturated state, except for around the sample boundaries (*boundary effects*), when the capillary pressure increases above zero or when macropores are present with sizes that are not capillaries (large macropores or large fractures). The capillary pressure required for NAPL to displace water and invade the largest water-filled pore is referred to as the *displacement pressure* and is related to the pore-size distribution of a sample. In general, lower-permeability media have higher displacement pressures than higher-permeability media due to their generally smaller pore throats.

A threshold, the *entry pressure*, is reached when the capillary pressure is increased to a value where the NAPL can invade a network of pores that is continuous through the sample so that NAPL will flow through the sample; this corresponds to a NAPL relative permeability greater than zero, as discussed in Section 4.2.

The relationship between capillary pressure and saturation is non-linear. This is controlled by the distribution of pore sizes in the porous medium, with smaller and smaller pores being drained as capillary pressure is increased.

The water saturation does not reach zero at high capillary pressure. As the wetting fluid in most media, water preferentially coats the surface of mineral grains, and exists as films on grain surfaces and around grain contact points (pendular rings), which cannot be displaced by an increase in nonwetting fluid pressure. This results in a *residual water saturation* ( $S_r$ ).

Other important capillary pressures and saturations that characterize capillary pressure-saturation curves are listed in Table 4 and illustrated in Figure 12. The key features of capillary pressure-saturation curves—including displacement pressure, entry pressure, and residual water saturation—have been given different names by different disciplines that use such curves (e.g., hydrogeologists, petroleum engineers, soil scientists, or material scientists; Corey, 1994) and care should be taken when transferring values from one discipline to another.

Importantly, the primary drainage curve is not the only capillary pressure-saturation relationship that occurs in porous media. For example, if drainage continues along the primary drainage curve to the residual water saturation and then capillary pressure is decreased, the result is the displacement of the nonwetting fluid by the wetting fluid along a separate *secondary imbibition curve* (lower red curve in Figure 12). The dependence of capillary pressure on the direction of saturation change is referred to as *hysteresis*. Hysteresis is generally the result of differences in contact angle (receding and advancing) during drainage and imbibition, often referred to as *raindrop effect*, and the resistance of pore throats or pore bodies to NAPL or water invasion, often referred to as *ink-bottle effect* (Hillel, 1980). One result of hysteresis is lower capillary pressures along the secondary imbibition curve compared to along the primary drainage curve at the same water saturations.

An important characteristic of capillary pressure-saturation relationships is that as capillary pressure returns to zero during imbibition, the water saturation will not return to 100 percent. This is due to NAPL entrapment during imbibition, which is discussed further in Section 3.4. The entrapped NAPL is immobile and is commonly referred to as a *residual NAPL saturation* ( $S_{nr}$ ), including in the petroleum industry, but it is also referred to as an *entrapped NAPL saturation* in three-fluid (air–NAPL–water) systems (Parker & Lenhard, 1987; Lenhard et al., 2004). The latter definition avoids potential confusion with residual water saturation, which exists at much higher capillary pressure, and distinguishes between immobile NAPL that is entrapped by water and immobile NAPL that is not entrapped by water (further explained in Section 5.2 for three-fluid systems). In two-fluid (NAPL–water) systems, all immobile NAPL is entrapped by water.

The curves shown in Figure 12 illustrate that hysteresis results in a non-unique capillary pressure-saturation relationship. In fact, an infinite number of capillary pressure-saturation combinations are possible, depending on the history of the capillary pressure changes, including the location of the *reversal point* at which the change in direction occurs.

These pathways are referred to as *scanning curves* (Figure 12) and, assuming an initially water-saturated porous medium, occur between the primary drainage curve and secondary imbibition curve. The scanning curves will never overlap the primary curves, and subsequent scanning curves will not overlap earlier (previous) scanning curves.

As is the case for the names of various capillary pressures and saturations that define key features of the capillary pressure-saturation curves, even the curves themselves are referred to by different names in different disciplines. For example, the bounding (outside) curves have been called primary or main curves, and all other curves have been called scanning curves.

In addition to the features of capillary pressure curves listed in Table 4, the shape of a capillary pressure-saturation curve also provides information concerning the pore-size distribution of the porous medium. As mentioned above, the non-linear relationship between capillary pressure and saturation is controlled by the distribution of pore sizes. Consider, for example, an initially water-saturated porous medium undergoing drainage once the displacement pressure has been reached. According to Equation (15) applied at the scale of a single pore throat, this is a capillary pressure sufficient to enter that size of pore space subject to the relevant contact angle. The smaller the pore, typically associated with finer-grained, lower-permeability media, the higher the displacement pressure (Figure 13). In addition, if all the pore throats in a medium were the same size (i.e., an extremely well-sorted granular medium), a capillary pressure equal to the displacement pressure would be sufficient to enter all pores, and the capillary pressure-saturation curve would appear as a horizontal line between  $S_w = 1$  and  $S_w = S_r$ . Conversely, if there is a broad range of pore sizes, then successive increases in capillary pressure are required to drain the medium. For example, the slopes of the curves shown in Figure 13b are much shallower than those in Figure 13a.

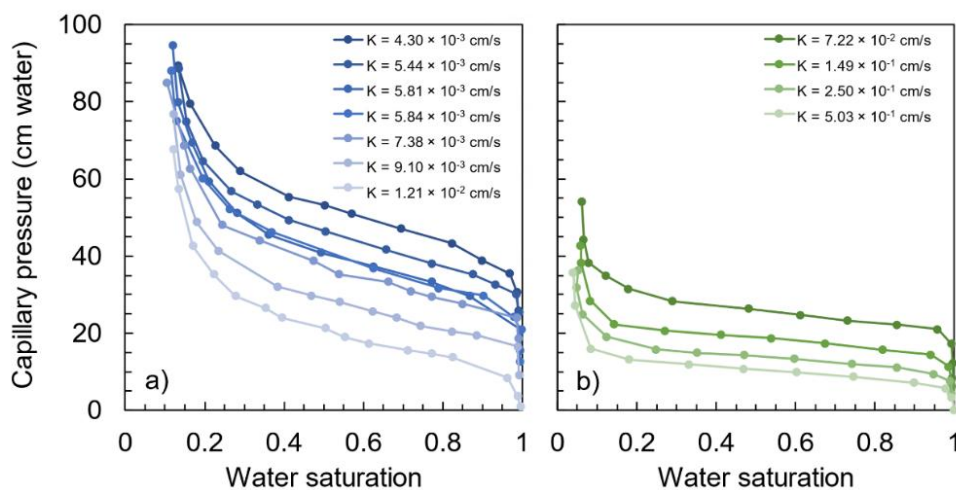


**Figure 13** - Example drainage capillary pressure-saturation curves measured in sand by a) Kueper and Frind (1991) using tetrachloroethene (PCE) as the nonwetting phase and water as the wetting phase, and b) by Schroth and others (1996) using air as the nonwetting phase and water as the wetting phase. Both sets of data show progressively higher curves for finer-grained, lower-permeability sand. The data for (b) was collected in well-sorted sands that exhibit shallower (flatter) drainage curves than the Borden aquifer sands used to gather the data shown in (a).

### 3.4 Residual Formation and Fluid Trapping

The formation of immobile wetting and nonwetting fluid is important in multiphase flow. They are often both referred to as a residual and both represent a saturation at which that phase becomes immobile, but the similarities end there. As discussed above, wetting fluid residual consists of a collection of films and pendular rings that are formed at the end of drainage at relatively high capillary pressure. Wetting fluid can also be trapped in larger pores that are surrounded by very small pores that do not drain at high capillary pressures, and through which the rate of wetting fluid movement is negligible.

In a NAPL–water system, the consequence of a residual water saturation is that the pore space of an initially water-saturated medium will not become completely filled with NAPL ( $S_n < 1$ ) following a NAPL release. Even highly-saturated NAPL zones (often referred to as *pools*; discussed further in Section 5) are not completely NAPL-saturated.

Nonwetting fluid residual is quite different than wetting fluid residual. Nonwetting fluid residual in a NAPL–water system is *entrapped* and consists of disconnected blobs and ganglia that are formed at the end of water imbibition at relatively low capillary pressures. These are generally conceptualized as being formed by pore-scale snap-off and bypass processes, whereby unstable wetting fluid configurations redistribute and fragment nonwetting fluid in pore throats, or wetting fluid becomes connected in surrounding smaller pores leaving disconnected nonwetting fluid in the adjacent pores (Dullien, 1992). In a NAPL–water system, the consequence of a residual NAPL saturation is that once NAPL enters a region of an initially water-saturated porous medium, that porous medium will not return to being completely water-saturated ( $S_w < 1$ ) even if the macroscopic capillary pressure returns to zero. A non-zero capillary pressure still exists at the scale of a single blob due to the curvature of the local NAPL–water interface, but the macroscopic capillary pressure is equal to zero because the NAPL is not continuous at the macroscopic scale.

The formation of nonwetting residual is an important consequence of capillary pressure-saturation hysteresis and has important implications on the distribution of NAPL at field sites, as well as efforts to remove it. The disconnected blobs and ganglia that exist at a residual NAPL saturation generally cannot flow under most conditions. Consequently, residual NAPL will not be mobilized by groundwater flow after drainage and imbibition during a NAPL release to the subsurface. In most cases, residual NAPL can only be removed by mass transfer (dissolution or vaporization), potentially aided by the application of in situ remediation technologies. Therefore, NAPL residual can serve as a persistent source of groundwater contamination. As discussed in Section 5.2, immobile NAPL in three-fluid (air–NAPL–water) systems includes discontinuous NAPL blobs and ganglia occluded by water. However, it also includes NAPL films and pendular rings that result from NAPL drainage (resulting from a process similar to how residual water develops).

### 3.5 Mathematical Capillary Pressure-Saturation Expressions

The relationship between capillary pressure and saturation can be described using mathematical expressions. These mathematical expressions are useful for performing screening calculations. They are also incorporated in sophisticated numerical models used to simulate NAPL flow, although tabulated capillary pressure-saturation data can also be used. Several mathematical expressions are available to characterize the relationship between capillary pressure and saturation; two of the more commonly-used expressions are the *Brooks-Corey* equation (Brook & Corey, 1966) and the *van Genuchten* equation (van Genuchten, 1980), examples of which are shown in Figure 14.

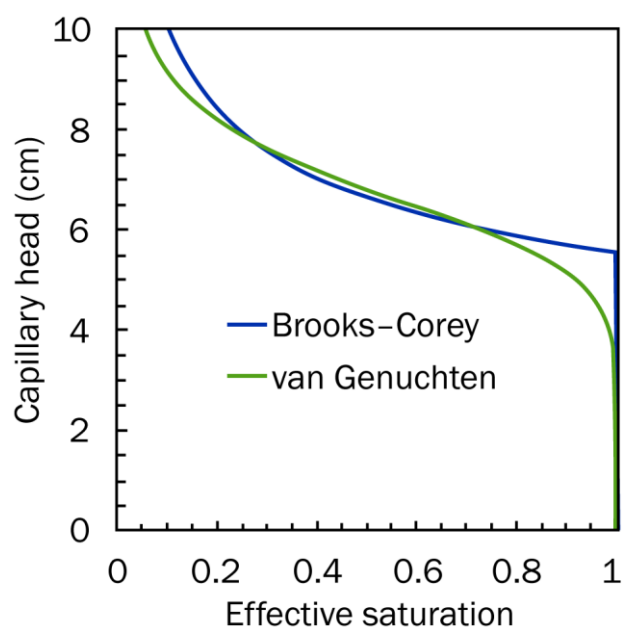


**Figure 14** - Example capillary pressure-saturation curves modeled using the Brooks-Corey (1966) and van Genuchten (1980) expressions (adapted from Lenhard et al., 1989).

Both of these equations make use of an *effective wetting saturation* that scales the water saturation between the residual water saturation and a maximum water saturation as shown in Equation (16).

$$S_e = \frac{S_w - S_r}{S_m - S_r} \quad (16)$$

where:

$S_e$  = effective wetting saturation (dimensionless)

$S_m$  = maximum water saturation (dimensionless)

For primary drainage,  $S_m = 1$ . When plotting capillary pressure versus water saturation, the primary drainage curve is asymptotic to  $S_w = S_r$  at high capillary pressure. However, when plotting capillary pressure versus effective saturation, the curve is asymptotic to  $S_e = 0$  at high capillary pressure. Using effective saturation, the

Brooks-Corey equation describes the relationship between capillary pressure and saturation as shown by Equations (17) and (18).

$$S_e = \left(\frac{P_c}{P_d}\right)^{-\lambda} \text{ for } P_c \geq P_d \quad (17)$$

$$S_e = 1 \text{ for } P_c < P_d \quad (18)$$

where:

$\lambda$  = pore-size distribution index (**dimensionless**)

The value of  $P_d$  in Equations (17) and (18) can be determined by extending the  $P_c$ - $S_e$  relationship to  $S_e = 1$ , which can overestimate the true displacement pressure. It is also important to note that Equations (17) and (18) are not continuously differentiable over all  $P_c$ , which requires additional care when implementing the equations in numerical models. Nevertheless, the description of  $S_e = 1$  for some  $P_c > 0$  accurately represents NAPL behavior in porous media and is particularly important for modelling the effect of water-saturated capillary barriers and their effect on NAPL distribution (Kueper & Frind, 1991).

The van Genuchten equation describes the relationship between capillary pressure and saturation as shown in Equation (19).

$$S_e = [1 + (\alpha P_c)^n]^{-m} \quad (19)$$

where:

$\alpha$  = fitting parameter related to a characteristic capillary pressure ( $M^{-1}LT^2$ )

$m$  and  $n$  = fitting parameters related to the pore-size distribution (**dimensionless**)

Commonly,  $m$  is assumed to be  $(1 - 1/n)$ , which simplifies calculation of the relative permeability. Unlike Equations (17) and (18), Equation (19) is continuously differentiable, which is computationally advantageous for use in numerical models. However, Equation 19 predicts  $S_e < 1$  for any  $P_c > 0$ , which cannot reproduce the exclusion of NAPL from water-saturated capillary barriers that occurs. It is clear from laboratory and field experiments that NAPL will be excluded from entering water-saturated capillary barriers if the capillary pressure at the base of the accumulated NAPL does not exceed the displacement pressure of the barrier (Kueper et al., 1993; Pankow & Cherry, 1996). Therefore, simulations that do not allow for this exclusion are unable to accurately represent NAPL distributions in many cases where such barriers are present, including at field sites. Equations (17), (18), and (19) are empirical relationships, and the parameters  $P_e$  and  $\lambda$ , or  $\alpha$ ,  $m$  and  $n$ , as well as  $S_m$  and  $S_r$ , are often determined by fitting experimental  $P_c$  versus  $S_w$  data.

### 3.6 Scaling Capillary Pressure Curves

The mathematical expressions of macroscopic capillary pressure are related to the properties of the fluids and porous media. For example, inspection of Equation (15) indicates that capillary pressure increases with increasing interfacial tension, all other factors remaining equal. It is also reasonable that capillary pressure will be higher at the same effective wetting fluid saturation in finer-grained porous media, which typically have smaller pore spaces and lower intrinsic permeability than coarser-grained porous media. Given these relationships, it is convenient to have an expression that allows capillary pressure to be scaled between similar porous media. A dimensionless expression developed by Leverett (1941) to correlate capillary pressure-saturation data of similar porous media with different intrinsic permeabilities, porosities and interfacial tensions is called the Leverett J-function (Amyx et al., 1960) as shown by Equation (20).

$$J = \frac{P_c}{\sigma} \sqrt{\frac{k}{\theta_T}} \quad (20)$$

where:

$J$  = dimensionless capillary pressure (dimensionless)

$k$  = intrinsic permeability ( $L^2$ )

Later, Rose and Bruce (1949) added cosine of the contact angle ( $\cos\theta$ ) to the Leverett J-function when investigating capillary pressure data but did not publish a revised equation. Subsequently, Brown (1951) wrote the Leverett J-function with  $\cos\theta$  in their analyses. Other investigators have followed Brown (1951) by including  $\cos\theta$  in the denominator next to the interfacial tension ( $\sigma$ ) in the Leverett J-function to address wettability effects (Anderson, 1987; Dullien, 1992; Tiab & Donaldson, 1996). For similar porous media where  $J$  is considered constant and the contact angle is not considered, this allows scaling relationships to be established as shown by Equation (21).

$$\frac{P_{c1}}{\sigma_1} \sqrt{\frac{k_1}{\theta_{T1}}} = \frac{P_{c2}}{\sigma_2} \sqrt{\frac{k_2}{\theta_{T2}}} \quad (21)$$

Different, but similar, media and/or fluid pairs are denoted by the subscripts 1 and 2. Equation (21) is particularly useful in the case of scaling between different fluid pairs in the same medium ( $k_1 = k_2$  and  $\theta_{T1} = \theta_{T2}$ ), where capillary pressure can be scaled by the ratio of interfacial tensions if contact angles are ignored (fluid-pair scaling is discussed in Section 5.2 for three fluid air–LNAPL–water systems). This allows, for example, capillary pressure-saturation relationships for NAPL–water and air–NAPL systems to be estimated from air–water experiments as was done by Lenhard and Parker (1987a). For example, the various capillary pressure drainage curves presented in Figure 13a, which employed PCE as the nonwetting phase and water as the wetting phase, were successfully scaled using the

Leverett J-function to arrive at a common dimensionless displacement pressure applicable to sands of different permeability (Kueper & Frind, 1991).

### 3.7 Relevant Exercises

The following Exercises provide the reader with an opportunity to work with the material presented in this section.

[Exercise 5](#)  prompts the reader to sketch capillary pressure-saturation curves.

[Exercise 6](#)  asks the reader to estimate displacement pressure.

## 4 Relative Permeability

### 4.1 Effective Permeability and The Extension of Darcy's Law

Darcy's law (Darcy, 1856) relates the specific discharge of a single fluid (typically water in a water-saturated system) to the hydraulic-head gradient and hydraulic conductivity. Although proposed for a system saturated with a single fluid, Darcy's law can also be used to describe specific discharge in unsaturated (multiphase) systems. The saturated hydraulic conductivity is a function of both the fluid properties and the porous medium, where the porous medium property is the intrinsic permeability. For multiphase flow, assuming that each fluid is able to flow within its own separate network of connected pores, Darcy's law can be extended as shown by Equation (22).

$$q_{\alpha} = -\frac{k_{\alpha}\rho_{\alpha}g}{\mu_{\alpha}}\nabla h_{\alpha} \quad (22)$$

where:

- $q_{\alpha}$  = specific discharge ( $LT^{-1}$ )
- $k_{\alpha}$  = effective permeability ( $L^2$ )
- $\rho_{\alpha}$  = density ( $ML^{-3}$ )
- $\mu_{\alpha}$  = dynamic viscosity ( $ML^{-1}T^{-1}$ )
- $\nabla h_{\alpha}$  = hydraulic-head gradient (**dimensionless**)
- $\alpha$  = fluid identifier (wetting or nonwetting)

The effective permeability represents the influence of the porous medium on the resistance to flow within only the network of connected pores occupied by fluid  $\alpha$ . The effective permeability is often expressed as a relative permeability as shown by Equation (23).

$$k_{r\alpha} = \frac{k_{\alpha}}{k} \quad (23)$$

where:

- $k_{r\alpha}$  = relative permeability of fluid indicated by  $\alpha$  (**dimensionless**)

Relative permeability is less than unity (i.e.,  $k_{r\alpha} < k$ ) because of the reduced ability of a fraction of the pore space to conduct fluid, as well as the increased tortuosity induced by flow around pores occupied by the second fluid. Taking the two fluids to be water and NAPL ( $a = w, n$ ) and separating the pressure and elevation components of hydraulic head, Equations (22) and (23) can be combined to give Equations (24) and (25).

$$q_{iw} = -\frac{k_{ij}k_{rw}}{\mu_w}\left(\frac{\partial P_w}{\partial x_j} + \rho_w g \frac{\partial z}{\partial x_j}\right) \quad (24)$$

$$q_{in} = -\frac{k_{ij}k_{rn}}{\mu_n} \left( \frac{\partial P_n}{\partial x_j} + \rho_n g \frac{\partial z}{\partial x_j} \right) \quad (25)$$

where:

$z$  = elevation (L)

$i, j$  =  $x, y,$  and  $z$  directional identifiers

Although intrinsic permeability is a tensor (potentially having different values depending on direction), relative permeability is assumed to be a scalar (a singular value independent of direction).

Equations (24) and (25) are analogous to Darcy's law, where the specific discharge of each fluid is related to a driving force defined by the hydraulic-head gradient and a resistance defined by properties of the fluid and porous medium through which it flows. Importantly, the resistance depends on the fluid saturation, and that resistance decreases as the number of pores occupied by the fluid increases. Therefore, the flow of one fluid depends on the second fluid, and the relative permeability depends on the fluid saturation.

## 4.2 Relative Permeability Curves

Much in the same way as was described for capillary pressure, there is a need to represent the relationship between relative permeability and saturation at the macroscopic scale. This relationship is represented by a set of relative permeability curves (Figure 15). Together with capillary pressure-saturation curves, they form a set of  $k$ - $S$ - $P$  relationships that couple the mathematical descriptions of water and NAPL flow in porous media.

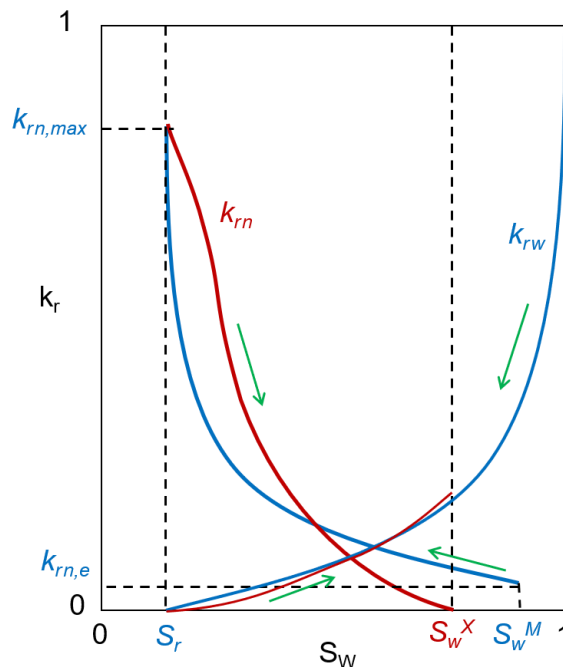


**Figure 15** - Conceptual representation of relative permeability curves. Drainage curves are shown in blue and imbibition curves are shown in red (modified after Kueper & Gerhard, 2014).

The relationships between relative permeability and saturation for the wetting (water) and nonwetting (NAPL) fluids are different because they occupy different size pores, with the wetting fluid occupying the smaller, less conductive pores and the continuous nonwetting fluid occupying the larger, more conductive pores. Consider an initially water-saturated ( $S_w = 1$ ) sample undergoing drainage by NAPL invasion (blue curve starting at  $k_{rw} = 1$  on the right side in Figure 15). The water relative permeability decreases from its initial value of  $k_{rw} = 1$  as the water saturation decreases. That initial decrease is steep, as the largest, most conductive pores are first occupied by NAPL.

At the same time, the NAPL relative permeability does not increase ( $k_{rn} = 0$ ) because NAPL has yet to form a sample-spanning connected pathway through which NAPL can flow. That is, the capillary pressure is less than the entry pressure ( $P_c < P_e$ ). Only after the emergence saturation is reached ( $S_w = S_w^M$ ) does  $k_{rn}$  increase ( $k_{rn} = k_{rn,e} > 0$ ).

As water drainage continues, the water relative permeability continues to decrease, until reaching a value of zero at the residual water saturation. That is, water becomes essentially immobile ( $k_{rw} = 0$ ) even though water is still present in the sample ( $S_w = S_r$ ). Meanwhile, the NAPL relative permeability increases, reaching a maximum value less than unity ( $k_{rn} = k_{rn,max} < 1$ ) because all of the pore space is not accessible to the NAPL at the residual water saturation. While less than unity, it is typically close to unity because the pore space not occupied by NAPL is comprised of the smallest pore spaces. Inspection of Figure 15 shows that the sum of the relative permeabilities (i.e., the superposition of either the two blue curves or the two red curves) is less than unity whenever two fluids are present.

Like capillary pressure-saturation curves, relative permeability curves are hysteretic. This hysteresis is more pronounced for the nonwetting fluid and is often negligible (Lenhard & Parker, 1987b) for the wetting fluid. During imbibition, the water relative permeability does not return to unity ( $k_{rw} < 1$ ) due to NAPL entrapment at the extinction saturation ( $S_w = S_w^X$ ).

### 4.3 Mathematical Relative Permeability-Saturation Expressions

Like the relationship between capillary pressure and saturation, the relationships between relative permeability and saturation are empirical. Multiple steady-state and unsteady-state measurement techniques are available (Honarpour et al., 1986), but are difficult, time-consuming, and costly. For this reason, estimates based on fits to capillary pressure-saturation measurements are often used to estimate relative permeability. Two such models for two-fluid systems are the combination of the *Brooks-Corey* (Brooks & Corey, 1966; Equations (17) and (18)) and *Burdine* (Burdine, 1953) models as shown by Equations (26) and (27),

$$k_{rw} = S_e^{3+\frac{2}{\lambda}} \quad (26)$$

$$k_{rn} = (1 - S_e)^2 \left(1 - S_e^{1+\frac{2}{\lambda}}\right) \quad (27)$$

and the combination of the *van Genuchten* (van Genuchten, 1980) (Equation 19) and *Mualem* (Mualem, 1976) models as shown by Equations (28) and (29).

$$k_{rw} = S_e^{\frac{1}{2}} \left[1 - \left(1 - S_e^{\frac{1}{m}}\right)^m\right]^2 \quad (28)$$

$$k_{rn} = (1 - S_e)^{\frac{1}{2}} \left(1 - S_e^{\frac{1}{m}}\right)^{2m} \quad (29)$$

where:

$$m = 1 - 1/n \text{ (dimensionless)}$$

Note that other expressions, and other combinations are also available (e.g., Leij et al., 1996). The latter set of equations was proposed for air-water systems but can be applied to other two-fluid systems, such as NAPL–water. Equations (26), (27), (28), and (29) are for non-hysteretic capillary pressure-saturation relations, and equations that consider hysteresis are more complex (Parker & Lenhard, 1987; Lenhard & Parker, 1987a).

Mass balance expressions can make use of Equations (24) and (25) to derive the governing equations for multiphase flow in porous media, analogous to the governing equation for groundwater flow (Woessner & Poeter, 2020). Written for water and NAPL, these are expressed as shown by Equations (30) and (31).

$$\frac{\partial}{\partial t} (S_w \theta_T \rho_w) = \frac{\partial}{\partial x_i} \left[ \frac{k_{ij} k_{rw} \rho_w}{\mu_w} \left( \frac{\partial P_w}{\partial x_j} + \rho_w g \frac{\partial z}{\partial x_j} \right) \right] \quad (30)$$

$$\frac{\partial}{\partial t} (S_n \theta_T \rho_n) = \frac{\partial}{\partial x_i} \left[ \frac{k_{ij} k_n \rho_w}{\mu_n} \left( \frac{\partial P_n}{\partial x_j} + \rho_n g \frac{\partial z}{\partial x_j} \right) \right] \quad (31)$$

Equations (30) and (31) are then coupled using Equations (8) and (16) combined with (17), (18), (26) and (27). Alternatively, Equations (8) and (16) can be combined with (19), (28) and (29). These equations, and modified versions where the dependent variables do not involve the phase pressures (Kueper & Frind, 1991), form the basis of complex, numerical multiphase flow simulators. The equations need to be solved simultaneously along with appropriate boundary conditions because the fluid pressure from one equation is needed for the other.

## 5 DNAPL and LNAPL Distribution

### 5.1 DNAPL Distribution in DNAPL-Water Systems

Upon release to the subsurface, DNAPL will distribute itself in the form of disconnected blobs and ganglia of organic liquid referred to as *residual DNAPL*, and in connected distributions referred to as *pooled DNAPL* (Section 3.4). Residual DNAPL always forms at the trailing edge of a migrating DNAPL body and typically occupies between 5 and 30 percent of pore space (Wilson et al., 1990; Cohen & Mercer, 1993; Pankow & Cherry, 1996). Figure 5b illustrates residual PCE DNAPL in sand (Kueper et al., 1993). Residual DNAPL is trapped by capillary forces and typically will not enter a monitoring well, even if it is present directly adjacent to the monitoring well sand pack and even under aggressive groundwater pumping conditions (Cohen & Mercer, 1993; Pankow & Cherry, 1996).

Pooling of DNAPL can occur above capillary barriers, which are typically layers or lenses of relatively less permeable material. Figure 5c illustrates a pool of PCE DNAPL that was perched upon a 1 cm thick silt lens (Kueper et al., 1993). The silt lens had a higher displacement pressure than the sand occupied by the DNAPL pool; consequently, the DNAPL did not penetrate the silt lens. One important observation here is that the thickness of the capillary barrier is generally not a factor in whether DNAPL will penetrate the barrier. Of relevance is that there is a permeability contrast, and the permeability contrast represents a difference in displacement pressures.

A second important point is that DNAPL pooling can occur at any elevation within an aquifer, not just above a major feature such as a clay or silt aquitard. Pools represent a connected distribution of DNAPL in the pore space, and typically correspond to DNAPL saturations on the order of 30 percent to 80 percent of pore space (Kueper et al., 1993; Pankow & Cherry, 1996).

The thickness of DNAPL pools is dependent upon the DNAPL density, the DNAPL–water interfacial tension, the vertical component of the groundwater hydraulic gradient, and the displacement pressure of the capillary barrier upon which the pool has formed (Kueper et al., 1993; Longino & Kueper, 1999). Kueper and others (1993) provide the following expression for the maximum stable pool height that can accumulate above a capillary barrier (Equation (32)).

$$H = \frac{P_c'' - P_c'}{\Delta\rho g} \quad (32)$$

where:

- $H$  = the maximum height (thickness) of DNAPL such that the capillary barrier is not penetrated (L)
- $P_c''$  = entry pressure of the capillary barrier ( $\text{ML}^{-1}\text{T}^{-2}$ )

$P_c'$  = capillary pressure at the top of the pool ( $ML^{-1}T^{-2}$ )

$\Delta\rho$  = difference in density between the DNAPL and water ( $ML^{-3}$ )

$g$  = gravitational acceleration ( $LT^{-2}$ )

The capillary pressure at the top of the DNAPL pool ( $P_c'$ ) is dependent on the saturation history associated with pool placement. The maximum value of  $P_c'$  will be the entry pressure of the porous medium within which the pool resides. This assumes that the top of the pool exists under drainage conditions. However, if the top of the pool exists under imbibition conditions,  $P_c'$  may be as low as the terminal pressure. As discussed by Gerhard and Kueper (2003), the terminal pressure can be reasonably approximated as half the entry pressure. Of note is that the pool height predicted by Equation (32) is independent of the depth below the water table. Equation (32) assumes a one-dimensional hydrostatic system; the pressure profiles for this system are illustrated in Figure 16 for the case of the top of the DNAPL pool existing under drainage conditions (Kueper et al., 2014).

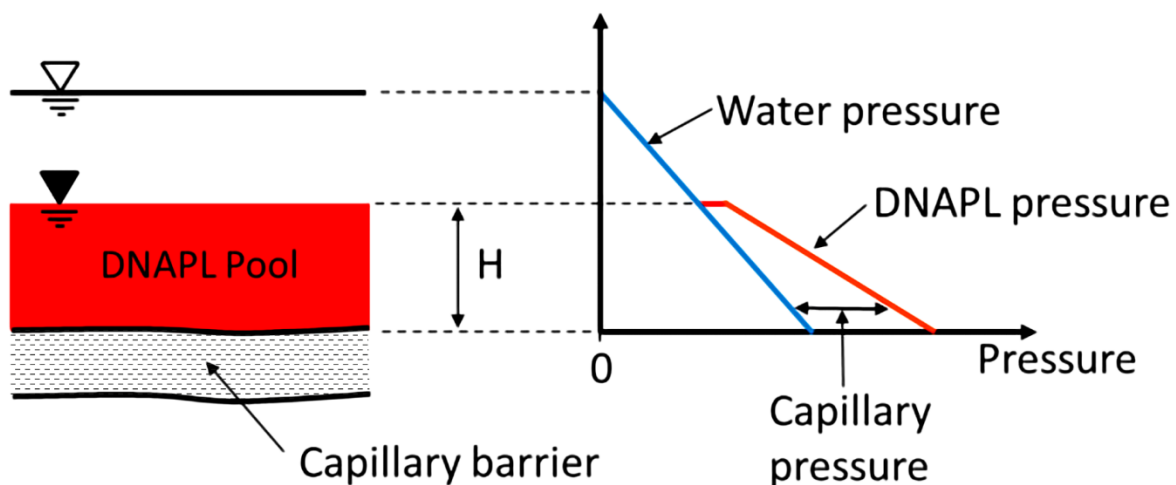


**Figure 16** - Hydrostatic distribution of water and DNAPL pressures for DNAPL pooled upon a capillary barrier (Kueper et al., 2014). The top of the DNAPL pool has a non-zero capillary pressure.

Figure 17 shows the relationship between the maximum stable DNAPL pool height and hydraulic conductivity of the capillary barrier for a variety of chlorinated solvent DNAPLs (Kueper et al., 2014). The calculations supporting Figure 17 assume that the DNAPL pools reside in a medium-grained sand having a hydraulic conductivity of  $1 \times 10^{-2}$  cm/s and a porosity of 40 percent. The entry pressure of the capillary barrier ( $P_c'$ ) is calculated using Equation (20) and a dimensionless entry pressure of 0.11 and assumes that the top of the pool exists under wetting conditions (i.e.,  $P_c'$  in Equation (32) is set to half of the entry pressure). Each DNAPL is assumed to have an interfacial tension with water of 0.025 N/m. Figure 17 illustrates that lower density DNAPLs and lower hydraulic conductivity capillary barriers promote larger DNAPL pool heights.

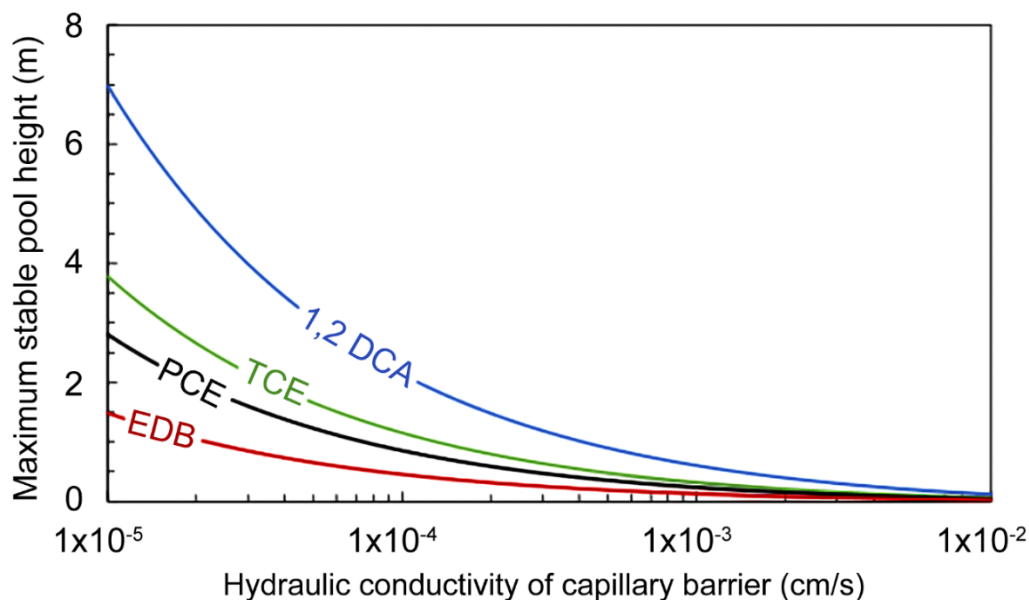


**Figure 17** - Maximum stable DNAPL pool height accumulated above a water-saturated capillary barrier versus hydraulic conductivity of the barrier for four different DNAPLs (details provided in Kueper & Gerhard, 2014). The volume of DNAPL in a pool under drainage conditions can be estimated using the calculations in Longino and Kueper (1995).

As discussed in Section 3.6, the displacement pressure of a particular lamination, lens, or layer correlates with its hydraulic conductivity. It is well established that aquifers are heterogeneous with respect to the distribution of hydraulic conductivity, and that it is not uncommon for macroscopic-scale hydraulic conductivities within an aquifer to vary by between three to six orders of magnitude. It follows that displacement pressures within an aquifer will vary widely between various laminations, lenses, and layers. Consequently, DNAPL will migrate through saturated porous media according to displacement pressure, always following the path of least capillary resistance (lowest displacement pressure at the advancing DNAPL front). The result of this selective nature of migration is a very tortuous, sinuous distribution of DNAPL residual and pools (i.e., the source zone architecture) as shown in Figure 2. One implication of the selective nature of DNAPL migration is that delineating the DNAPL source zone can be challenging and subject to uncertainty. This, in turn, is one of the major reasons why many remediation implementations do not achieve desired groundwater clean-up goals.

A concept related to DNAPL distribution is the bulk retention capacity, typically used to characterize DNAPL-impacted sites, defined as shown by Equation (33).

$$R_b = \frac{V_n}{V_{SZ}} \quad (33)$$

where:

$R_b$  = bulk retention capacity (dimensionless)

$V_n$  = volume of NAPL in a source zone ( $L^3$ )

$V_{SZ}$  = total volume of the source zone ( $L^3$ )

This appears similar to the definition of NAPL saturation (Equation (5)) but the difference lies in the scale at which it is applied. NAPL saturation is determined at the scale of a single soil sample, where much of the pore space in that sample could contain NAPL. The bulk retention capacity is determined at the scale of a NAPL source zone in which, because of the heterogeneous distribution of NAPL, much of the subsurface volume contains no NAPL at all (Kueper et al., 2014). Therefore, while local-scale residual NAPL saturations may be on the order of 0.05 to 0.3 (5 to 30 percent of pore space) and local-scale NAPL saturations in pools may be on the order of 0.3 to 0.8, bulk retention capacity is typically on the order of 0.005 to 0.03 (Kueper & Davies, 2009). Importantly, bulk retention capacity accounts for the presence of both NAPL residual and NAPL pools.

DNAPL distribution in the subsurface is also dependent on the elapsed time since the original DNAPL release occurred. As discussed in Section 1.6, the DNAPL source zone goes through five primary life cycle stages. This life cycle begins with an initial release of DNAPL to the subsurface and culminates in complete DNAPL depletion with contamination persisting as a result of diffusion from low permeability zones and desorption from solids. In theory, a sixth life cycle stage exists where all former contaminants are non-detectable in soil, groundwater, and vapor. To our knowledge, there are no documented cases of sites reaching Stage 6. The reader is referred to Kueper and others (2014) for a detailed discussion of the various life cycle stages of a DNAPL source zone, within which the distributions of DNAPL can vary significantly.

[Exercise 7](#) asks the reader to calculate DNAPL pressures, capillary pressure, and maximum pool height.

## 5.2 NAPL Distribution in Three-Fluid Systems

In the previous sections, the focus was on two-fluid (NAPL–water) systems in porous media. Unless NAPL is released directly at the water-saturated capillary fringe above the water table or directly at the water table, a three-fluid (e.g., air–NAPL–water) system will be created (Figure 18a). Whenever the NAPL pressure is greater than or equal to zero (gauge pressure) in a region, a two-fluid, NAPL–water system will exist in that region, except for possibly entrapped air. Whenever the NAPL pressure is less than zero, a three-fluid, air–NAPL–water system will exist. Therefore, the subsurface may contain regions of two-fluid (NAPL–water) and three-fluid (air–NAPL–water) systems. This is true for NAPLs with a density less than water (LNAPLs) and greater than water (DNAPLs). In this section, the focus is on LNAPLs as a prelude to Section 5.3.

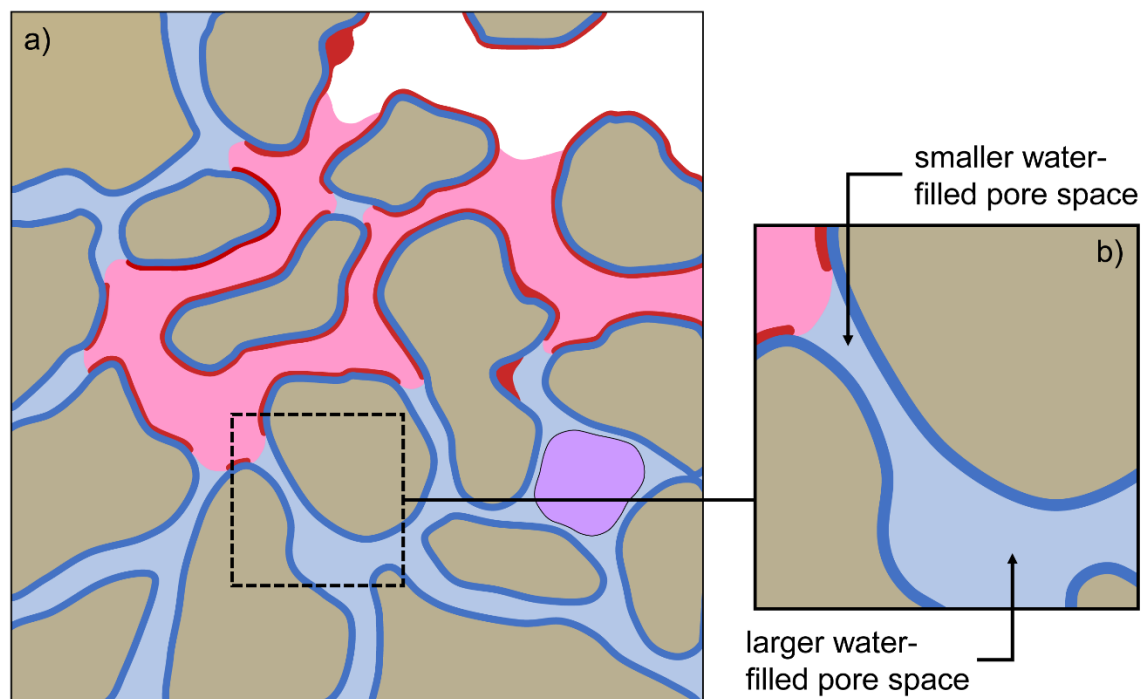


**Figure 18** - A drawing of a) an air–LNAPL–water system in porous media showing free LNAPL (pink), entrapped LNAPL (purple), and residual LNAPL (red), which consist of continuous thin LNAPL films and relatively immobile LNAPL in wedges, with mobile (light blue) and residual water (dark blue), and b) LNAPL that is unable to displace water from a larger pore space because it cannot enter the smaller water-filled pore space at the current capillary pressure.

In a three-fluid (air–NAPL–water) system in porous media where water wets the solid surfaces (i.e., wetting fluid), water will be in the smallest pore spaces, air will be in the largest pore spaces, and NAPL will be in pores spaces not occupied by either water or air (i.e., the intermediate pore sizes). This depends on the accessibility of air–NAPL and NAPL–water interfaces to pores—these are the interfaces that separate the continuous air and continuous NAPL; and those that separate the continuous NAPL and continuous water, respectively. For example, it is not uncommon for larger pores to be adjacent to (i.e., be surrounded by) smaller water-filled pores, which prevent nonwetting fluid from entering the larger pore space until the relevant capillary pressure is reached. Consequently, NAPL cannot displace water from the larger pore space in Figure 18b because a smaller pore space exists between the NAPL and the larger pore space containing water. Only after the NAPL–water capillary pressure becomes large enough to displace water from the smaller pore space will the NAPL be able to displace water from the larger space. This can occur with LNAPL as well as DNAPL in the vadose zone. The pore size distributions in porous media can be very complex and the general statement in the beginning of this paragraph depends on accessibility of fluid–fluid interfaces separating the immiscible fluids to all pores.

Which fluid will occupy the pore sizes depends on the wettability order. For cases where water is the wetting fluid (i.e., water wets the porous media relative to other fluids) it is generally assumed for air–NAPL–water systems that NAPL will wet water surfaces

relative to air, which occurs almost without exception. Ordinarily, a liquid will wet either the solids or other liquid phase surfaces relative to air. An exception is a two-fluid, air–mercury system where air wets the solid surfaces relative to liquid mercury (i.e., air is the wetting fluid and mercury is the nonwetting fluid). An air–mercury system is employed in mercury porosimetry which is used in the petroleum industry to measure the pore-size distribution of solid cores. The solid and fluid molecular properties determine the wettability order. In an air–NAPL–water fluid system in water-wet porous media, there will be air–NAPL and NAPL–water fluid–fluid interfaces separating the immiscible fluids. The fluid pressure difference across the air–NAPL interfaces is the air–NAPL capillary pressure shown by Equation (34).

$$P_c^{an} = P_a - P_n \quad (34)$$

where:

$$P_c^{an} = \text{air-NAPL capillary pressure (ML}^{-1}\text{T}^{-2}\text{)}$$

$$P_a = \text{air pressure (ML}^{-1}\text{T}^{-2}\text{)}$$

$$P_n = \text{NAPL pressure (ML}^{-1}\text{T}^{-2}\text{)}$$

Commonly, the air pressure in the near subsurface is assumed to be at atmospheric pressure (zero-gauge pressure) because of its connectivity to the atmosphere through networks of pores and fractures. However, the subsurface air pressures change in time and location with varying time-dependent atmospheric conditions (weather); therefore, an assumption of zero-gauge pressure (i.e.,  $P_c^{an} = -P_n$ ) is not always appropriate.

As discussed in Section 3.1, the fluid pressure difference across NAPL–water interfaces is the NAPL–water capillary pressure shown by Equation (35).

$$P_c^{nw} = P_n - P_w \quad (35)$$

where:

$$P_c^{nw} = \text{NAPL–water capillary pressure (ML}^{-1}\text{T}^{-2}\text{)}$$

$$P_n = \text{NAPL pressure (ML}^{-1}\text{T}^{-2}\text{)}$$

$$P_w = \text{water pressure (ML}^{-1}\text{T}^{-2}\text{)}$$

Equation (35) is similar to Equation (8), but explicitly defines the capillary pressure as being the NAPL–water capillary pressure. Because both NAPL–water and air–NAPL capillary pressures exist in air–NAPL–water systems in porous media, a single  $P_c$  cannot be used for defining the capillary pressure as originally presented in Equation (8). Therefore, a superscript is used in Equation ((35) and elsewhere in this section for capillary pressure symbols, where the first superscript indicates the relative nonwetting fluid at the interface and the second superscript indicates the relative wetting fluid at the interface.

In special cases where NAPL may behave as a wetting fluid relative to water in the pore spaces—as discussed in Section 2.4 for NAPL-wet and mixed-wet systems in porous media—the capillary pressures in air-NAPL-water fluid systems will be defined differently. The capillary pressure separating the continuous NAPL and water would be the water-NAPL capillary pressure ( $P_c^{wn}$ ) and the capillary pressure separating the continuous air and water would be the air–water capillary pressure ( $P_c^{aw}$ ).

For this book, the focus is three-fluid (air–LNAPL–water) systems where water is a strongly wetting fluid. Additional work has been done on fluid systems that are not strongly water wet (e.g., Anderson, 1987; Lenhard & Oostrom, 1998; Morrow, 1990).

In addition to the definitions of capillary pressure for each fluid pair presented above, descriptions of air-NAPL-water systems also require more specific definitions of saturation. For example, the *total liquid saturation* is the ratio of the water- and NAPL- occupied pore space to the total pore space. It is typically assumed to be governed by the air-NAPL capillary pressure while the water saturation is governed by the NAPL-water capillary pressure. *Effective total liquid saturation* and *effective air saturation* can also be defined by accounting for the residual water saturation, similar to Equation (16). A mathematical description of these parameters is provided in [Box 1](#).

Accounting for different forms of NAPL in air-NAPL-water systems requires different terminology than that used in Section 3.4 for two-fluid systems (i.e., residual and pooled NAPL). Lenhard and others (2004) developed alternative terminology to label LNAPL that is:

1. free LNAPL, which is continuous and can move under LNAPL pressure gradients;
2. entrapped LNAPL, which is occluded by water during water imbibition; and
3. residual LNAPL, including LNAPL as thin films, LNAPL in pore wedges that is not entrapped by water, and LNAPL in bypassed pores.

While LNAPL present as thin films may move under LNAPL pressure gradients, its velocity is expected to be negligible compared to LNAPL in the center of pores and is typically treated as being immobile. In the case of nonspreading LNAPLs (i.e., with a spreading coefficient less than one, as discussed in Section 2.4), residual LNAPL also includes discontinuous LNAPL lenses. Theoretically, continuous LNAPL films will result following drainage of LNAPL-filled pores for spreading LNAPLs, but discontinuous LNAPL lenses will result following drainage of LNAPL-filled pores for nonspreading LNAPLs. All discontinuous LNAPL, whether entrapped or residual, is assumed to be immobile.

Figure 19 shows free LNAPL internal to LNAPL films. Figure 19 also shows residual LNAPL as continuous thin LNAPL films and LNAPL that may remain following LNAPL drainage in the vadose zone (an air-LNAPL-water system). The LNAPL films wet the water films adjacent to the solid porous media (i.e., water films lie between the LNAPL films and

the solid grains). Because the water films are assumed to be immobile, the LNAPL films also are assumed to be immobile. The LNAPL that remains after LNAPL has drained from pores is generally in pore wedges as shown in Figure 19 and pores bypassed during the LNAPL drainage. This LNAPL in pore wedges and bypassed pores is also typically treated as being immobile because it is connected by only LNAPL films (for spreading LNAPLs) or is discontinuous (for nonspreading LNAPLs).

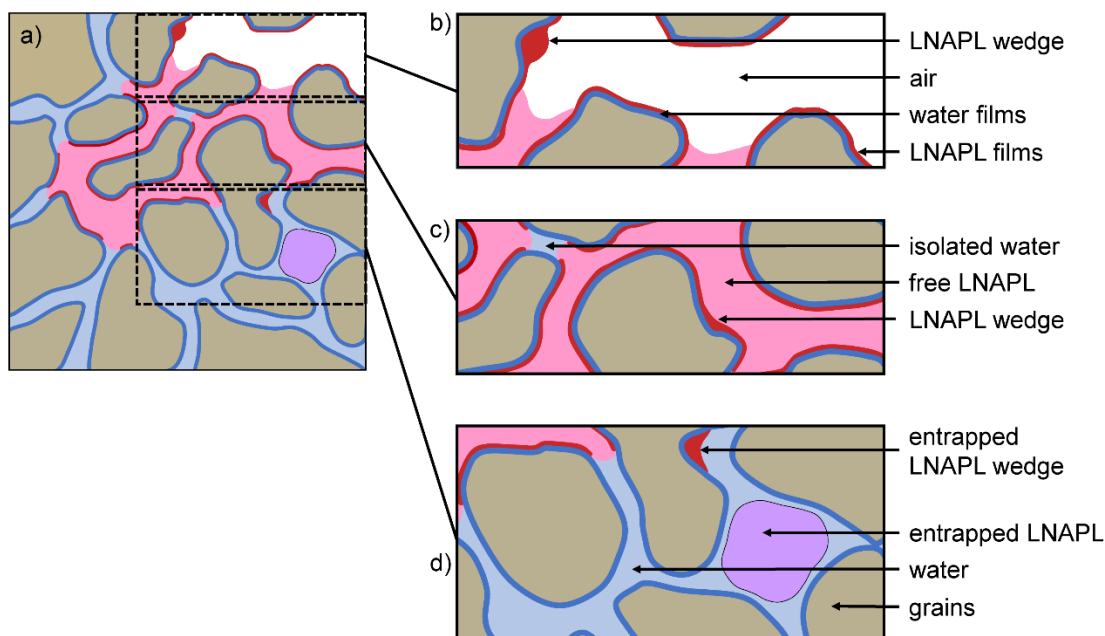


**Figure 19** - This drawing shows a) potential forms of LNAPL and water in a water-wet porous medium, where b) shows relatively immobile LNAPL in films and pore wedges (red) following LNAPL drainage, and free LNAPL (pink), c) shows immobile isolated (discontinuous) water (light blue) and water films (dark blue), and d) shows entrapped LNAPL in pore wedges (red) and pore bodies (purple), as well as free water (light blue).

Figure 19a shows LNAPL in a three-phase, air–LNAPL–water system in water–wet porous media where some water is isolated because it remains connected by only water films during water drainage as LNAPL invades pore spaces. The formation of isolated water develops as LNAPL displaces water from larger pores that surround smaller pores containing water (also shown in Figure 19c). The water in the small pores will not drain as the LNAPL invades nearby larger pores because of capillary forces. The isolated water may be in a single pore (pore throat) or may be in multiple pores.

Furthermore, the isolated water and the water films wetting the solids can be called residual water and are typically treated as being immobile because water film flow will be very slow (Sections 3.3 and 3.4), that is, water that will not drain under high LNAPL–water capillary pressures.

Figure 19b shows LNAPL in films on water surfaces (water films) and in pore wedges, as well as LNAPL that is subject to LNAPL pressure gradients (free LNAPL). Figure 19d shows entrapped LNAPL where water-occluded LNAPL ganglia can be in pore bodies (larger pore spaces at the junction of several pores), pore wedges, and pore throats.

In Sections 3.3 and 3.4 (which refer to LNAPL–water systems), residual NAPL is synonymous with entrapped NAPL. According to the approach by Lenhard and others (2004), residual LNAPL in NAPL–water systems would only be the LNAPL films on water surfaces and in narrow pore wedges.

Entrapped LNAPL can be in pore bodies and created by snap-off mechanisms (Deng et al., 2015) when water displaces LNAPL from pore bodies during water imbibition (Figure 19d). Entrapped LNAPL also can be created when water displaces LNAPL in pores adjacent to larger LNAPL pore wedges as water passes over the LNAPL wedges and occludes the LNAPL (Figure 19d). Additionally, entrapped LNAPL can form similarly to how isolated water forms when water displaces LNAPL, where LNAPL can remain in smaller pore spaces as water displaces LNAPL from surrounding larger pores.

To estimate total liquid and water saturations in air–NAPL–water systems in water-wet porous media, a similar approach to Section 3.5 (e.g., using the van Genuchten equation) can be used for nonhysteretic, capillary pressure–saturation relations. Using this approach, the air–NAPL capillary pressure is used to estimate the effective total liquid saturation and the NAPL–water capillary pressure is used to estimate the effective water saturation. In addition, scaling factors are often used to estimate parameters using air–water capillary pressure–saturation data rather than measuring air–NAPL or NAPL–water curves directly.

Analogous to the approach discussed in Section 4.3, the relative permeabilities of air, NAPL and water as a function of fluid saturation can also be estimated. These relationships are needed to predict fluid flow in air–NAPL–water systems and, along with capillary pressure–saturation relationships, are incorporated into the governing equations that form the basis of numerical multiphase flow simulators. Equations for estimating capillary pressure and relative permeability functions, as well as the governing equations for flow in air–NAPL–water systems, are presented in detail in Box 1.

### 5.3 LNAPL Distribution

Following a release of LNAPL, its distribution and movement through the unsaturated zone will be controlled as described in Section 5.2 and will be affected by spatial variations in subsurface properties. This can result in the formation of various forms of immobile LNAPL, including films, wedges and occluded LNAPL, and mobile LNAPL above lower-permeability layers and water-saturated layers or lenses. When the vertical movements of LNAPL and water have ceased (becoming static; the vertical equilibrium assumption) after the LNAPL reaches the capillary fringe, then the LNAPL and water pressure distributions become linear and equal to their mass densities. For example, when vertical water movement has ceased, then the water pressure at a given elevation ( $z$ ) can be determined from Equation (36).

$$P_w = \rho_w g z_{aw} - \rho_w g z \quad (36)$$

where:

$z_{aw}$  = elevation of the water table ( $P_w = 0$ ), which is the elevation of the air-water interface in a well (borehole) screened only in the water-saturated zone (L)

Water pressures will be negative above the water table and positive below. When vertical LNAPL movement has ceased, then the LNAPL pressure at a given elevation ( $z$ ) can be determined from Equation (37).

$$P_n = \rho_n g z_{an} - \rho_n g z \quad (37)$$

where:

$z_{an}$  = elevation of the air-LNAPL interface ( $P_n = 0$ ) in a well (borehole) screened in the subsurface containing LNAPL and water (L)

As  $z_{aw}$  is the elevation of the water table,  $z_{an}$  is the elevation of the LNAPL table. LNAPL pressures will be negative above the LNAPL table and positive below.

From Equations (36) and (37), the elevation of the LNAPL-water interface (i.e.,  $z_{nw}$ , the elevation where  $P_n = P_w$ ) in a well (borehole) screened in the subsurface containing LNAPL and water can be determined from Equation (38).

$$z_{nw} = \frac{\rho_n z_{an} - \rho_w z_{aw}}{\rho_n - \rho_w} \quad (38)$$

Equation (38) can be rearranged to calculate  $z_{aw}$  (i.e., the elevation where  $P_w = 0$ ) if only a well screened across the water table is available. The air-LNAPL and LNAPL-water capillary pressures can be determined from the elevations of the air-LNAPL ( $z_{an}$ ) and LNAPL-water ( $z_{nw}$ ) interfaces in a well as shown by Equations (39) and (40).

$$P_c^{an} = \rho_n g (z - z_{an}) \quad (39)$$

$$P_c^{nw} = (\rho_w - \rho_n) g (z - z_{nw}) \quad (40)$$

Knowing the distribution of air-LNAPL and LNAPL-water capillary pressures, the total liquid and water saturation distributions can be determined from Equations Box (1-5) and Box (1-6) of Box 1, respectively. Figure 20 shows the general approach for determining the vertical air, LNAPL and water saturation distributions in the subsurface near a well where the air-LNAPL ( $z_{an}$ ) and LNAPL-water ( $z_{nw}$ ) interfaces in the well were measured.

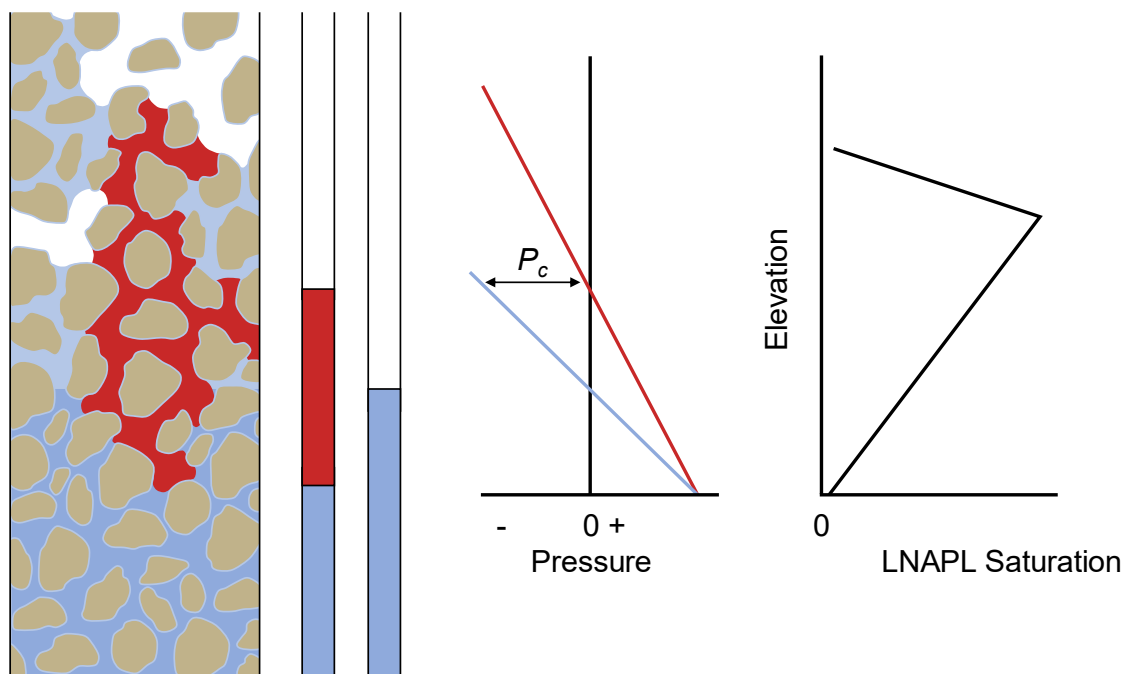


**Figure 20** - Predicting air (white), LNAPL (red) and water (blue) saturation distributions in the subsurface when the vertical equilibrium condition exists.

The LNAPL saturation distribution with height typically has a “shark fin” shape as shown in Figure 20, which is consistent with what is found in field investigations. Once the total liquid and water saturation distributions are known, then the LNAPL relative permeability distribution can be calculated using Equation Box (1-10).

From the LNAPL saturation and relative permeability distributions, the LNAPL volume and the LNAPL transmissivity can be predicted, which is useful information for planning LNAPL cleanup operations. Such analyses have been developed by Farr and others (1990) and Lenhard and Parker (1990). Later, Lenhard and others (2017) expanded the approach to predict the distributions of free, entrapped, and residual LNAPL saturations from the historic fluid levels in wells.

The work of Farr and others (1990) and Lenhard and Parker (1990) showed that when LNAPL collects above the water-saturated capillary fringe, an LNAPL layer with  $S_n = 1$  does not develop as some earlier investigators assumed. Instead, above the water-saturated capillary fringe, the LNAPL saturation varies depending on the air-LNAPL and LNAPL-water capillary pressures.

The amount of LNAPL at any location above the water-saturated capillary fringe will be a function of the shape of the capillary pressure-saturation curves. If the curves are relatively flat, indicating a significant volume of similar pore sizes, then there can be a high LNAPL saturation (greater than 80 percent of pore space) above the water-saturated capillary fringe. Uniform sands (i.e., sands with similarly sized grains) are likely to have uniform pore sizes. If the shape of the curves is more gradual, indicating the pores sizes are not uniform, then there will not be such a high LNAPL saturation above the

water-saturated capillary fringe; there will be a more gradual change in LNAPL saturation with height. Regardless of the shape of the capillary pressure-saturation curves, water will be present above the water-saturated capillary fringe and there will be no zone where the LNAPL saturation is equal to 1.

The approach to determine NAPL saturation and relative permeability distributions when the vertical equilibrium condition applies is only applicable for LNAPLs. A fluctuating water table will move LNAPL vertically, causing LNAPL and air to become entrapped during a rising water table and releasing entrapped LNAPL during a falling water table. This process can result in a *smear zone* as described by LNAPL remediation practitioners, where LNAPL can be present above and below the water table as a combination of free, residual, and entrapped LNAPL and distributed over a larger depth interval than would be predicted under hydrostatic conditions.

In addition, the formation of a smear zone can be affected by other processes including biological activity and changing LNAPL composition and fluid properties over time. Free LNAPL will not enter a monitoring well screen unless the LNAPL pressure is greater than atmospheric pressure but may enter the sand pack surrounding the monitoring well by capillary forces. The LNAPL will be contained in the pore spaces of the sand pack because of capillary forces when the LNAPL pressure is less than atmospheric.

## 5.4 Relevant Exercises

The following exercises provide the reader with an opportunity to work with the material presented in this section.

[Exercise 8](#) asks the reader to calculate fluid saturations related to LNAPL in a three-fluid system.

[Exercise 9](#) asks the reader to calculate total liquid saturations, water saturations and LNAPL saturations as a function of elevation based on measurements of LNAPL in a monitoring well.

## 6 Visual Examples of DNAPL and LNAPL Migration

Practitioners infer NAPL behavior from site history, the analysis of soil and groundwater samples, inspection of fluids in monitoring wells and soil cores, data from geophysical surveys, and information concerning site geology and hydrogeology. These site-specific data are complemented by laboratory experiments and numerical models, in simplified settings, that are used to investigate NAPL migration and build a fundamental and transferable understanding of the governing processes.

In the spirit of the tank experiments performed by Schwille (1981), two laboratory-scale demonstrations are presented here to illustrate key aspects of DNAPL and LNAPL migration.

### 6.1 DNAPL Migration through Heterogeneous Sand

In this demonstration, approximately 350 mL of PCE DNAPL was released into a water-saturated, coarse-sand layer near the top of a heterogeneous sand pack in a 1.5 m x 1.5 m x 2 cm flow cell (Figure 21). The flow cell was made from glass walls sealed to a stainless-steel frame and was backlit to promote clear observation of the fluids over the entire thickness of the pack (perpendicular to the glass walls). This backlit technique is commonly referred to as the light transmission method (Tidwell & Glass, 1995; Niemet & Selker, 2001).

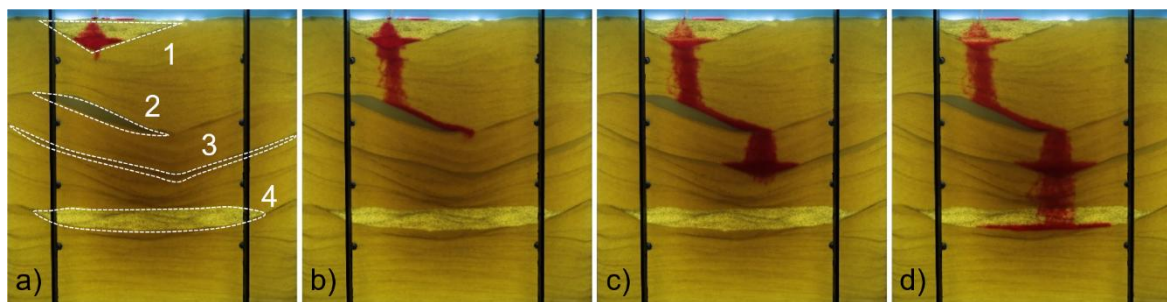


**Figure 21** - Selected images from a release of PCE DNAPL (red) into a) water-saturated heterogeneous sand showing b) migration along and c) breakthrough of capillary barriers before d) accumulating in a coarse sand lens. Numbered features are described in the text. Black vertical bars are supports on the outside of the front glass wall. Darker region in the middle portion of the sand is caused by variation in lighting. [A video of the PCE DNAPL release is available here](#).

The PCE DNAPL was dyed using Oil-Red-O so that it appeared distinct from the water. Three sand sizes were used and appear as different colors in Figure 21, with finer sand appearing darker when backlit. Capillary pressure-saturation curves for these sands are shown in Figure 13b (top-most and two bottom-most curves).

The four key features of the heterogeneous pack are

1. a triangular layer of coarse sand that contained the release point,
2. a sloping, discontinuous capillary barrier of fine sand,
3. a continuous capillary barrier of fine sand, and
4. a lens of coarse sand.

These features are surrounded by medium sand (Figure 21 includes the numbered features). Layering of the medium sand during packing created minor spatial differences in sand properties.

Once released into the triangular coarse sand, the PCE accumulated as a pool on the underlying medium sand until it accumulated to its critical pool height (Figure 21a). After breakthrough into the medium sand, the PCE migrated downward until it encountered the discontinuous sloping capillary barrier of fine sand. Unable to overcome the entry pressure of that capillary barrier, the PCE migrated laterally to the right along the top of the barrier (Figure 21b). As additional PCE was released, downward migration continued past the sloping capillary barrier and accumulated on the continuous fine-sand capillary barrier below. There, the PCE accumulated as a pool (Figure 21c). Importantly, because of the geometry of these barriers, this pool was not underneath the release point, which is a common finding at DNAPL-impacted sites.

After the DNAPL accumulated to a height equal to the critical pool height of the continuous capillary barrier, DNAPL continued to migrate downward. That migration was not stopped at the top of the coarse sand lens because the entry pressure of that sand is less than that of the medium sand above it. An additional PCE pool was formed at the base of the coarse sand lens, with the medium sand acting as a capillary barrier similar to the release in the triangular coarse sand surrounding the release point (Figure 21d). It is important to note that although the PCE was able to continue its migration after the release was stopped, a PCE pool remained in the triangular coarse sand at a height lower than the critical pool height, which is defined by the terminal pressure rather than the displacement pressure of the medium sand.

Overall, Figure 21 (and the accompanying video) highlights the importance of capillary barriers in controlling DNAPL migration, which results in the formation of both residual and pools. In this case, capillary barriers were created using sands that differed in their permeabilities by only one order-of-magnitude. Greater differences are typically encountered at most field sites. The result is that DNAPL must move laterally to move downward, either by flowing along and around discontinuous barriers or accumulating and breaking through barriers after reaching the critical pool height.

## 6.2 LNAPL Migration Followed by a Water Table Fluctuation

In this demonstration, approximately 1,000 mL of heptane LNAPL was released above the water table and into a homogeneous medium sand pack in the same 1.5 m x 1.5 m x 2 cm flow cell that was described in Section 6.1 (Figure 22). The water table was set at the top of the sand during sand emplacement but was lowered below the release point prior to heptane emplacement. Therefore, the water above the water table is on a drainage pathway when the LNAPL is introduced, with all water saturations greater than or equal to the residual water saturation.

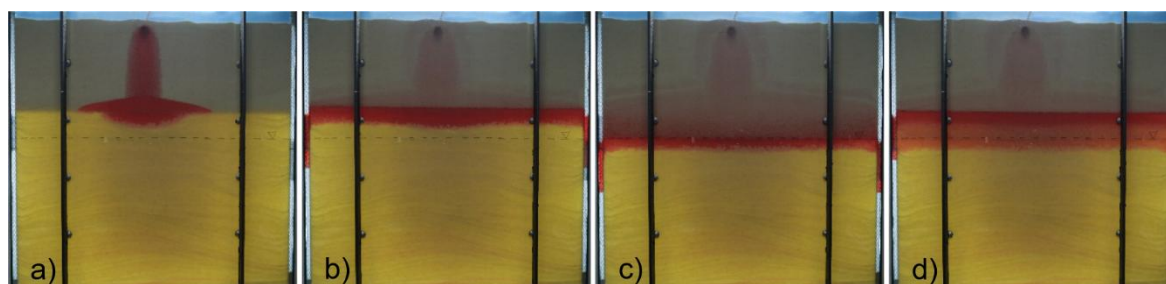


**Figure 22** - Selected images from a release of heptane LNAPL (red) into an unsaturated homogeneous sand pack (darker grey) above a water-saturated homogeneous sand pack (yellow) showing a) downward migration to and pooling along the capillary fringe with b) further migration towards the water table, followed by c) lowering and d) raising the water table to create a smear zone. Black vertical bars are supports on the front glass wall. The original water table position is marked by a dashed black line drawn on the glass wall. Clear wells along the edges of the cell appear lighter. Darker region in the middle portion of the sand is caused by variation in lighting. [A video of the heptane LNAPL release is available here](#) .

The difference between unsaturated sand and water-saturated sand can be seen in the backlit images of Figure 22, with the unsaturated sand appearing as a darker grey and the water-saturated sand (both below the water table and in the capillary fringe) appearing as yellow. The abrupt change in water saturation is a result of the uniformity of the sand and the relatively shallow capillary pressure-saturation curve (Figure 13b).

As in the PCE demonstration described in Section 6.1, the heptane was dyed using Oil-Red-O so that it appeared distinct from the water. During the demonstration, the water table was lowered and then raised by extracting or injecting water from ports in the bottom of the cell. Heptane released in the unsaturated zone migrated downward as the intermediate wetting fluid until reaching the capillary fringe where it began to pool. Importantly, this pooling does not occur at the water table because the capillary fringe is also water-saturated. Once pooling began, the heptane moved laterally along the capillary fringe and continued to move downward toward the water table as heptane accumulated and heptane pressure increased (Figure 22a). Relatively early in the heptane release—and only beneath the release point—the heptane pressure exceeded that of water and displaced some water from the capillary fringe.

Under field conditions, within a larger domain and for a greater volume of LNAPL released, LNAPL can penetrate below the water table. This highlights the oversimplification of early conceptual models of LNAPL migration, which assumed that LNAPL pooled as a “pancake” on the water table. In fact, LNAPL presence above and below the water table is common, just as most of an iceberg is beneath the ocean’s surface.

Continued heptane release was followed by redistribution and further lateral migration. After the release stopped, the LNAPL below the release point transitioned to LNAPL residual as LNAPL drained and was replaced by air. This residual appears as a lighter red color in the unsaturated zone below the release point (Figure 22b). Continued lateral migration resulted in heptane entry into wells along the edges of the flow cell (Figure 22b). This was possible because the LNAPL pressure was positive (greater than atmospheric), which allowed entry through the well screen.

If monitoring wells are installed through a LNAPL source that has reached hydrostatic equilibrium, the lack of further LNAPL migration into the well or the lack of LNAPL in the well does not indicate a lack of LNAPL presence in the adjacent (subsurface) material. LNAPL can be held in the pore space by capillary forces in the capillary fringe and above, and not enter a well because the LNAPL pressure is negative. Within the wells, it is important to note that the water table does not coincide with the air–LNAPL interface or the LNAPL–water interface. The LNAPL–water interface in a well is the elevation where the LNAPL and water pressures are equal (the LNAPL–water capillary pressure is zero), not where the water pressure is zero (the water table).

Following redistribution, the water table was lowered (Figure 22c) and raised (Figure 22d). Pooled heptane was mobilized downward, leaving LNAPL residual in its previous location. In turn, only a fraction of the heptane returned to that location as the water table was raised, with a portion remaining at lower elevations as water-occluded LNAPL. This “smearing” of the LNAPL source by lowering and raising the water table creates an LNAPL source that is deeper than the source created by the initial release (Figure 22b versus Figure 22d) with greater LNAPL–water interfacial area, which enhances dissolution.

Overall, Figure 22 (and the accompanying video) highlights the importance of water saturation in controlling LNAPL migration, with primarily downward migration under unsaturated conditions where LNAPL is the intermediate wetting fluid and lateral migration and pooling when encountering water-saturated conditions in the capillary fringe. It should not be assumed that LNAPL pools exist solely at the water table; LNAPL can exist both above and below the water table. This is exacerbated by water table fluctuations that create a smear zone of residual LNAPL above and/or water-occluded LNAPL below an original LNAPL pool. This sensitivity to water saturation can be further complicated by heterogeneity in permeability and entry pressure (e.g., grain size) which also influences capillary forces in three-fluid (air–LNAPL–water) systems (e.g., Schroth et al., 1998; Wipfler et al., 2004).

## 7 Summary

Understanding the flow of NAPL in porous media is an important component of the conceptual models that are foundational to the investigation and remediation of soil and groundwater following the release of LNAPL or DNAPL to the subsurface, many of which are hazardous industrial chemicals. NAPL flow is dictated by a combination of porous media and fluid properties, notably interfacial tension and wettability, that define the difference in pressure between two fluids (capillary pressure).

Relationships between capillary pressure, the curvature of fluid-fluid interfaces, and pore geometry result in the preferential entry of NAPL into a sub-set of the (larger) pores, which leads to complex distributions of NAPL that are controlled primarily by geological features, particularly capillary barriers that cause NAPL to spread laterally and form NAPL pools. These relationships also lead to increased occupancy of the pore space (saturation) by NAPL with increasing capillary pressure, and non-linear relationships between saturation and the resistance to fluid flow (relative permeability). Importantly, these relationships depend on the saturation history and direction of change (hysteresis), leading to non-uniqueness and the formation of trapped, discontinuous NAPL blobs (NAPL residual).

Where air is present in addition to NAPL and water, other forms of immobile NAPL are created, which include films and wedges as well as water-occluded NAPL. This book presents an introduction to these important concepts, including conceptual models used to plan the investigation and remediation of NAPL-impacted sites and many of the mathematical expressions that form the basis of numerical models used to simulate multiphase flow relevant to those sites.

## 8 Exercises

### Exercise 1

What are some examples of hazardous liquids you might have in your home? Which of these are non-aqueous phase liquids? Are they LNAPLs or DNAPLs?

[Solution to Exercise 1](#) ↴

[Return to where text linked to Exercise 1](#) ↴

### Exercise 2

Provide two examples of activities or sites associated with DNAPL releases.

[Solution to Exercise 2](#) ↴

[Return to where text linked to Exercise 2](#) ↴

### Exercise 3

Why are NAPLs at field sites often found to be multicomponent NAPLs?

[Solution to Exercise 3](#) ↴

[Return to where text linked to Exercise 3](#) ↴

### Exercise 4

Using information in Tables 1 and 2, what is the minimum volume of water required to dissolve: (a) 1 L of benzene and (b) 1 L of 1-2-dichloroethane?

[Solution to Exercise 4](#) ↴

[Return to where text linked to Exercise 4](#) ↴

### Exercise 5

Sketch three capillary pressure-saturation curves for the same medium but for three fluid pairs with different interfacial tensions.

[Solution to Exercise 5](#) ↴

[Return to where text linked to Exercise 5](#) ↴

## Exercise 6

The displacement pressure for air–water in a sand is measured to be 4,000 Pa. Estimate the displacement pressure for NAPL–water if the NAPL–water interfacial tension is 25 mN/m and the air–water interfacial tension is 72 mN/m.

[Solution to Exercise 6](#) ↴

[Return to where text linked to Exercise 6](#) ↴

## Exercise 7

Consider a 1 m thick DNAPL pool in sand above a silt lens. The top of the pool is 1.5 m below the water table and the top of the lens is 2.5 m below the water table. You know that:

The DNAPL–water displacement pressure in the sand is 3,000 Pa.

The DNAPL–water displacement pressure in the silt is 6,000 Pa.

The DNAPL density is 1.15 g cm<sup>3</sup>.

- What is the DNAPL pressure at the top of the pool?
- What is the DNAPL pressure at the bottom of the pool?
- What is the capillary pressure at the bottom of the pool?
- What pool height is required for DNAPL to invade the silt lens?

[Solution to Exercise 7](#) ↴

[Return to where text linked to Exercise 7](#) ↴

## Exercise 8

Consider a DNAPL pool within a sand that has accumulated on a silt lens. The top of the lens is located 10 m below the water table. The sand has an air–water displacement pressure of 2,500 Pa and the silt has an air–water displacement pressure of 6,900 Pa. The sand can be characterized by a Brooks-Corey  $P_c$ - $S_w$  function for DNAPL-water with a pore-size distribution index of 2.5 and a residual water saturation of 0.10. Assume the pool exists under drainage conditions and that it exists at its maximum height. Assume that the air-water interfacial tension is 72 mN/m and the DNAPL-water interfacial tension is 20 mN/m. Assume that the DNAPL density is 1.46 g/cm<sup>3</sup>.

- Plot the water and DNAPL pressures versus elevation above the top of the silt lens.
- Plot the water and DNAPL saturations versus elevation above the top of the silt lens.

[Solution to Exercise 8](#) ↴

[Return to where text linked to Exercise 8](#) ↴

## Exercise 9

Consider an LNAPL-impacted site where LNAPL has been detected in a monitoring well. The LNAPL thickness in the well is 40 cm, and the LNAPL–water interface in the well ( $z_{nw}$ ) is 100 cm above the datum [i.e., the air–LNAPL interface ( $z_{an}$ ) is 140 cm above the datum]. Analysis of the LNAPL shows that it has a density of  $700 \text{ kg/m}^3$  ( $\rho_n$ ), an LNAPL–water interfacial tension of  $0.030 \text{ N/m}$ , and an air–LNAPL interfacial tension of  $0.035 \text{ N/m}$ . Assume the water density is  $1,000 \text{ kg/m}^3$ . The monitoring well has been installed in a sandy soil that has an estimated porosity of  $0.43$ . Previous laboratory testing on this soil showed that the air–water capillary pressure–saturation relationship can be described by the van Genuchten equation, with  $\alpha_{aw} = 0.145 \text{ cm}^{-1}$ ,  $n = 2.68$ ,  $m = 1 - 1/n$ , and  $S_{rw} = 0.05$  (Carsel & Parrish, 1988).

- What will be the elevation of the air–water interface in a nearby monitoring well that does not contain LNAPL?
- Estimate the scaling factors  $\beta_{nw}$  and  $\beta_{an}$  for this LNAPL.
- Estimate the total liquid saturations ( $S_t$ ) and water saturations ( $S_w$ ) at elevations of 80 to 200 cm above the datum. Note that for negative air–LNAPL capillary pressure  $S_t = 1$  and for negative LNAPL–water capillary pressure  $S_w = 1$ . The air pressure can be assumed to be atmospheric.
- Plot the LNAPL saturations, calculated as the difference between the total saturations and water saturations ( $S_n = S_t - S_w$ ), as a function of elevation for 80 to 200 cm above the datum.
- Repeat parts (c) and (d) for the same LNAPL, LNAPL thickness and elevation of the LNAPL–water interface, but for a sandy clay soil with  $\alpha_{aw} = 0.03 \text{ cm}^{-1}$ ,  $n = 1.3$ ,  $m = 1 - 1/n$ , and  $S_{rw} = 0.10$ . How do the LNAPL saturations compare to those calculated in part (d)?

[Solution to Exercise 9](#) ↴

[Return to where text linked to Exercise 9](#) ↴

## 9 References

- Adamson, A. W. (1990). *Physical chemistry of surfaces* (5th ed.). John Wiley & Sons.
- Amyx, J. W., Bass, D. M., & Whiting, R. L. (1960). *Petroleum reservoir engineering: Physical properties*. McGraw-Hill.  
[https://books.google.com.br/books/about/Petroleum\\_Reservoir\\_Engineering\\_Physical.html?id=4rcAAAIAAJ&redir\\_esc=y](https://books.google.com.br/books/about/Petroleum_Reservoir_Engineering_Physical.html?id=4rcAAAIAAJ&redir_esc=y).
- Anderson, W. G. (1987). Wettability literature survey - Part 4: Effects of wettability on capillary pressure. *Journal of Petroleum Technology*, 39(10), 1283–1300.  
<https://doi.org/10.2118/15271-PA>.
- Brooks, R. H., & Corey, A.T. (1966). Properties of porous media affecting fluid flow. *Journal of the Irrigation and Drainage Division, American Society of Civil Engineers*, 92(2), 61–88,  
<https://ascelibrary.org/doi/10.1061/JRCEA4.0000425>.
- Brown, H. W. (1951). Capillary pressure investigations. *Journal of Petroleum Technology*, 3(3), 67–74. <https://doi.org/10.2118/951067-G>.
- Burdine, N. T. (1953). Relative permeability calculations from pore size distribution data. *Journal of Petroleum Technology*, 5(3), 71–78. <https://doi.org/10.2118/225-G>.
- Carsel, R. F., & Parrish, R. S. (1988). Developing joint probability distributions of soil water retention characteristics. *Water Resources Research*, 24(5), 755–769.  
<https://doi.org/10.1029/WR024i005p00755>.
- Cohen, R. M., & Mercer, J. W. (1993). *DNAPL site evaluation – Project summary* (EPA/600/R-93/022). US Environmental Protection Agency.  
[https://cfpub.epa.gov/si/si\\_public\\_record\\_report.cfm?Lab=NRMRL&dirEntryId=126385](https://cfpub.epa.gov/si/si_public_record_report.cfm?Lab=NRMRL&dirEntryId=126385).
- Corey, A. T. (1994). *Mechanics of immiscible fluids in porous media*. Water Resources Publications. <https://books.google.com.br/books>.
- Darcy, H. (1856). *Les Fontaines publiques de la ville de Dijon* [The public fountains of the City of Dijon]. Dalmont.
- Deng, W., Balhoff, M., & Cardenas, M. B. (2015). Influence of dynamic factors on nonwetting fluid snap-off in pores. *Water Resources Research*, 51(11), 9182–9189.  
<https://doi.org/10.1002/2015WR017261>.
- Dobson, R., Schroth, M. H., & Zeyer, Z. (2007). Effect of water-table fluctuation on dissolution and biodegradation of a multi-component, light non-aqueous phase liquid. *Journal of Contaminant Hydrology*, 94(3–4), 235–248.  
<https://doi.org/10.1016/j.jconhyd.2007.07.007>.
- Dullien, F. A. L. (1992). *Porous media: Fluid transport and pore structure* (2nd ed.). Elsevier.  
<https://www.elsevier.com/books/porous-media/brenner/978-0-12-223651-8>.

- Dussan, E. B., V. (1979). Spreading of liquids on solid surfaces: Static and dynamic contact lines. *Annual Review of Fluid Mechanics*, 11, 371–400.  
<https://doi.org/10.1146/annurev.fl.11.010179.002103>.
- Dwarakanath, V., Jackson, R. E., & Pope, G. A. (2002). Influence of wettability on the recovery of NAPLs from alluvium. *Environmental Science & Technology*, 36(2), 227–231. <https://doi.org/10.1021/es011023w>.
- Essaid, H. I., Bekins, B. A., & Cozzarelli, I. M. (2015). Organic contaminant transport and fate in the subsurface: Evolution of knowledge and understanding. *Water Resources Research*, 51(7), 4861–4906. <https://doi.org/10.1002/2015WR017121>.
- Ewing, R. P., & Berkowitz, B. (1998). A generalized growth model for simulating initial migration of dense non-aqueous phase liquids. *Water Resources Research*, 34(4), 611–622. <https://doi.org/10.1029/97WR03754>.
- Farr, A. M., Houghtalen, R. J., & McWhorter, D. D. (1990). Volume estimation of light nonaqueous phase liquids in porous media. *Groundwater*, 28(1), 48–56.  
<https://doi.org/10.1111/j.1745-6584.1990.tb02228.x>.
- Gerhard, J. I., & Kueper, B. H. (2003). Capillary pressure characteristics necessary for simulating DNAPL infiltration, redistribution, and immobilization in saturated porous media. *Water Resources Research*, 39(8).  
<https://doi.org/10.1029/2002WR001270>.
- Hillel, D. (1980). *Fundamental of soil physics*. Academic Press.
- Hofstee, C., Oostrom, N., Dane, J. H., & Walker, R.C. (1998). Infiltration and redistribution of perchloroethylene in partially saturated, stratified porous media. *Journal of Contaminant Hydrology*, 34(4), 293–313.  
[https://doi.org/10.1016/S0169-7722\(98\)00101-6](https://doi.org/10.1016/S0169-7722(98)00101-6).
- Honarpour, M., Koederitz, L., & Harvey, A. H. (1986). *Relative permeability of petroleum reservoirs*. CRC Press. <https://doi.org/10.1201/9781351076326>.
- Jackson, R. E., Dwarakanath, V., Ewing, J. E., & Avis, J. (2006). Migration of viscous non-aqueous phase liquids (NAPLs) in alluvium, Fraser River lowlands, British Columbia. *Canadian Geotechnical Journal*, 43(7), 694–703.  
<https://doi.org/10.1139/t06-034>.
- Korteland, S., Botterro, S., Hassanizadeh, S. M., & Berentsen, C. W. J. (2009). What is the correct definition of average pressure? *Transport in Porous Media*, 84, 153–175.  
<https://doi.org/10.1007/s11242-009-9490-2>.
- Kueper, B. H. (1996). *Water-saturated laboratory sand box experiment* [Unpublished photograph]. Department of Civil Engineering, Queen’s University.
- Kueper, B. H. (1989). *The behaviour of dense, non-aqueous phase liquid contaminants in heterogeneous porous media* (Doctoral dissertation, University of Waterloo).

- Kueper, B. H., & Davies, K. L. (2009). *Assessment and delineation of DNAPL source zones at hazardous waste sites* (EPA/600/R-09/119). US Environmental Protection Agency. [https://cfpub.epa.gov/si/si\\_public\\_record\\_report.cfm?Lab=NRMRL&dirEntryId=214252](https://cfpub.epa.gov/si/si_public_record_report.cfm?Lab=NRMRL&dirEntryId=214252).
- Kueper, B. H., & Frind, E. O. (1988). An overview of immiscible fingering in porous media. *Journal of Contaminant Hydrology*, 2(2), 95–110. [https://doi.org/10.1016/0169-7722\(88\)90001-0](https://doi.org/10.1016/0169-7722(88)90001-0).
- Kueper, B. H., & Frind, E. O. (1991). Two-phase flow in heterogeneous porous media 1. Model development. *Water Resources Research*, 27(6), 1049–1057. <https://doi.org/10.1029/91WR00266>.
- Kueper, B. H., & Gerhard, J. I. (2014). Hydraulic displacement of dense nonaqueous phase liquids. In B. H. Kueper, H. F. Stroo, C. M. Vogel, & C. H. Ward (Eds.), *Chlorinated solvent source zone remediation* (pp. 219–257). Springer. <https://doi.org/10.1007/978-1-4614-6922-3>.
- Kueper, B. H., Redman, D., Starr, R. C., Reitsma, S., & Mah, M. (1993). A field experiment to study the behavior of tetrachloroethylene below the water table: Spatial distribution of residual and pooled DNAPL. *Groundwater*, 31(5), 756–766. <https://doi.org/10.1111/j.1745-6584.1993.tb00848.x>.
- Kueper, B. H., Wealthall, G. P., Smith, J. W. N., Leharne, S. A., & Lerner, D. N. (2003). *An illustrated handbook of DNAPL transport and fate in the subsurface. Prepared for the United Kingdom Environment Agency* (R&D Publication 133). [dnapl handbook final.pdf](#).
- Kueper, B. H., Stroo, H. F., Vogel, C. M., & Ward, C. H. (Eds.). (2014). *Chlorinated solvent source zone remediation*. Springer. <https://doi.org/10.1007/978-1-4614-6922-3>.
- Leij, F. J., Alves, W. J., van Genuchten, M. Th., & Williams, J. R. (1996). *The UNSODA unsaturated soil hydraulic database - User's manual version 1.0* (EPA/600/R-96/095). US Environmental Protection Agency. [https://nepis.epa.gov/The\\_UNSDA\\_unsaturated\\_soil\\_hydraulic\\_database\\_user's\\_manual\\_version\\_1.0](https://nepis.epa.gov/The_UNSDA_unsaturated_soil_hydraulic_database_user's_manual_version_1.0).
- Lenhard, R. J., & Brooks, R. H. (1985). Comparison of liquid retention curves with polar and non-polar liquids. *Soil Science Society of America Journal*, 49(4), 816–821. <https://doi.org/10.2136/sssaj1985.03615995004900040005x>.
- Lenhard, R. J., & Oostrom, M. (1998). A parametric model for predicting relative permeability-saturation-capillary pressure relationships of oil-water systems in porous media with mixed wettability. *Transport in Porous Media*, 31(April), 109–131. <https://link.springer.com/article/10.1023/A:1006503406056>.

- Lenhard, R. J., & Parker, J. C. (1987a). Measurement and prediction of saturation-pressure relationships in three phase porous media systems. *Journal of Contaminant Hydrology*, 1(4), 407–424. [https://doi.org/10.1016/0169-7722\(87\)90017-9](https://doi.org/10.1016/0169-7722(87)90017-9).
- Lenhard, R. J., & Parker, J.C. (1987b). A model for hysteretic constitutive relations governing multiphase flow. 2. Permeability-saturation relations. *Water Resources Research*, 23(12), 2197–2206. <https://doi.org/10.1029/WR023i012p02197>.
- Lenhard, R. J., & Parker, J. C. (1988). Experimental validation of the theory for extending two phase saturation-pressure relations to three fluid phase systems for onotonic drainage paths. *Water Resources Research*, 24(3), 373–380. <https://doi.org/10.1029/WR024i003p00373>.
- Lenhard, R. J., & Parker, J. C. (1990). Estimation of free hydrocarbon volume from fluid levels in monitoring wells. *Groundwater*, 28(1), 57–67. <https://doi.org/10.1111/j.1745-6584.1990.tb02229.x>.
- Lenhard, R. J., Parker, J. C., & Mishra, S. (1989). On the correspondence between Brooks-Corey and van Genuchten models. *Journal of Irrigation and Drainage Engineering*, 115(4), 744–751.
- Lenhard, R. J., Oostrom, M., & Dane, J. H. (2002). Multi-fluid flow. In J. H Dane & G. C. Topp (Eds.), *Methods of soil analysis, part 4 - Physical methods* (p. 1596). Soil Science Society of America. [https://doi.org/10.1061/\(ASCE\)0733-9437\(1989\)115:4\(744\)](https://doi.org/10.1061/(ASCE)0733-9437(1989)115:4(744)).
- Lenhard, R. J., Oostrom, M., & Dane, J. H. (2004). A constitutive model for air–APL–water flow in the vadose zone accounting for immobile non-occluded (residual) NAPL in strongly water-wet porous media. *Journal of Contaminant Hydrology*, 73(1–4), 283–304. <http://doi.org/10.1016/j.jconhyd.2004.07.005>.
- Lenhard, R. J., Rayner, J. L., & Davis, G. B. (2017). A practical tool for estimating subsurface LNAPL distributions and transmissivity using current and historical fluid levels in groundwater wells: Effects of entrapped and residual LNAPL. *Journal of Contaminant Hydrology*, 205(October), 1–11. <https://doi.org/10.1016/j.jconhyd.2017.06.002>.
- Leverett, M. C. (1941). Capillary behavior in porous solids. *Transactions of the AIME*, 142(01), 152–169. <https://doi.org/10.2118/941152-G>.
- Longino, B. L., & Kueper, B. H. (1995). The use of upward gradients to arrest downward DNAPL migration in the presence of solubilizing surfactants. *Canadian Geotechnical Journal*, 32(2), 296–308. <https://doi.org/10.1139/t95-031>.
- Longino, B. L., & Kueper, B. H. (1999). Non-wetting phase retention and mobilization in rock fractures. *Water Resources Research*, 35(7), 2085–2093. <https://doi.org/10.1029/1999WR900100>.

- Mercer, J. W., & Cohen, R. M. (1990). A review of immiscible fluids in the subsurface: Properties, models, characterization and remediation. *Journal of Contaminant Hydrology*, 6(2), 107–163. [https://doi.org/10.1016/0169-7722\(90\)90043-G](https://doi.org/10.1016/0169-7722(90)90043-G).
- Morrow, N. R. (1976). Capillary pressure correlations for uniformly wetted porous media. *Journal of Canadian Petroleum Technology*, 15(4), 49–69. <https://doi.org/10.2118/76-04-05>.
- Morrow, N. R. (1990). Wettability and its effect on oil recovery. *Journal of Canadian Petroleum Technology*, 42(12), 1476–1484. <https://doi.org/10.2118/21621-PA>.
- Mualem, Y. (1976). A new model for predicting the hydraulic conductivity of unsaturated porous media. *Water Resources Research*, 12(3), 513–522. <https://doi.org/10.1029/WR012i003p00513>.
- Niemet, M. R., & Selker, J. S. (2001). A new method for quantification of liquid saturation in 2D translucent porous media systems using light transmission. *Advances in Water Resources*, 24(6), 651–666.
- Pankow, J. F., & Cherry, J. A. (1996). *Dense chlorinated solvents and other DNAPLs in groundwater*. Waterloo Press. <https://gw-project.org/books/dense-chlorinated-solvents-and-other-dnapls-in-groundwater/>.
- Parker, J. C., & Lenhard, R. J. (1987). A model for hysteretic constitutive relations governing multiphase flow. 1. Saturation-pressure relations. *Water Resources Research*, 23(12), 2187–2196. <https://doi.org/10.1029/WR023i012p02187>.
- Parker, J. C., Lenhard, R. J., & Koppusamy, T. A. (1987). Parametric model for constitutive properties governing multiphase flow in porous media. *Water Resources Research*, 23(4), 618–624. <https://doi.org/10.1029/WR023i004p00618>.
- Ramirez-Corredores, M. M. (2017). *The science and technology of unconventional oils: Finding refining opportunities*. Academic Press. <https://www.sciencedirect.com/book/9780128012253/the-science-and-technology-of-unconventional-oils>.
- Richards, L. A. (1931). Capillary conduction of liquids through porous mediums. *Physics*, 1(5), 318–333. <https://doi.org/10.1063/1.1745010>.
- Rivett, M. O. (Ed.), Tomlinson, D. W., Thornton, S. F., Thomas, A. O., Leharne, S. A., & Wealthall, G. P. (2014). *An illustrated handbook of LNAPL transport and fate in the subsurface*. CL:AIRE. [https://www.researchgate.net/publication/271766134\\_Illustrated\\_handbook\\_of\\_LNAPL\\_transport\\_and\\_fate\\_in\\_the\\_subsurface](https://www.researchgate.net/publication/271766134_Illustrated_handbook_of_LNAPL_transport_and_fate_in_the_subsurface).
- Rose, W., & Bruce, W. A. (1949). Evaluation of capillary character in petroleum reservoir rock. *Journal of Petroleum Technology*, 1(5), 127–142.

- <https://doi.org/10.2118/949127-G>.
- Roy, J. W., Smith, J. E., & Gillham, R. W. (2004). Laboratory evidence of natural remobilization of multicomponent DNAPL pools due to dissolution. *Journal of Contaminant Hydrology*, 74(1–4), 145–161.  
<https://doi.org/10.1016/j.jconhyd.2004.02.009>.
- Salathiel, R. A. (1973). Oil recovery by surface film drainage in mixed-wettability rocks. *Journal of Petroleum Technology*, 25(10), 1216–1224.  
<https://doi.org/10.2118/4104-PA>.
- Sale, T., Hopkins, H., & Kirkman, A. (2018). *Managing risk at LNAPL sites* (Soil and Groundwater Research Bulletin No. 18). American Petroleum Institute.  
<https://www.api.org/oil-and-natural-gas/environment/clean-water/ground-water/lnapl/lnapl-faqs>.
- Sale, T., Zimbron, J., & Dandy, D. (2008). Effects of reduced contaminant loading on downgradient water quality in an idealized two layer system. *Journal of Contaminant Hydrology*, 102(1–2), 72–85.  
<https://doi.org/10.1016/j.jconhyd.2008.08.002>.
- Schroth, M. H., Ahearn, S. J., Selker, J. S., & Istok, J. D. (1996). Characterization of Miller-similar silica sands for laboratory hydrologic studies. *Soil Science Society of America Journal*, 60(5), 1331–1339.  
<https://doi.org/10.2136/sssaj1996.03615995006000050007x>.
- Schroth, M. H., Istok, J. D., & Selker, J. S. (1998). Three-phase immiscible fluid movement in the vicinity of textural interfaces. *Journal of Contaminant Hydrology*, 32(1–2), 1–23.  
[https://doi.org/10.1016/S0169-7722\(97\)00069-7](https://doi.org/10.1016/S0169-7722(97)00069-7).
- Schwille, F. (1981). Groundwater pollution in porous media by fluids immiscible with water. *Studies in Environmental Science*, 17, 451–463.  
[https://doi.org/10.1016/S0166-1116\(08\)71937-X](https://doi.org/10.1016/S0166-1116(08)71937-X).
- Su, C., & Brooks, R. H. (1980). Water retention measurements for soils. *Journal of the Irrigation and Drainage Division, American Society of Civil Engineers*, 106(2), 105–112.  
<https://doi.org/10.1061/JRCEA4.0001295>.
- Tiab, D., & Donaldson, E. C. (1996). *Petrophysics: Theory and practice of measuring reservoir rocks and fluid transport properties*. Gulf Publishing Company.
- Tidwell, V. C., & Glass, R. J. (1994). X ray and visible light transmission for laboratory measurement of two-dimensional saturation fields in thin-slab systems. *Water Resources Research*, 30(11), 2873–2882.
- Toussaint, R., Mäløy, K. J., Méheust, Y., Løvoll, G., Jankov, M., Schäfer, G., & Schmittbuhl, J. (2012). Two-phase flow: Structure, upscaling, and consequences for macroscopic transport properties. *Vadose Zone Journal*, 11(3).

- <https://doi.org/10.2136/vzj2011.0123>.
- van Genuchten, M. Th. (1980). A closed-form equation for predicting the hydraulic conductivity of unsaturated soils. *Soil Science Society of America Journal*, 44(5), 892–898. <https://doi.org/10.2136/sssaj1980.03615995004400050002x>.
- Wildenschild, D., & Sheppard, A. P. (2013). X-ray imaging and analysis techniques for quantifying pore-scale structure and processes in subsurface porous medium systems. *Advances in Water Resources*, 51(January), 217–246. <https://doi.org/10.1016/j.advwatres.2012.07.018>.
- Wilson, J. L., Conrad, S. H., Mason, W. R., Peplinski, W., & Hagan, E. (1990). *Laboratory investigation of residual liquid organics from spills, leaks, and the disposal of hazardous wastes in groundwater* (EPA/600/6-90/004 NTIS 90-235797). US Environmental Protection Agency.
- Wipfler, E. L., Ness, M., Breedveld, G. D, Marsman, A., van der Zee, S. E. A. T. M. (2004). Infiltration and redistribution of LNAPL into unsaturated layered porous media. *Journal of Contaminant Hydrology*, 71(1–4), 47–66. <https://www.sciencedirect.com/science/article/abs/pii/S0169772203002055>.
- Woessner, W. W., & Poeter, E. P. (2020). *Hydrogeologic properties of earth materials and principles of groundwater flow*. The Groundwater Project. <https://gw-project.org/books/hydrogeologic-properties-of-earth-materials-and-principles-of-groundwater-flow/>.
- Zhou, D., & Blunt, M. (1997). Effect of spreading coefficient on the distribution of light non-aqueous phase liquid in the subsurface. *Journal of Contaminant Hydrology*, 25(1–2), 1–19. [https://doi.org/10.1016/S0169-7722\(96\)00025-3](https://doi.org/10.1016/S0169-7722(96)00025-3).
- Zogorski, J. S., Carter, J. M., Ivahnenko, T., Lapham, W. W., Moran, M. J., Rowe, B. L., Squillace, P. J., & Toccaline, P. L. (2006). *The quality of our nation's waters - Volatile organic compounds in the nation's ground water and drinking-water supply wells*. (Circular 1292). US Geological Survey. <https://pubs.usgs.gov/circ/circ1292/>.

## 10 Boxes

### Box 1 - Additional Equations for Air-NAPL-Water Systems

For air-NAPL-water systems in water-wet porous media, the air-NAPL capillary pressure governs the total liquid saturation; the ratio of the pore space volume occupied by NAPL and water to the total pore space volume (porosity) shown in Equation Box (1-1).

$$S_t = \frac{V_n + V_w}{V_v} = \frac{V_{tl}}{V_v} \quad (1-1)$$

where:

$S_t$  = total liquid saturation (dimensionless)

$V_{tl}$  = volume of the pore space occupied by NAPL and water (L<sup>3</sup>)

The effective total liquid saturation ( $\bar{S}_t$ ), similar in concept to the effective water saturation discussed in Section 3.5, is shown in Equation Box (1-2).

$$\bar{S}_t = \frac{S_w + S_n - S_{rw}}{1 - S_{rw}} \quad (1-2)$$

As addressed in Sections 3.2 and 3.3, the NAPL–water capillary pressure governs the water saturation; the ratio of the pore space volume occupied by water to the total pore space volume (porosity). The effective water saturation is defined as in Section 3.5, assuming maximum water saturation ( $S_m$ ) is equal to 1. Although the effective water saturation is commonly given the symbol  $S_e$  in two-fluid systems (Equation 16), it cannot be used in three-fluid systems. Instead, a single overbar is used in this section to indicate effective saturations as shown in Equation Box (1-3).

$$\bar{S}_w = \frac{S_w - S_{rw}}{1 - S_{rw}} \quad (1-3)$$

The effective air saturation, which also is a function of the air-NAPL capillary pressure, is illustrated by Equation Box (1-4).

$$\bar{S}_a = \frac{S_a}{1 - S_{rw}} = \frac{1 - S_t}{1 - S_{rw}} \quad (1-4)$$

where:

$S_a$  = air saturation (dimensionless)

Using only the van Genuchten (1980) equation as an example, the air-NAPL-water effective total liquid saturation in water-wet porous media is a function of the air-NAPL capillary pressure as shown by Equation Box (1-5).

$$\bar{S}_t = [1 + (\beta_{an} \alpha_{aw} P_c^{an})^n]^{-m} \quad (1-5)$$

where:

$\beta_{an}$  = air–NAPL scaling factor (dimensionless)  
 $\alpha_{aw}$  and  $n$  = van Genuchten (1980) parameters determined using nonhysteretic, air-water capillary pressure-saturation data ( $M^{-1}LT^2$  and dimensionless, respectively)

The corresponding effective water saturation is a function of the NAPL-water capillary pressure as shown by Equation Box (1-6).

$$\bar{S}_w = [1 + (\beta_{nw}\alpha_{aw}P_c^{nw})^n]^{-m} \quad (1-6)$$

where:

$\beta_{nw}$  = NAPL–water scaling factor (dimensionless)

Both Equations Box (1-5) and (1-6) were proposed by Parker and others (1987) to convert two-fluid, air-water capillary pressure-saturation relations, which are more commonly measured, to three-fluid, air-NAPL-water capillary pressure-saturation relations. The scaling factors  $\beta_{an}$  and  $\beta_{nw}$  can be determined from ratios of interfacial tensions (Lenhard & Parker, 1987a) as shown by Equation Box (1-7a) and (1-7b).

$$\beta_{an} = \frac{\sigma_{aw}}{\sigma_{an}} \quad (1-7a)$$

$$\beta_{nw} = \frac{\sigma_{aw}}{\sigma_{nw}} \quad (1-7b)$$

where:

$\sigma_{aw}$  = air-water interfacial tension ( $MT^{-2}$ )

$\sigma_{an}$  = air-NAPL interfacial tension ( $MT^{-2}$ )

$\sigma_{nw}$  = NAPL-water interfacial tension ( $MT^{-2}$ )

This scaling approach neglects contact angle, similar to Leverett (1941), whereas contact angle is included in a common version of the Leverett J-function (Dullien, 1992, Tiab & Donaldson, 1996). Alternatively, the scaling factors can be determined using nonlinear regression on air-water, air-NAPL and NAPL-water data from capillary pressure-saturation measurements, which requires substantially more effort than either measuring or relying on published interfacial tension data. Ideally, the interfacial tension measurements should be conducted after the NAPL and water have been in contact with each other for a period.

To ensure there is no discontinuity in fluid saturations as a two-fluid, air-water system transitions into a three-fluid, air-NAPL-water system in rigid porous media for spreading NAPLs, the following condition is needed (Lenhard et al, 2002) as shown by Equation Box (1–8).

$$\frac{1}{\beta_{an}} + \frac{1}{\beta_{nw}} = 1 \quad (1-8)$$

which infers:  $\sigma_{an} + \sigma_{nw} = \sigma_{aw}$

When considering hysteretic, three-fluid (air-NAPL-water) capillary pressure-saturation relations, it is useful to introduce the concept of apparent saturations. The apparent total liquid and water saturations account for entrapped air and NAPL. As a result of relative nonwetting fluid entrapment by the corresponding wetting fluid (i.e., entrapment of air by water in air–water systems, and entrapment of air by NAPL and entrapment of NAPL by water in air–NAPL–water systems), the relative wetting fluids (i.e., NAPL and water) will be displaced into larger pore spaces following the relative nonwetting fluid entrapment. This is important for predicting the mobility (relative permeabilities) of the fluids. Readers are referred to Parker and Lenhard (1987) and Lenhard and others (2004) for further information.

Air, NAPL, and water relative permeabilities as a function of fluid saturation are needed to predict fluid flow in air-NAPL-water systems. It is well accepted that the air relative permeability is a function of only the total liquid saturation, the NAPL relative permeability is a function of both the total liquid and water saturations, and the water relative permeability is a function of only the water saturation. Using the van Genuchten (1980) and Mualem (1976) equations, Parker and others (1987) calculated the air, NAPL, and water relative permeabilities for nonhysteretic capillary pressure-saturation relations as shown in Equation Box (1-9), (1-10), and (1-11).

$$k_{ra} = \bar{S}_a^{\frac{1}{2}} \left(1 - \bar{S}_t^{\frac{1}{m}}\right)^{2m} \quad (1-9)$$

$$k_{rn} = (\bar{S}_t - \bar{S}_w)^{\frac{1}{2}} \left\{ \left[1 - \bar{S}_w^{\frac{1}{m}}\right]^m - \left[1 - \bar{S}_t^{\frac{1}{m}}\right]^m \right\}^2 \quad (1-10)$$

$$k_{rw} = \bar{S}_w^{\frac{1}{2}} \left\{1 - \left[1 - \bar{S}_w^{\frac{1}{m}}\right]^m\right\}^2 \quad (1-11)$$

where:

$k_{ra}$  = air relative permeability (dimensionless)

$k_{rn}$  = NAPL relative permeability (dimensionless)

$k_{rw}$  = water relative permeability (dimensionless)

When capillary pressure-saturation hysteresis is considered, equations for predicting air, NAPL, and water relative permeabilities can be complex. Readers are referred to the literature for further information (Lenhard & Parker, 1987b).

The capillary pressure-saturation and relative-permeability/saturation relations described in this section for three-fluid air-NAPL-water systems are needed to predict the

movement of air, NAPL, and water in porous media. To predict (calculate) LNAPL distributions for evaluating potential health and environment risks or for planning remedial efforts, one needs to be able to estimate fluid saturations and relative permeabilities based on the air, NAPL, and water pressures. The capillary pressure-saturation and relative permeability-saturation relations are critical for solving the fluid flow equations for the separate fluid phases, which include those for NAPL and water presented in Section 4.3—that is, Equation (30) and Equation (31), reproduced here—as well as an additional equation for the flow of air shown as Equation Box (1–12).

$$\frac{\partial}{\partial t}(S_w \theta_T \rho_w) = \frac{\partial}{\partial x_i} \left[ \frac{k_{ij} k_{rw} \rho_w}{\mu_w} \left( \frac{\partial P_w}{\partial x_j} + \rho_w g \frac{\partial z}{\partial x_j} \right) \right] \quad (30)$$

$$\frac{\partial}{\partial t}(S_n \theta_T \rho_n) = \frac{\partial}{\partial x_i} \left[ \frac{k_{ij} k_{rn} \rho_n}{\mu_n} \left( \frac{\partial P_n}{\partial x_j} + \rho_n g \frac{\partial z}{\partial x_j} \right) \right] \quad (31)$$

$$\frac{\partial}{\partial t}(S_a \theta_T \rho_a) = \frac{\partial}{\partial x_i} \left[ \frac{k_{ij} k_{ra} \rho_a}{\mu_a} \left( \frac{\partial P_a}{\partial x_j} + \rho_a g \frac{\partial z}{\partial x_j} \right) \right] \quad (1-12)$$

These three equations are difficult to solve because the fluid pressures are linked via the capillary pressures and they must be solved simultaneously. In addition, the fluid (and possibly porous medium) properties are changing with respect to time and space.

It is important to note that although Equation (30) and Equation (31) appear as they do in Section 4.3, the solution of them here requires the three-fluid capillary pressure-saturation and relative permeability-saturation relations and not the two-fluid capillary pressure-saturation and relative permeability-saturation relations. Although the solution to these equations is complex, these equations do not account for the mass transfer of compounds between fluid phases (i.e., dissolution or vaporization), which is important for estimating long-term fate or remedial efforts.

The solution to Equations (30), (31), and (1-12) generally requires numerical methods using computers after stipulating initial and boundary conditions. One simplification to solving the set of equations is to assume that porous medium properties do not change with time.

Another is to neglect the air phase, so Equation Box (1-12) does not need to be solved. When developing an equation to predict water flow in a two-fluid, air–water system in soils, Richards (1931) assumed the air phase pressure is constant (generally assumed to be atmospheric) and the air phase does not affect water flow in a non-deformable porous medium. With these assumptions, the air flow equation—Equation Box (1-12)—is not needed. Richards' (1931) assumption, which originally pertained to two-fluid air-water systems, has been extended to air-NAPL-water systems so

only Equation (30) and Equation (31) with simplifications need to be solved simultaneously to predict NAPL and water flow and subsurface distributions. Unfortunately, assuming constant air pressure is not valid for all subsurface conditions.

The capillary pressure-saturation scaling format by Parker and others (1987) and Lenhard and Parker (1987a) minimizes the number of parameters needed to solve Equations (29) and (30). The capillary pressure-saturation and relative permeability-saturation relations needed for Equations (29) and (30) can be obtained from more easily measured air-water capillary pressure-saturation relations and interfacial tensions.

[Return to where text linked to Box 1](#)↑

# 11 Exercise Solutions

## Solution Exercise 1

There are many examples of hazardous liquids, including household cleaners that you might be familiar with, but most are solutions (e.g., bleach) and are soluble in water. The most common example of NAPLs that might be found in a home setting are petroleum fuels like gasoline and diesel, which are LNAPLs. Mineral spirits used for cleaning are another example of a common LNAPL found in homes.

[Return to Exercise 1](#) ↑

[Return to where text linked to Exercise 1](#) ↑

## Solution Exercise 2

There are many DNAPLs with a variety of uses and used by multiple industries. Therefore, DNAPL can be found at many types of sites. These include sites associated with storage tanks and fluids handling, burn pits and waste lagoons, as well as manufacturing facilities, solvent recyclers, dry cleaners, and chemical production facilities.

[Return to Exercise 2](#) ↑

[Return to where text linked to Exercise 2](#) ↑

## Solution Exercise 3

Some NAPLs, such as petroleum fuels, contain a variety of chemicals and are therefore referred to as multicomponent NAPLs. Others are created through the use of those chemicals, such as using DNAPL solvents to remove LNAPL in degreasing operations. Still others are formed through co-disposal, where multiple NAPLs are released at the same location over time.

[Return to Exercise 3](#) ↑

[Return to where text linked to Exercise 3](#) ↑

## Solution Exercise 4

The minimum volume of water required can be calculated from the maximum concentration (i.e., solubility) and the density.

$$Volume_{\text{water required to dissolve NAPL}} = \frac{(Volume_{\text{NAPL to dissolve}}) (Density_{\text{NAPL}})}{(Solubility_{\text{NAPL in water}})}$$

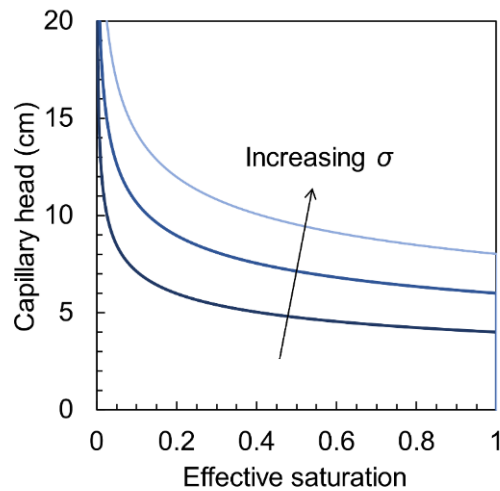
$$V_{w \text{ to dissolve benzene}} = \frac{(1 \text{ L}) \left( \frac{0.87 \text{ g}}{\text{cm}^3} \frac{1,000 \text{ cm}^3}{1 \text{ L}} \right)}{\left( \frac{1,750 \text{ mg}}{1 \text{ L}} \frac{1 \text{ g}}{1,000 \text{ mg}} \right)} = 497 \text{ L}$$

$$V_{w \text{ to dissolve 1-2-dichloroethane}} = \frac{(1 \text{ L}) \left( \frac{1.25 \text{ g}}{\text{cm}^3} \frac{1,000 \text{ cm}^3}{1 \text{ L}} \right)}{\left( \frac{8,500 \text{ mg}}{1 \text{ L}} \frac{1 \text{ g}}{1,000 \text{ mg}} \right)} = 147 \text{ L}$$

[Return to Exercise 4](#) ↑

[Return to where text linked to Exercise 4](#) ↑

## Solution Exercise 5



(a) Assume  $P_d = 8$  cm (of water) and  $\lambda = 4$

$$\therefore P_c = P_d S_e^{-1/2} \text{ (rearrangement of Equation (17))}$$

→ plot  $P_c$  for  $S_e = 0$  to 1

(b) Scale  $P_d$  using Equation (21) given:

$$P_{d1} = P_{c1} = 8 \text{ cm}$$

$$P_{d2} = P_{c2}$$

$$k_1 = k_2$$

$$\theta_{T1} = \theta_{T2}$$

$$\therefore \frac{P_{c1}}{\sigma_1} \sqrt{\frac{k_1}{\theta_{T1}}} = \frac{P_{c2}}{\sigma_2} \sqrt{\frac{k_2}{\theta_{T2}}}$$

$$P_{d2} = P_{d1} \frac{\sigma_2}{\sigma_1}$$

$$\text{Assume } \sigma_1 = 72 \frac{\text{mN}}{\text{m}} \text{ and } \sigma_2 = 54 \frac{\text{mN}}{\text{m}}$$

$$\therefore P_{d2} = 8 \text{ cm} \cdot \frac{54 \frac{\text{mN}}{\text{m}}}{72 \frac{\text{mN}}{\text{m}}} = 6 \text{ cm}$$

→ repeat (a) for  $P_d = 6$  cm

(c) Assume  $\sigma_1 = 72 \frac{\text{mN}}{\text{m}}$  and  $\sigma_2 = 36 \frac{\text{mN}}{\text{m}}$

$$\therefore P_{d2} = 8 \text{ cm} \cdot \frac{36 \frac{\text{mN}}{\text{m}}}{72 \frac{\text{mN}}{\text{m}}} = 4 \text{ cm}$$

→ repeat (a) for  $P_d = 4$  cm

[Return to Exercise 5](#) ↑

[Return to where text linked to Exercise 5](#) ↑

## Solution Exercise 6

Using Equation (20) with constant permeability and porosity; let the capillary pressures equal the displacement pressures, and let condition 1 be air–water (aw) and condition 2 be NAPL–water (nw).

$$\frac{P_{c1}}{\sigma_1} \sqrt{\frac{k_1}{\theta_{T1}}} = \frac{P_{c2}}{\sigma_2} \sqrt{\frac{k_2}{\theta_{T2}}} \text{ with } k \text{ \& } \theta \text{ constant, \& letting } P_c = P_d \quad \frac{P_{d1}}{\sigma_1} \sqrt{\frac{k}{\theta}} = \frac{P_{d2}}{\sigma_2} \sqrt{\frac{k}{\theta}}$$

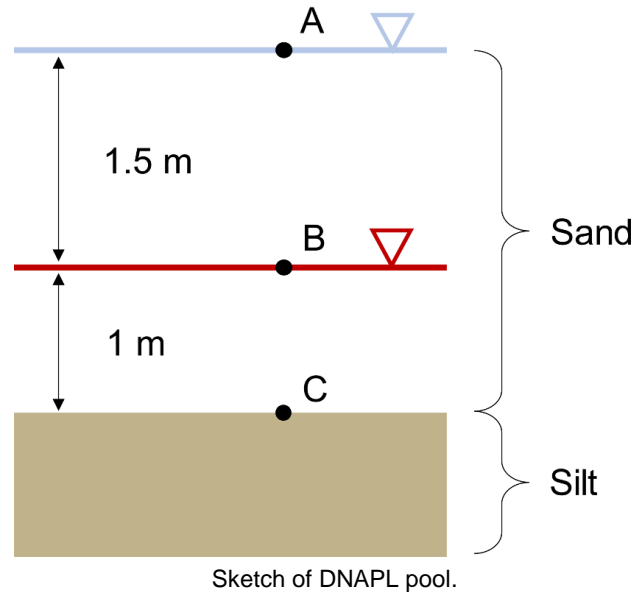
$$\begin{aligned} P_d^{nw} &= P_d^{aw} \frac{\sigma^{nw}}{\sigma^{aw}} \\ &= 4,000 \text{ Pa} \frac{25 \frac{\text{mN}}{\text{m}}}{72 \frac{\text{mN}}{\text{m}}} \\ &= 1,389 \text{ Pa} \end{aligned}$$

[Return to Exercise 6](#) ↗

[Return to where text linked to Exercise 6](#) ↗

## Solution Exercise 7

Start by sketching the DNAPL pool and identifying important locations for calculating fluid pressures (A, B, and C) as shown in this image.



- a) The water pressure at the water table (A) is defined as zero (gauge pressure) and the water pressure at the top of the DNAPL pool (B) is  $P_w^B$  (assuming hydrostatic conditions).

$$\begin{aligned}
 P_w^B &= P_w^A + \rho_w g z_{AB} \\
 &= 0 + 1 \frac{\text{g}}{\text{cm}^3} 9.81 \frac{\text{m}}{\text{s}^2} 1.5 \text{m} \frac{1 \text{kg}}{1000 \text{g}} \frac{(100)^3 \text{cm}^3}{\text{m}^3} = 14,715 \frac{\text{kg}}{\text{m s}^2} \frac{1 \text{Pa}}{1 \frac{\text{kg}}{\text{m s}^2}} \\
 &= 14,715 \text{Pa}
 \end{aligned}$$

Assuming that the capillary pressure at the top of the pool is equal to the displacement pressure in the sand, the DNAPL pressure is given by a rearranged Equation (8).

$$\begin{aligned}
 P_n^B &= P_c^B + P_w^B \\
 &= 3,000 \text{ Pa} + 14,715 \text{ Pa} \\
 &= 17,715 \text{ Pa}
 \end{aligned}$$

- b) The DNAPL pressure at the bottom of the pool (C) can also be calculated assuming hydrostatic conditions using the density of the DNAPL.

$$P_n^C = P_n^B + \rho_n g z_{BC}$$

$$\begin{aligned}
 &= 17,715 \text{ Pa} + 1.15 \frac{\text{g}}{\text{cm}^3} 9.81 \frac{\text{m}}{\text{s}^2} 1\text{m} \frac{1\text{kg}}{1000\text{g}} \frac{(100)^3 \text{cm}^3}{\text{m}^3} \frac{1\text{Pa}}{1 \frac{\text{kg}}{\text{m s}^2}} \\
 &= 17,715 \text{ Pa} + 11,281.5 \text{ Pa} = 28,996.5 \text{ Pa}
 \end{aligned}$$

- c) The water pressure at the bottom of the pool (recall that the water is present alongside the DNAPL) is calculated as for the top of the pool shown in (a).

$$\begin{aligned}
 P_w^C &= P_w^A + \rho_w g z_{AB} \\
 &= 0 + 1 \frac{\text{g}}{\text{cm}^3} 9.81 \frac{\text{m}}{\text{s}^2} 2.5\text{m} \frac{1\text{kg}}{1000\text{g}} \frac{(100)^3 \text{cm}^3}{\text{m}^3} \frac{1\text{Pa}}{1 \frac{\text{kg}}{\text{m s}^2}} \\
 &= 24,525 \text{ Pa}
 \end{aligned}$$

and the capillary pressure is:

$$\begin{aligned}
 P_c^C &= P_n^C - P_w^C \\
 &= 28,996.5 \text{ Pa} - 24,525 \text{ Pa} \\
 &= 4,471.5 \text{ Pa}
 \end{aligned}$$

- d) To invade the silt, the capillary pressure at the bottom of the pool must exceed the displacement pressure of the silt. Using Equation (32) and again assuming that the capillary pressure at the top of the pool is equal to the displacement pressure of the sand, the maximum stable pool height is as shown here.

$$\begin{aligned}
 H &= \frac{P_d^{\text{silt}} - P_d^{\text{sand}}}{\Delta \rho g} \\
 &= \frac{(6000\text{Pa} - 3000\text{Pa}) \frac{1 \frac{\text{kg}}{\text{m s}^2}}{1\text{Pa}}}{\left(1.15 \frac{\text{g}}{\text{cm}^3} - 1 \frac{\text{g}}{\text{cm}^3}\right) 9.81 \frac{\text{m}}{\text{s}^2} \frac{1\text{kg}}{1000\text{g}} \frac{(100)^3 \text{cm}^3}{1 \text{m}^3}} = 2.04\text{m}
 \end{aligned}$$

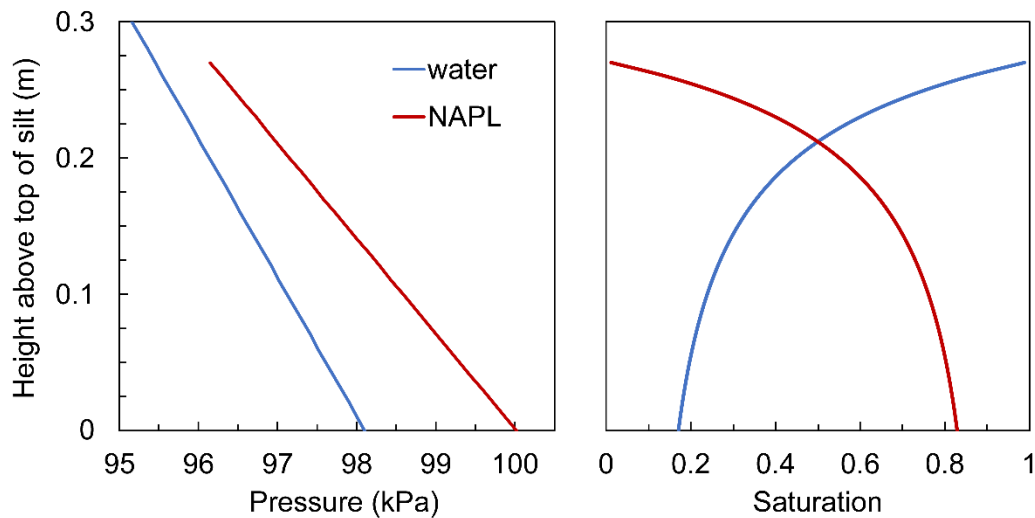
Therefore, any DNAPL pool height greater than 2.04 m will invade the silt lens.

[Return to Exercise 7](#) ↗

[Return to where text linked to Exercise 7](#) ↗

## Solution Exercise 8

Pressures and saturations are shown in this image. If your calculations do not match these values, you may want to keep working on it to sort it out or read on for an explanation of how the values were calculated.



Fluid pressure as a function of elevation above the top of the silt and corresponding water saturation.

Fluid pressures can be calculated assuming hydrostatic conditions using the same approach as shown in the solution to Exercise 7 and subsequently used to calculate capillary pressures and fluid saturations.

The water pressure at the water table is defined as zero (gauge pressure) and the water pressure at the top of the silt, 10 m below the water table is  $P_w^{top\ silt}$  (assuming hydrostatic conditions).

$$\begin{aligned}
 P_w^{top\ silt} &= P_w^{wt} + \rho_w g z_{water\ column\ above\ silt} \\
 &= 0 + 1 \frac{\text{g}}{\text{cm}^3} 9.81 \frac{\text{m}}{\text{s}^2} 10\text{m} \frac{1\text{kg}}{1000\text{g}} \frac{(100)^3 \text{cm}^3}{\text{m}^3} = 98,100 \frac{\text{kg}}{\text{m s}^2} \frac{1\text{Pa}}{1 \frac{\text{kg}}{\text{m s}^2}} \\
 &= 98,100 \text{ Pa}
 \end{aligned}$$

So, the water pressure is a straight line from 0 kPa at the water table to 98.1 kPa at the top of the silt, which is 10 m below the water table.

To estimate the NAPL-water displacement pressure for sand and silt, use Equation (21) with constant permeability and porosity, let the capillary pressures equal the displacement pressures, and let condition 1 be air-water (aw) and condition 2 be NAPL-water (nw).

$$\frac{P_{c1}}{\sigma_1} \sqrt{\frac{k_1}{\theta_{T1}}} = \frac{P_{c2}}{\sigma_2} \sqrt{\frac{k_2}{\theta_{T2}}} \text{ with } k \text{ \& } \theta \text{ constant, letting } P_c = P_d \quad \frac{P_{d1}}{\sigma_1} \sqrt{\frac{k}{\theta}} = \frac{P_{d2}}{\sigma_2} \sqrt{\frac{k}{\theta}}$$

$$P_d^{nw-sand} = P_d^{aw-sand} \frac{\sigma^{nw}}{\sigma^{aw}} = 2,500 \text{ Pa} \frac{20 \frac{mN}{m}}{72 \frac{mN}{m}} = 694 \text{ Pa}$$

$$P_d^{nw-silt} = P_d^{aw-silt} \frac{\sigma^{nw}}{\sigma^{aw}} = 6,900 \text{ Pa} \frac{20 \frac{mN}{m}}{72 \frac{mN}{m}} = 1917 \text{ Pa}$$

The maximum height of the DNAPL pool is the height that causes a capillary pressure at the top of the silt that is equal to (but not greater than) the NAPL-water displacement pressure of the silt. Using Equation (32) and assuming that the capillary pressure at the top of the pool is equal to the displacement pressure of the sand, the maximum pool height is  $H$  as shown here.

$$H = \frac{P_d^{silt} - P_d^{sand}}{\Delta\rho_{nw}g}$$

$$= \frac{(1,917 \text{ Pa} - 794 \text{ Pa}) \frac{1 \frac{\text{kg}}{\text{m s}^2}}{1 \text{ Pa}}}{\left(1.46 \frac{\text{g}}{\text{cm}^3} - 1 \frac{\text{g}}{\text{cm}^3}\right) 9.81 \frac{\text{m}}{\text{s}^2} \frac{1 \text{ kg}}{1000 \text{ g}} \frac{(100)^3 \text{ cm}^3}{1 \text{ m}^3}} = \frac{1,222.2 \frac{\text{kg}}{\text{m s}^2}}{4,512.6 \frac{\text{kg}}{\text{m}^2 \text{ s}^2}} = 0.27 \text{ m}$$

The NAPL pressure at the bottom of the pool is  $P_n^{top \text{ silt}}$  and can be calculated as the sum of the water and capillary pressures.

$$P_n^{top \text{ silt}} = P_w^{top \text{ silt}} + P_d^{nw-silt} = 98,100 \text{ Pa} + 1,917 \text{ Pa} = 100,017 \text{ Pa}$$

Similar to the calculation of water pressure, NAPL pressure at various elevations can be calculated assuming hydrostatic conditions. An example is shown here for the elevation equal to the top of the pool.

$$P_n^{top \text{ pool}} = P_n^{top \text{ silt}} - \rho_n g Z_{DNAPL \text{ height above silt}}$$

$$= 100,017 - 1.46 \frac{\text{g}}{\text{cm}^3} 9.81 \frac{\text{m}}{\text{s}^2} 0.27 \text{ m} \frac{1 \text{ kg}}{1000 \text{ g}} \frac{(100)^3 \text{ cm}^3}{\text{m}^3} = 96,150 \frac{\text{kg}}{\text{m s}^2} \frac{1 \text{ Pa}}{1 \frac{\text{kg}}{\text{m s}^2}}$$

$$= 96,150 \text{ Pa}$$

So, the NAPL pressure is a straight line from 96.15 kPa at the top of the pool to 100.017 kPa at the top of the silt (bottom of the pool).

The corresponding water saturations are calculated using Equations (16) and (17). DNAPL saturations can then be calculated as  $S_n = 1 - S_w$ .

$$S_e = \frac{S_w - S_r}{S_m - S_r}$$

$$S_e = \left(\frac{P_c}{P_d}\right)^{-\lambda} \text{ for } P_c \geq P_d$$

For example, for the water saturation at the bottom of the pool:

$$P_w = 98,100 \text{ Pa}$$

$$P_n = 100,017 \text{ Pa}$$

$$P_c = 100,017 - 98,100 \text{ Pa} = 1,917 \text{ Pa}$$

$$S_e = \left(\frac{1,917 \text{ Pa}}{694 \text{ Pa}}\right)^{-2.5} = 0.08$$

$$\begin{aligned} S_w &= S_e (S_m - S_r) + S_r \\ &= 0.08 (1 - 0.1) + 0.1 \\ &= 0.17 \end{aligned}$$

[Return to Exercise 8](#) ↑

[Return to where text linked to Exercise 8](#) ↑

## Solution Exercise 9

(a) Find  $z_{aw}$  given

$$z_{nw} = 100 \text{ cm}, z_{an} = 140 \text{ cm}, \rho_w = 1,000 \text{ kg/m}^3, \text{ and } \rho_n = 700 \text{ kg/m}^3$$

$$z_{nw} = \frac{\rho_n z_{an} - \rho_w z_{aw}}{\rho_n - \rho_w} \quad (\text{Equation (38)})$$

$$\begin{aligned} \therefore z_{aw} &= \frac{\rho_n z_{an} - z_{nw}(\rho_n - \rho_w)}{\rho_w} \\ &= \frac{700 \frac{\text{kg}}{\text{m}^3} 140 \text{ cm} - 100 \text{ cm} \left( 700 \frac{\text{kg}}{\text{m}^3} - 1,000 \frac{\text{kg}}{\text{m}^3} \right)}{1,000 \frac{\text{kg}}{\text{m}^3}} \\ &= 128 \text{ cm} \end{aligned}$$

$$(b) \beta_{an} = \frac{\sigma_{aw}}{\sigma_{an}} \quad (\text{Equation Box 1-7a})$$

$$\text{and } \sigma_{aw} = \sigma_{an} + \sigma_{nw} \quad (\text{Equation Box 1-8})$$

$$\therefore \beta_{an} = \frac{0.035 \frac{\text{N}}{\text{m}} + 0.030 \frac{\text{N}}{\text{m}}}{0.035 \frac{\text{N}}{\text{m}}} = 1.857$$

$$\beta_{nw} = \frac{\sigma_{aw}}{\sigma_{nw}} \quad (\text{Equation Box 1-7b})$$

$$= \frac{0.035 \frac{\text{N}}{\text{m}} + 0.030 \frac{\text{N}}{\text{m}}}{0.030 \frac{\text{N}}{\text{m}}} = 2.167$$

(c) Given:

$$\bar{S}_t = [1 + (\beta_{an} \alpha_{aw} P_c^{an})^n]^{-m} \quad (\text{Equation Box 1-5})$$

$$\bar{S}_w = [1 + (\beta_{nw} \alpha_{aw} P_c^{nw})^n]^{-m} \quad (\text{Equation Box 1-6})$$

$$\bar{S}_t = \frac{S_w + S_n - S_{rw}}{1 - S_{rw}} \quad (\text{Equation Box 1-2})$$

$$\bar{S}_w = \frac{S_w - S_{rw}}{1 - S_{rw}} \quad (\text{Equation Box 1-3})$$

$$\alpha_{aw} = 0.145 \text{ cm}^{-1}$$

$$n = 2.68$$

$$m = 1 - \frac{1}{n} = 1 - \frac{1}{2.68} = 0.627$$

$$S_{rw} = 0.05$$

Because  $\alpha_{aw}$  is given in units of  $\text{cm}^{-1}$ , it is easiest to express each of  $P_c^{nw}$  and  $P_c^{an}$  as an equivalent head of water (in cm) by dividing by  $\rho_w g$

$$P_c^{nw} = (\rho_w - \rho_n)g(z - z_{nw}) \quad (\text{Equation (40)})$$

$$\therefore h_c^{nw} = \frac{(\rho_w - \rho_n)}{\rho_w}(z - z_{nw})$$

$$\text{and } P_c^{an} = \rho_n g(z - z_{an}) \quad (\text{Equation (39)})$$

$$\therefore h_c^{an} = \frac{\rho_n}{\rho_w}(z - z_{an})$$

Next calculate  $S_t$  and  $S_w$  at elevations from  $z = 80$  cm to  $z = 200$  cm.

For example, for  $z = 120$  cm:

$$h_c^{nw} = \left( \frac{1,000 - 700}{1,000} \right) (120 - 100) = 6 \text{ cm}$$

$$h_c^{an} = \left( \frac{700}{1,000} \right) (120 - 140) = -14 \text{ cm}$$

for  $h_{an} < 0$   $S_t = 1$

to calculate  $S_w$ :

$$\bar{S}_w = [1 + \{(2.167)(0.145 \text{ cm}^{-1})(6 \text{ cm})\}^{2.68}]^{-0.627} = 0.310$$

$$S_w = \bar{S}_w(1 - S_{rw}) + S_{rw} = 0.310(1 - 0.05) + 0.05 = 0.345$$

as another example, at  $z = 150$  cm:

$$h_c^{nw} = \left( \frac{1,000 - 700}{1,000} \right) (150 - 100) = 15 \text{ cm}$$

$$h_c^{an} = \left( \frac{700}{1,000} \right) (150 - 140) = 7 \text{ cm}$$

$$\bar{S}_t = [1 + \{(1.857)(0.145 \text{ cm}^{-1})(7 \text{ cm})\}^{2.68}]^{-0.627} = 0.310$$

$$\bar{S}_w = [1 + \{(2.167)(0.145 \text{ cm}^{-1})(15 \text{ cm})\}^{2.68}]^{-0.627} = 0.073$$

$$S_w = 0.073(1 - 0.05) + 0.05 = 0.120$$

$$\bar{S}_t = \frac{S_w + S_n - S_{nw}}{1 - S_{nw}} \text{ and } S_t = S_n + S_w$$

$$\therefore S_t = \bar{S}_t(1 - S_{rw}) + S_{rw} = 0.310(1 - 0.05) + 0.05 = 0.345$$

(d) Calculate  $S_n = S_t - S_w$  for  $z = 80$  cm to  $z = 200$  cm.

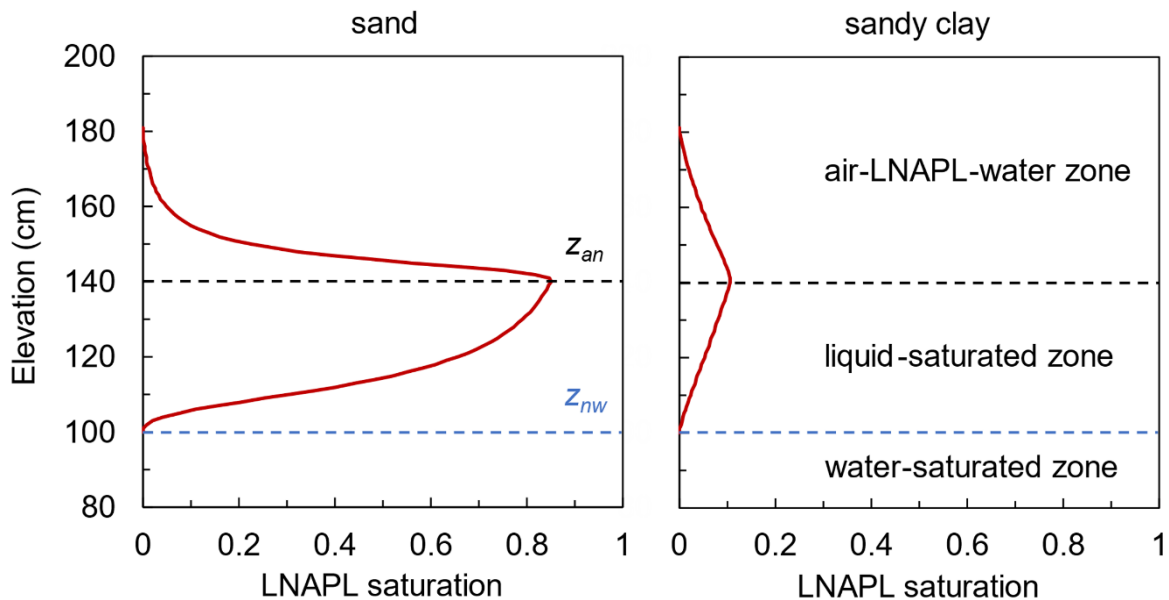
For example,

$$\text{for } z = 120 \text{ cm: } S_n = 1 - 0.345 = 0.655$$

$$\text{for } z = 150 \text{ cm: } S_n = 0.345 - 0.120 = 0.225$$

The calculated LNAPL saturations ( $S_n$ ) are shown in this image (left-hand side) as a red solid line;  $z_{an}$  and  $z_{nw}$  are shown as horizontal broken black and blue lines, respectively. The LNAPL distribution curve has the “shark fin” shape found by field investigators. Above  $z_{an}$ , the sand is unsaturated with respect to liquids; air, LNAPL, and water are in the pore spaces.

Below  $z_{nw}$ , the sand is saturated with only water; there is neither air nor LNAPL.



(e) Repeat part (d) using:

$$\alpha_{aw} = 0.03 \text{ cm}^{-1}$$

$$n = 1.3$$

$$S_{rw} = 0.10$$

The resulting LNAPL saturations are shown on the right-hand side of the previous image. For the same thickness of LNAPL in a well, the LNAPL saturations are far less in this sandy-clay soil than in the sandy soil.

[Return to Exercise 9](#) ↑

[Return to where text linked to Exercise 9](#) ↑

## 12 Notations

- $\alpha$  = Equation (19): fitting parameter related to a characteristic capillary pressure ( $M^{-1}LT^2$ )
- $\alpha$  = Equation (22) and (23): fluid identifier (wetting or nonwetting) – dimension is not relevant
- $\alpha_{aw}$  = van Genuchten (1980) parameter determined using nonhysteretic, air–water capillary pressure-saturation data ( $M^{-1}LT^2$ )
- $\beta_{an}$  = air–NAPL scaling factor (dimensionless)
- $\beta_{nw}$  = NAPL–water scaling factor (dimensionless)
- $g$  = gravitational acceleration ( $LT^{-2}$ )
- $H$  = the maximum height (thickness) of DNAPL such that the capillary barrier is not penetrated (L)
- $\nabla h_\alpha$  = hydraulic-head gradient (dimensionless)
- $h_c$  = height of water in capillary tube (L)
- $i, j$  = x, y, and z directional identifiers
- $J$  = dimensionless capillary pressure (dimensionless)
- $k$  = intrinsic permeability ( $L^2$ )
- $k_\alpha$  = effective permeability of fluid  $\alpha$  ( $L^2$ )
- $k_{r\alpha}$  = relative permeability of fluid  $\alpha$  (dimensionless)
- $k_{ra}$  = relative permeability of air (dimensionless)
- $k_{rn}$  = relative permeability of NAPL (dimensionless)
- $k_{rw}$  = relative permeability of water (dimensionless)
- $\lambda$  = pore-size distribution index (dimensionless)
- $m$  and  $n$  = Equation (19): fitting parameters related to the pore-size distribution (dimensionless)
- $\mu_\alpha$  = dynamic viscosity ( $ML^{-1}T^{-1}$ )
- $P_\alpha$  = air pressure ( $ML^{-1}T^{-2}$ )
- $P_c$  = capillary pressure ( $ML^{-1}T^{-2}$ )
- $P_c^{an}$  = air–NAPL capillary pressure ( $ML^{-1}T^{-2}$ )
- $P_c^{nw}$  = NAPL–water capillary pressure ( $ML^{-1}T^{-2}$ )
- $P'_c$  = capillary pressure at top of pool ( $ML^{-1}T^{-2}$ )
- $P''_c$  = entry pressure of capillary barrier ( $ML^{-1}T^{-2}$ )
- $P_n$  = NAPL pressure ( $ML^{-1}T^{-2}$ )
- $P_w$  = water pressure ( $ML^{-1}T^{-2}$ )

- $q_\alpha$  = specific discharge ( $\text{LT}^{-1}$ )  
 $R$  = mean radius of curvature ( $\text{L}$ )  
 $r$  = tube radius ( $\text{L}$ )  
 $R_b$  = bulk retention capacity (dimensionless)  
 $R_1$  and  $R_2$  = principal radii of curvature ( $\text{L}$ )  
 $\Delta\rho$  = difference in density between DNAPL and water ( $\text{ML}^{-3}$ )  
 $\rho_\alpha$  = density of fluid represented by  $\alpha$  ( $\text{ML}^{-3}$ )  
 $\rho_w$  = water density ( $\text{ML}^{-3}$ )  
 $S_a$  = air saturation (dimensionless)  
 $S_e$  = effective wetting saturation (dimensionless)  
 $S_m$  = maximum water saturation (dimensionless)  
 $S_n$  = NAPL saturation (dimensionless)  
 $S_t$  = total liquid saturation (dimensionless)  
 $S_w$  = water saturation (dimensionless)  
 $\sigma_{an}$  = air–NAPL interfacial tension ( $\text{MT}^{-2}$ )  
 $\sigma_{aw}$  = air–water interfacial tension ( $\text{MT}^{-2}$ )  
 $\sigma_{nw}$  = NAPL–water interfacial tension ( $\text{MT}^{-2}$ )  
 $\sigma_{sn}$  = solid–NAPL interfacial tension ( $\text{MT}^{-2}$ )  
 $\sigma_{sw}$  = solid–water interfacial tension ( $\text{MT}^{-2}$ )  
 $\theta$  = contact angle (dimensionless)  
 $\theta_a$  = volumetric air content (dimensionless)  
 $\theta_n$  = volumetric NAPL content (dimensionless)  
 $\theta_w$  = volumetric water content (dimensionless)  
 $V_a$  = volume of air ( $\text{L}^3$ )  
 $V_n$  = volume of NAPL in a source zone ( $\text{L}^3$ )  
 $V_{sz}$  = total volume of the source zone ( $\text{L}^3$ )  
 $V_T$  = total volume of pore space ( $\text{L}^3$ )  
 $V_{tl}$  = volume of the pore space occupied by NAPL and water ( $\text{L}^3$ )  
 $V_w$  = volume of water ( $\text{L}^3$ )  
 $z$  = elevation ( $\text{L}$ )  
 $z_{an}$  = elevation of the air–LNAPL interface ( $P_n = 0$ ) in a well (borehole) screened in the subsurface containing LNAPL and water ( $\text{L}$ )

$z_{aw}$  = elevation of the water table ( $P_w = 0$ ), which is the elevation of the air-water interface in a well (borehole) screened only in the water-saturated zone (L)

## 13 About the Authors



**Kevin Mumford** received a bachelor's degree in environmental engineering and master's degree in civil engineering from the University of Waterloo, and PhD in civil engineering from McMaster University before joining the faculty of Queen's University in 2010. His research is focused on the study of multiphase flow in porous media and its application to the remediation of non-aqueous phase liquids in soil and groundwater, with particular specialization in the behavior of gases in contaminated groundwater systems including in situ thermal remediation, bubble-facilitated transport, and the numerical simulation of gas migration and mass transfer. His research includes high-resolution laboratory experiments, often using quantitative visual techniques, coupled with process-based numerical modelling of multiphase flow and reactive transport.



**Bernard Kueper** is a popular short-course instructor who has lectured on the topic of DNAPL and LNAPL migration and remediation in courses held in Switzerland, Australia, Denmark, England, the United States, Brazil, and Canada. He is a former associate editor of the *Journal of Ground Water*, the *Journal of Contaminant Hydrology*, and the *Canadian Geotechnical Journal*. Dr. Kueper is the lead editor of the textbook *Chlorinated Solvent Source Zone Remediation*, published by Springer Science + Business Media, LLC, New York.



**Robert Lenhard** studied under Drs. A. T. Corey, R. H. Brooks, and B. P. Warkentin at Oregon State University. Later, he had a productive post-doc under Dr. J. C. Parker at Virginia Tech. Afterwards, he largely worked for US National Laboratories (Pacific Northwest National Laboratory and Idaho National Laboratory) but spent four years at Sultan Qaboos University in the Sultanate of Oman as the head of the Soil & Water Department. He also spent 1.5 years near Perth, Australia, working for CSIRO (Commonwealth Scientific & Industrial Research Organization). During his long career as a scientist, he mainly addressed the behavior of nonaqueous-phase liquids (NAPL) in the subsurface. He published seminal work in the area of predicting and measuring NAPL behavior in

three-phase air–NAPL–water systems. His work is still being utilized by investigators to address subsurface NAPL contamination. Knowledge obtained from his work has been employed to design and apply new innovative techniques to remediate contaminated areas and to better understand the subsurface behavior of fluids. Before his PhD studies at Oregon State University, he worked as a forest soil scientist in the state of Oregon, USA.

Please consider signing up to the GW-Project mailing list and stay informed about new book releases, events, and ways to participate in the GW-Project. When you sign up to our email list it helps us build a global groundwater community. [Sign up](#)<sup>↗</sup>.

